

Tesi di Dottorato di PINNA GIOVANNI

Matricola 738513

**POLITECNICO DI
MILANO**



**DIPARTIMENTO
DI
CHIMICA,
MATERIALI
E
INGEGNERIA CHIMICA
"Giulio Natta"**

**SYNTHESIS OF ^{18}F -LABELLED
COMPOUNDS AS TARGETS FOR
APPLICATION IN
PET RADIOCHEMISTRY.**

Dottorato di Ricerca in Chimica
Industriale e Ingegneria Chimica
(CII)

**XXIV ciclo
2009 - 2011**

Coordinatore: prof. Dr. Tiziano FARAVELLI
Tutore: prof. Dr. Elisabetta BRENNNA
Relatore: prof. Dr. Alessandro VOLONTERIO

List of Publications

1. Bigotti, S., Olimpieri, F., Shankar P.S., Pinna, G., Altomonte, S., Zanda, M. The trifluoroethylamine function as peptide bond replacement: new developments and findings. *Chimica Oggi*(Chemistry Today) **2009**, 27,(3).
2. Pinna, G., Bellucci, M. C., Malpezzi, L., Pisani, L., Superchi, S., Volonterio, A., Zanda, M. An umpolung sulfoxide reagent for use as a functionalized benzyl carbanion equivalent. *Tetrahedron*, **2011**, 67, 5268-5281.
3. **SYMPOSIUM PRESENTATION – POSTER: “Targeting Tumor Hypoxia: Synthesis of a Novel Potential PET radioligand”**
Pinna, G., Domarkas, J., Schweiger, L., Mingarelli, M., Welch, A., Dall’Angelo, S., Delibegovic, M., Zanda, M. 11th Annual Postgraduate Meeting of the RSC Fluorine Fubject Group, September 2011, Aberdeen, Scotland

Table of Contents

List of Figures	VII
List of Tables	IX
List of Schemes	X
ABSTRACT	XII
Chapter 1. Positron Emission Tomography	25
1.1 Introduction	25
1.2 Positron Emission Tomography principles.....	28
1.3 PET radionuclide production.....	30
1.3.1 Fluorine-18 radionuclide	30
1.4 PET radiopharmaceuticals.....	31
1.4.1 2-[¹⁸ F]fluoro-2-D-deoxyglucose ([¹⁸ F]FDG)	34
1.4.2 6-[¹⁸ F]fluoro-L-dihydroxyphenyl alanine ([¹⁸ F]L-DOPA)	36
1.4.3 3'-Deoxy-3'-[¹⁸ F]fluorothymidine ([¹⁸ F]FLT)	37
1.4.4 [¹⁸ F]Fluoromisonidazole ([¹⁸ F]FMISO)	38
1.4.5 [¹¹ C]choline and [¹⁸ F]Fluorocholine ([¹⁸ F]FCH)	40
1.5 Synthetic strategies for radiolabeling with fluorine-18	41
1.5.1 Electrophilic fluorination.....	42
1.5.2 Nucleophilic fluorination.....	43
Chapter 2. PET-Imaging of Hypoxia	50
2.1 What is Hypoxia?	50
2.2 Physiological changes related to hypoxia.....	50
2.3 Tumour hypoxia measurement	51
2.3.1 Molecular imaging of hypoxia with PET	52
Chapter 3. Synthesis of [¹⁸F]FAZA	60
3.1 Introduction	60
3.2 State of the art on FAZA synthesis.....	61
3.3 Results and discussion.....	62

3.3.1 Chemical synthesis of [¹⁸ F]FAZA precursor	62
3.3.2 Radiosynthesis of [¹⁸ F]FAZA	63
3.3.3 [¹⁸ F]FAZA hypoxia PET imaging.....	69
3.4 Conclusions.....	69
Chapter 4. Synthesis of a novel potential PET radioligand for hypoxia imaging	70
4.1 Aim of the project	70
4.2 Results and discussion	71
4.2.1 Synthesis of trifluoro- <i>N</i> -alcoxycarbonylimino intermediate.....	71
4.2.2 Synthesis of <i>N</i> -ethylamino-2-nitroimidazole	73
4.2.3 Introduction of 2-nitroimidazole functionality.....	73
4.2.4 Synthesis of the precursor for ¹⁸ F-radiolabeling	74
4.2.5 Introduction of ¹⁸ F-radionuclide	76
4.3 Conclusions.....	78
Chapter 5. Sulfoxides as carbanion equivalents.....	79
5.1 Introduction.....	79
5.2 Results and discussion	80
5.2.1 Synthesis of sulfoxides 5.1.....	80
5.2.2 Alkylation of sulfoxides 5.1	82
5.2.3 Use of umpolung sulfoxide reagents 5.2.....	87
5.3 Conclusions.....	92
Chapter 6. Experimental section	93
Chapter 7. References.....	110

List of Figures

Chapter 1. Positron Emission Tomography

Figure 1.1. *Image of a commercial cyclotron.*

Figure 1.2. *From left: hot cells for the production of radiopharmaceuticals and automated synthesizer.*

Figure 1.3. *From left: a combined PET/CT scanner and a processed PET image of whole body.*

Figure 1.4. *Schematic representation of annihilation event.*

Figure 1.5. *Glucose and its analogs: 2-deoxyglucose (DG) and fluorodeoxyglucose (FDG).*

Figure 1.6. *Metabolic trapping of ^{18}F -fluorodeoxyglucose and catabolic path of glucose metabolism.*

Figure 1.7. *Intracellular synthesis of dopamine from L-tyrosine.*

Figure 1.8. *Transport and decarboxylation of [^{18}F]6-Fluoro-L-DOPA to [^{18}F]6-Fluorodopamine in the CNS.*

Figure 1.9. *Chemical structures of thymidine radiolabeled with ^{18}F (1.9) and ^{11}C (1.10).*

Figure 1.10. *Metabolic trapping of [^{18}F]fluorothymidine.*

Figure 1.11. *Chemical structures of [^{18}F]Fluoromisonidazole (1.11), [^{18}F]fluoroarabinofuranosylnitroimidazole (1.12) and [^{64}Cu]copper-diacetyl-bis-methylthiosemicarbazone (1.13).*

Figure 1.12. *Intracellular mechanism of nitroimidazole compounds trapping.*

Figure 1.13. *[^{18}F]FECH and [^{11}C]Choline uptake mechanism.*

Figure 1.14. *Radiolabelled choline derivatives.*

Chapter 2. PET-Imaging of Hypoxia

Figure 2.1. *Mechanism of intracellular trapping of nitroimidazoles under hypoxic conditions.*

Figure 2.2. *Nitroimidazole agents for tumor hypoxia PET imaging.*

Chapter 3. Synthesis of [¹⁸F]FAZA

Figure 3.1. *Schematic representation of the production and preparation of “naked” [¹⁸F]fluoride with Kryptofix 2.2.2. and by azeotropic evaporation.*

Figure 3.2. *Scheme of the TRACERlab FX_{FDG} for the automated production of precursor 3.12.*

Figure 3.3. *Radio-TLC chromatograms.*

(a) After fluorination

(b) After Hydrolysis

Figure 3.4. *HPLC analysis of [¹⁸F]FAZA co-eluted with cold FAZA.*

Figure 3.5. *PET images of two transgenic hypoxic mice (PTP1B) after PET imaging with [¹⁸F]FAZA.*

Chapter 4. Synthesis of a novel potential PET radioligand for hypoxia imaging

Figure 4.1. *General synthetic route to the new potential hypoxia tracer.*

List of Tables

Chapter 1. Positron Emission Tomography

Table 1.1. *The most commonly used positron emitting radionuclides in PET.*

Table 1.2. *Some PET-radiopharmaceuticals and their application.*

Chapter 3. Synthesis of [¹⁸F]FAZA

Table 3.1. *Flow chart of [¹⁸F]FAZA radiosynthesis scheme.*

Chapter 4. Synthesis of a novel potential PET radioligand for hypoxia imaging

Table 4.1. *Attempts to introduce 2-nitroimidazole, and introduction of imidazole and piperidine.*

Table 4.2. *“Cold” fluorination conditions.*

Chapter 5. Sulfoxides as carbanion equivalents

Table 5.1. *Synthesis of sulfoxides (±)-5.1.*

Table 5.2. *Reaction conditions for alkylation of (±)-5.1a.*

Table 5.3. *Alkylation of ortho-[(N-alkyl)carbamoyl]phenyl sulfoxide.*

Table 5.4. *Synthesis of alcohols 5.3, chlorides 5.4 and acetamides 5.5.*

List of Schemes

Chapter 1. Positron Emission Tomography

Scheme 1.1. *Synthesis of EF5 by direct electrophilic fluorination with $[^{18}\text{F}]\text{F}_2$.*

Scheme 1.2. *Electrophilic synthesis of $[^{18}\text{F}]$ fluoro-L-DOPA, starting from an organotin precursor.*

Scheme 1.3. *Synthesis of $[^{18}\text{F}]$ FDG via electrophilic fluorination by using $[^{18}\text{F}]$ acetyl hypofluorite.*

Scheme 1.4. *Synthesis of $[^{18}\text{F}]$ FDG through aliphatic nucleophilic reaction and deprotection.*

Scheme 1.5. *Synthetic routes to $[^{18}\text{F}]$ fluoroethylcholine.*

Scheme 1.6. *Reaction scheme for the synthesis of $[^{18}\text{F}]$ FMISO: ^{18}F -fluorination of NITTP precursor and subsequent removal of the THP protecting group under acidic conditions.*

Scheme 1.7. *Synthesis of $[^{18}\text{F}]$ FMISO via the $[^{18}\text{F}]$ EPI-F intermediate: nucleophilic displacement of GOTS precursor with ^{18}F -fluoride and epoxide ring opening by coupling with 2-NIM.*

Scheme 1.8. *Radiosynthesis of $[^{18}\text{F}]$ Fluorothymidine starting from protected precursor (1.31), then sequentially submitted to $[^{18}\text{F}]$ labeling and hydrolysis.*

Scheme 1.9. *General scheme of aromatic nucleophilic fluorinations.*

Scheme 1.10. *Radiosynthesis of $[^{18}\text{F}]$ flumazenil.*

Scheme 1.11. *Aromatic nucleophilic fluorinations on pyridinyl rings.*

Scheme 1.12. *Synthesis of the PET radioligand for imaging the 5-HT_{1A} receptor ($[6\text{-pyridinyl-}^{18}\text{F}]$ fluoro-WAY-100635).*

Scheme 1.13. *^{18}F -labelling of the meta position of pyridines.*

Scheme 1.14. *^{18}F -fluorination of 3- $[^{18}\text{F}]$ fluoropyridine starting from a diaryl-iodonium salt.*

Scheme 1.15. *Nucleophilic fluorination of an electron-rich arene.*

Chapter 3. Synthesis of $[^{18}\text{F}]$ FAZA

Scheme 3.1. *Synthesis of FAZA by Kumar.*

Scheme 3.2. *Alternative route to FAZA.*

Scheme 3.3. *$[^{18}\text{F}]$ FAZA precursor synthesis.*

Scheme 3.4. *$[^{18}\text{F}]$ Fluorination of $[^{18}\text{F}]$ FAZA precursor.*

Scheme 3.5. *Hydrolysis of diacetyl[¹⁸F]FAZA.*

Chapter 4. Synthesis of a novel potential PET radioligand for hypoxia imaging

Scheme 4.1. *Retrosynthetic pathway for the new PET hypoxia radiopharmaceutical.*

Scheme 4.2. *Synthesis of trifluoro-N-alcoycarbonylimino intermediate (4.4).*

Scheme 4.3. *Planned introduction of nitroimidazole by using a base.*

Scheme 4.4. *Alternative synthetic route to different nitroimidazole compounds.*

Scheme 4.5. *Synthesis of 2-(2-nitro-1H-imidazolyl)ethylamine (4.8).*

Scheme 4.6. *Synthesis of nitroimidazole peptidomimetic derivative 4.13.*

Scheme 4.7. *Retrosynthetic approach towards the new potential fluorinated 2-nitroimidazole tracer.*

Scheme 4.8. *Synthesis of the precursor for [¹⁸F]-radiolabeling.*

Scheme 4.9. *Derivatization of syn-1,2-diol (4.19) into cyclic carbonate (4.21).*

Scheme 4.10. *Cold fluorination with KF/Kryptofix 2.2.2.*

Scheme 4.11. *Epoxidation of alkene function of 4.13.*

Chapter 5. Sulfoxides as carbanion equivalents

Scheme 5.1. *Planned synthetic strategy.*

Scheme 5.2. *Synthesis of racemic sulfoxides (±)-5.1.*

Scheme 5.3. *Preparation of enantiomerically pure sulfoxides (+)-5.1a and (-)-5.1a.*

Scheme 5.4. *Alkylation of (±)-5.1a with 1-Br-3-methylbutane.*

Scheme 5.5. *Alkylation of ortho-[(N-alkyl)carbonyl]phenyl sulfoxides.*

Scheme 5.6. *NOPR on sulfoxide (±)-5.2a.*

Scheme 5.7. *Synthesis of alcohols 5.3, chlorides 5.4 and acetamides 5.5.*

Scheme 5.8. *Pummerer reaction on enantiomerically pure (S_SR)-5.2a.*

Scheme 5.9. *Recycle of the co-product 5.6.*

Scheme 5.10. *Proposed mechanism for the Pummerer reactions.*

Scheme 5.11. *Potential synthetic strategy for the introduction of fluorine-18 and production of new PET-tracers.*

ABSTRACT

Positron emission tomography (PET) is a highly sensitive molecular imaging technique which allows for the visualization and investigation of biochemical/pathological processes by detection of radioactive compounds, commonly administered to the subject (typically 10^{-10} g in humans)¹ by intravenous injection.

The radioactive compound (tracer) for PET research is labelled with a radioactive isotope, which emits a positively charged anti-matter particle, namely the positron (β^+). The positron encounters an electron in the surrounding matter in the body and annihilates, thus producing two high energy (511 KeV) gamma ray photons (γ) that travel at 180° with respect to each other. These gamma rays are recorded with a special camera and elaborated, then a computer calculates the spatial distribution of the tracer within the patient's body. A 2D or 3D image of the investigated region is the final result of the PET imaging experiment. Many millions of annihilation events are required for the construction of a PET image.

PET images allows the quantitative measurement, although at relatively low resolution, of the real concentration of the tracer in the tissue.

The typical duration of a PET-imaging procedure is about 30 min, although it can be reduced to 10 min., using the most recent PET scanners.

PET radiopharmaceuticals are commonly labelled with short-lived positron emitters, such as ^{11}C ($t_{1/2} = 20.4$ min), ^{13}N ($t_{1/2} = 9.97$ min), ^{15}O ($t_{1/2} = 2.04$ min), ^{18}F ($t_{1/2} = 110$ min), however some tracers labelled with longer-lived radionuclides, such as ^{68}Ga ($t_{1/2} = 68.1$ min), ^{124}I ($t_{1/2} = 60$ 192 min), and ^{64}Cu ($t_{1/2} = 762$ min) are available.

^{18}F -Fluorine is the most used PET radionuclide because of its relatively long half-life (110 min) which allows the delivery of ^{18}F -labelled PET radiopharmaceuticals to other PET centres, which are not equipped with a cyclotron.

Radionuclides for labelling are produced by means of a cyclotron, where accelerated beams of protons or deuterons are generated and used to irradiate a target material (e.g. N_2 , Ne, H_2^{18}O , etc), giving rise to the desired radioisotope through a nuclear reaction.

¹ Paans, A. M. J., van Waarde, A., Elsinga, P. H., Willemsen, A. T. M., Vaalburg, W. Positron emission tomography: the conceptual idea using a multidisciplinary approach. *Methods* **2002**, 27, 195-207.

^{18}F -Fluorine is the most widely used radioisotope for labelling procedures. It is produced by proton irradiation of ^{18}O -enriched water, through the nuclear reactions $^{18}\text{O} (p, n) ^{18}\text{F}$ and $^{20}\text{Ne} (d, \alpha) ^{18}\text{F}$ ^{II}.

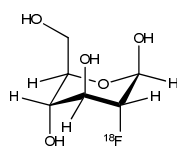
The radiolabelling and synthesis of PET radiopharmaceuticals are performed in lead shielded automated systems, referred to as “hot cells”, in order to avoid the prolonged exposure of the operator to radiations, particularly when high amounts of radiotracers are produced for PET clinical application.

The half-lives - the period of time over which half the radionuclides undergo disintegration - of the commonly used positron emitters for PET imaging are too short, hence represent a limiting factor for PET, given that the half-life of the radioisotope should be commensurate to the time of the biochemical process to be investigated.

The spatial resolution of the human PET cameras is relatively low, between 1 and 2 mm. This represents an important limiting factor in PET practice, but can be overcome by combining a PET scan with a higher resolution CT or MRI scan. PET-CT scanners are nowadays routinely used for clinical and pre-clinical imaging.

Medical diagnosis by means of PET is rather expensive. All the procedures performed approaching a PET imaging experiment require expensive facilities, namely the cyclotron for the production of radionuclides, the automated system for the synthesis of the radiopharmaceutical and the PET camera for detection and elaboration of radiations.

2- ^{18}F fluoro-2-D-deoxyglucose (^{18}F FDG) [Figure I] is by far the most widely used radiopharmaceutical for PET imaging of a number of pathological conditions related to an alteration of glucose metabolism.



1.3

2- ^{18}F Fluoro-2-deoxy-D-glucose (^{18}F FDG)

Figure I. Structure of ^{18}F FDG

Although ^{18}F FDG PET imaging has many applications in several types of cancers, ^{18}F FDG is not a “specific” radiotracer for malignancy assessment, as different biochemical processes involve the utilisation of glucose (e.g. inflammatory cells and macrophages accumulate higher amounts of

^{II} Le Bars, D. Fluorine-18 and medical imaging: radiopharmaceutical for positron emission tomography. *J. Fluorine Chem.* **2006**, *127*, 1488-1493.

FDG than tumor cells). It is well known that several solid tumors are often associated to a deficiency in oxygen supply, resulting in the condition of hypoxia. This represents a very limiting factor during the treatment of cancer patients, as it decreases the efficacy of radiotherapy and chemotherapy. Thus, highly “tumor specific” radiotracers are essential for PET detection of those tissues characterized by a low O₂ partial pressure.

Radiolabelled 2-nitroimidazole compounds [**Figure II**] are a specific class of PET-tracers used for the detection of hypoxia. Their role as hypoxia markers was first proposed in 1979 by Chapman and co-workers^{III, IV}.

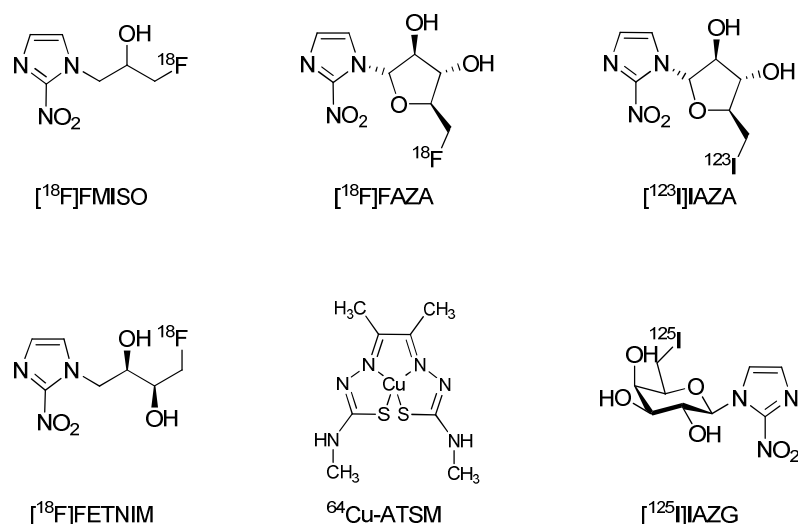


Figure II. Radiolabelled tracers for imaging hypoxia.

2-Nitroimidazole derivatives are selectively trapped inside the hypoxic cells through a biochemical mechanism, which is related to the oxygen concentration. Under hypoxic conditions, the 2-nitroimidazole compound undergoes a reduction process, leading to a highly reactive intermediary, which covalently binds to intracellular macromolecules and accumulates within the hypoxic cell [**Figure III**]. Furthermore, the presence of a positron emitter radionuclide in the 2-nitroimidazole derivative structure allows the detection *via* PET imaging of the radiations produced during the annihilation event and, finally the construction of the image of tissue affected by hypoxia.

^{III} Chapman, J.D. Hypoxic sensitizers: implications for radiation therapy. *N. Engl. J. Med.* **1979**, *301*, 1429-1432.

^{IV} Chapman, J.D., Franko, A.J., Sharplin, J. A marker for hypoxic cells in tumours with potential clinical applicability. *Br. J. Cancer* **1981**, *43*, 546-550.

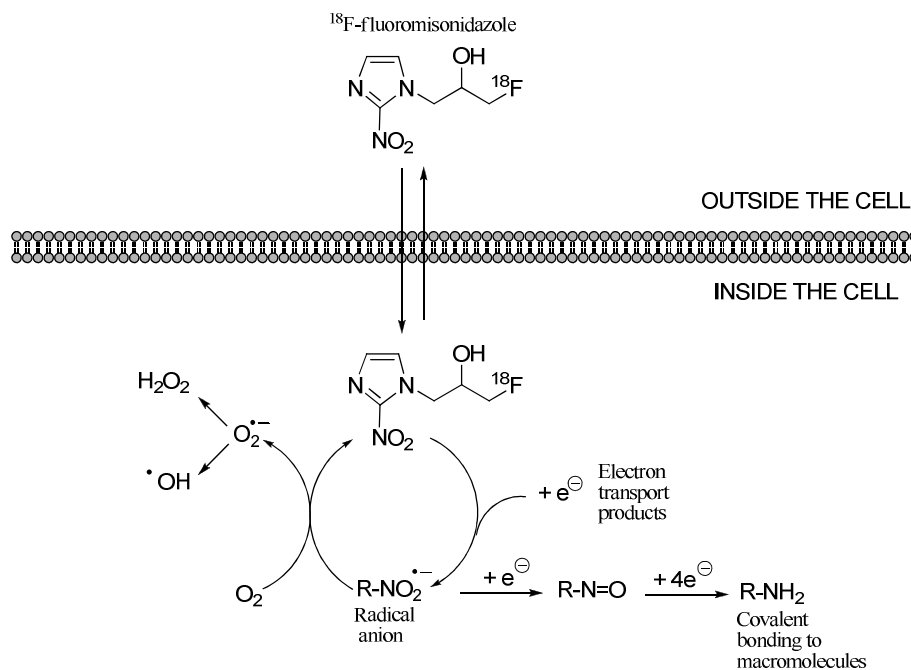


Figure III. Mechanism of 2-nitroimidazole derivatives trapping inside hypoxic cells.

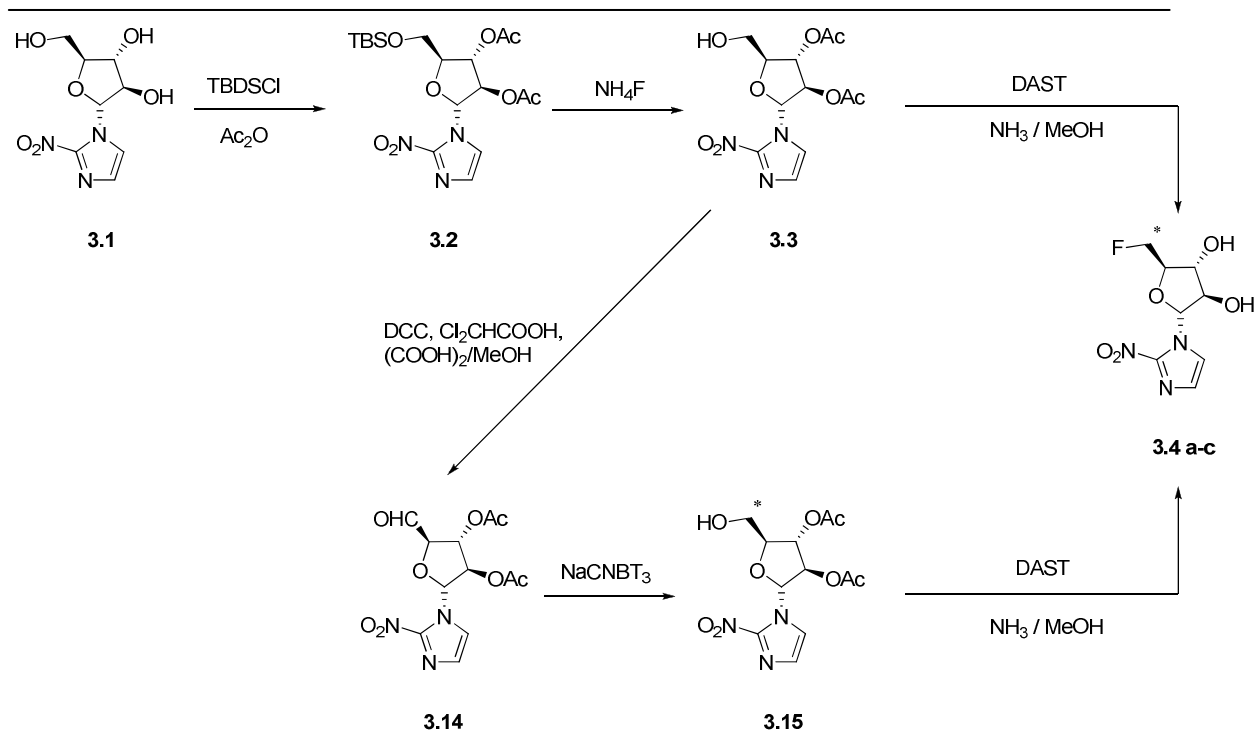
^{18}F -Fluoromisonidazole (^{18}F FMISO) is the most commonly used radiotracer for detecting tumor hypoxia by PET. However, given its slow clearance from the body and a significant metabolism rate, other 2-nitroimidazole derivatives have been investigated and used as hypoxia markers [Figure II]. Amongst them, ^{18}F fluoroazomycinarabinofuranoside (^{18}F FAZA) was shown to be the most promising hypoxia PET radiotracer because of its low lipophilicity, hence a fast elimination from the body, relative to ^{18}F FMISO^V.

The synthesis of 1- α -D-(5-fluoro-5-deoxyarabinofuranosyl)-2-nitroimidazole (FAZA) (3.4 a-c, Scheme I) was first reported in 1999 by Kumar *et al*^{VI, VII}, who synthesised the ^2H and ^3H -labeled FAZA derivatives [Scheme I] and investigated their pharmacokinetics.

^V Sorger, D., Patt, M., Kumar, P., Wiebe, L. I., Barthel, H., Seese, A., Dannenberg, C., Tannapfel, A., Kluge, R., Sabri, O. ^{18}F Fluoroazomycinarabinofuranoside (^{18}F FAZA) and ^{18}F Fluoromisonidazole (^{18}F FMISO): A comparative study of their selective uptake in hypoxic cells and PET imaging in experimental rat tumors. *Nucl. Med. Biol.* **2003**, *30*, 317-326.

^{VI} Kumar, P., Stypinski, D., Xia, H., McEwan, A. J. B., Machulla, H.-J., Wiebe, L. I. FLUOROAZOMYCIN ARABINOSIDE (FAZA): Synthesis, ^2H and ^3H -labeling and preliminary biological evaluation of a novel 2-nitroimidazole marker of tissue hypoxia. *J. Labelled Cpd. Radiopharm.* **1999**, *42*, 3-16.

^{VII} Kumar, P., Emami, S., McEwan, A. J. B., Wiebe, L. I. Development of an economical, single step synthesis of FAZA, a clinical hypoxia marker, and potential synthons to prepare its positional analogs. *Letters in Drug Design & Discovery* **2009**, *6*, 82-85.



Scheme I. Synthesis of FAZA by Kumar et al. * = H/D/T.

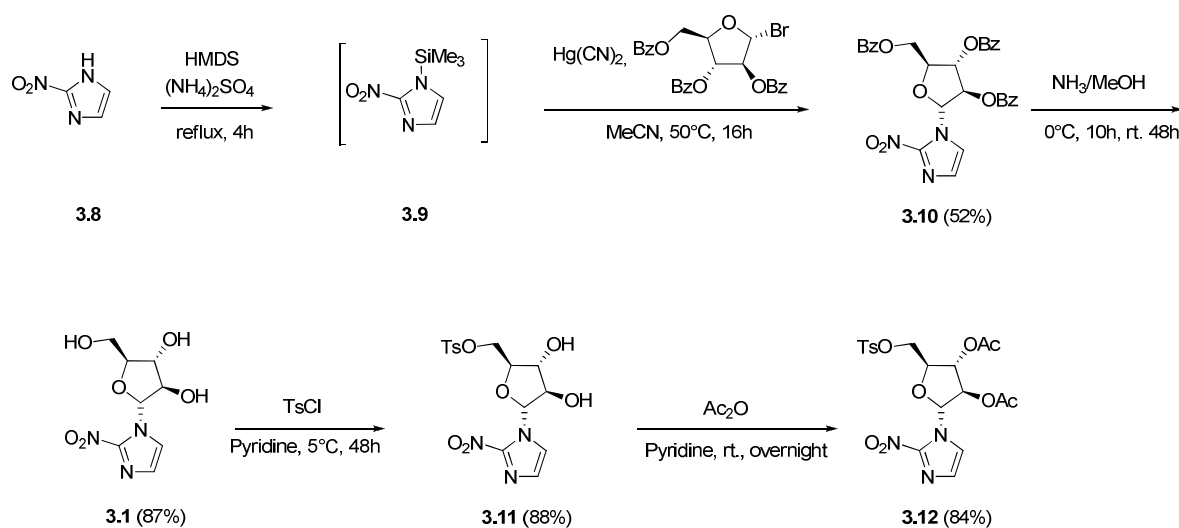
Given the increasing importance and diffusion of [¹⁸F]FAZA as a PET hypoxia marker along with its high cost and low availability in PET centres, we aimed at achieving an efficient synthesis of the [¹⁸F]FAZA precursor and its subsequent labelling procedure, in order to have satisfactory radiochemical yields (RCYs) of the [¹⁸F]FAZA, to be finally used for pre-clinical and clinical hypoxia imaging *via* PET.

[¹⁸F]FAZA synthesis

The synthetic strategy for the preparation of the FAZA precursor (3.12) [Scheme II] started from the production of 1-*N*-trimethylsilyl-2-nitroimidazole (3.9) by treating the commercially available 2-nitroimidazole (3.8) with hexamethyldisilazide (HMDS), in the presence of (NH₄)₂SO₄, at reflux temperature. The following coupling of intermediate 3.9 with stoichiometric amounts of the tribenzoyl-protected α -bromosugar, in the presence of Hg(CN)₂, gave the corresponding tribenzoylarabinofuranosylazomycin (3.10) in reasonable yields.

Deprotection of compound 3.10 with ammonia in methanol afforded satisfactory yields of arabinofuranosyl-2-nitroimidazole (α -AZA) (3.1), which was then reacted with tosyl chloride to yield the α -AZA protected at the C-5' hydroxyl group (3.11).

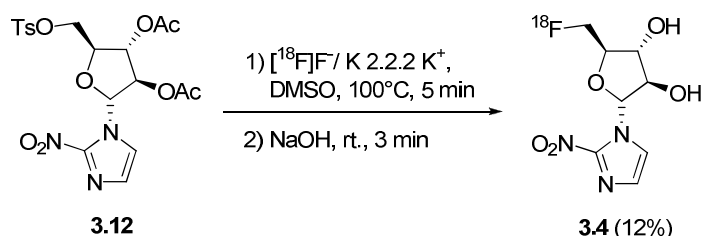
Finally, the reaction of **3.11** with acetic anhydride resulted in the production of the desired Ts-diAc- α -AZA (**3.12**) in good yield. [Scheme II].



Scheme II. Synthetic route to [^{18}F]FAZA precursor (**3.12**).

The radiosynthesis of ^{18}F -labelled FAZA was achieved under standard nucleophilic substitution conditions, by using non-carrier-added (NCA) ^{18}F -fluoride, in the presence of the phase transfer reagent Kryptofix 2.2.2 in order to enhance the ^{18}F -fluoride nucleophilicity towards Ts-diAc- α -AZA (**3.12**). Currently, this is the typical procedure adopted for ^{18}F -labelling in [^{18}F]FAZA production^{VIII, IX}.

The ^{18}F -labelled intermediate thus obtained was then hydrolysed with NaOH at rt. to give [^{18}F]FAZA (**3.4**) with a radiochemical yield (RCY) of ca. 12% (non-decay-corrected) [Scheme III].



Scheme III. Synthesis of [^{18}F]FAZA

^{VIII} Reischl, G., Ehrlichmann, W., Bieg, C., Solbach, C., Kumar, P., Wiebe, L. I., Machulla, H.-J. Preparation of the hypoxia PET tracer [^{18}F]FAZA: reaction parameters and automation. *Appl. Rad. Isot.* **2005**, *62*, 897-901.

^{IX} Hayashi, K., Furutsuka, K., Takei, M., Muto, M., Nakao, R., Aki, H., Suzuki, K., Fukumura, T. High-yield automated synthesis of [^{18}F]fluoroazomycin arabinoside ([^{18}F]FAZA) for hypoxia-specific tumor imaging. *Appl. Rad. Isot.* **2011**, 1007-1013.

The last step of the [^{18}F]FAZA project was the hypoxia assessment in animal models by PET imaging, after injection of a sterile saline solution of the radiotracer.

Two transgenic hypoxic mice (PTP1B) were submitted to [^{18}F]FAZA PET imaging, which showed the selective uptake of [^{18}F]FAZA in the fat of mice, the area affected by hypoxia.

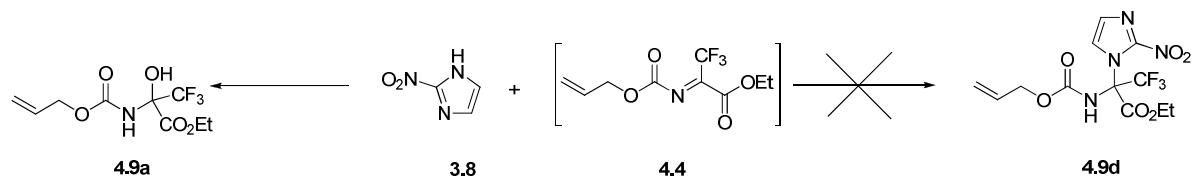
Further investigations will involve the [^{18}F]FAZA PET hypoxia imaging of animal models bearing hypoxic tumors, aiming at PET hypoxia measurement of cancer patients.

Synthesis of a new potential hypoxia PET-radiotracer

With regard to hypoxia radiotracers, we commenced a project aimed at developing a new radiolabelled nitroimidazole-based compound for detecting tumor hypoxia *via* PET.

In order to achieve an azomycin derivative as a leading compound to be then ^{18}F -labelled, an initial coupling of 2-nitroimidazole (**3.8**) with the intermediary imine (**4.4**) was performed.

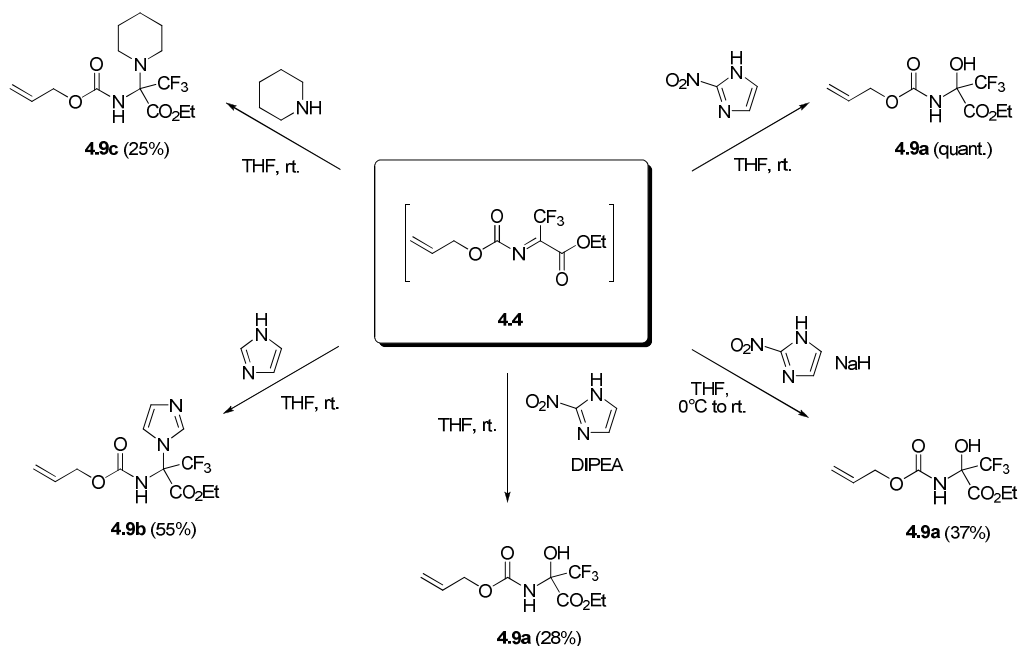
However, the desired imidazole-adduct (**4.9d**), could not be isolated and the hydrate form of imine (**4.9a**) was formed instead [**Scheme IV**].



Scheme IV. The coupling of azomycin with imine 4.4 afforded the hydrate instead of the desired coupled product.

Further attempts to obtain the product **4.9d** were performed without success: in fact the formation of hydrate (**4.9a**) was also observed when either NaH or DIPEA [**Scheme V**] were used to enhance the reactivity of azomycin and allow its coupling to imine **4.4**.

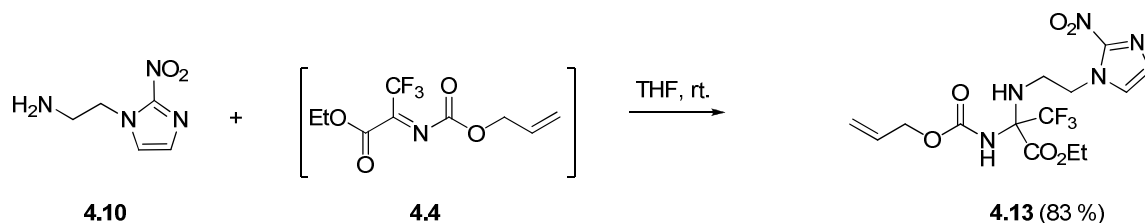
When the intermediary imine (**4.4**) was reacted with more nucleophilic species, such as imidazole and piperidine, the corresponding coupling products (**4.9b** and **4.9c**, respectively) took place [**Scheme V**], thus demonstrating the poor nucleophilicity of nitroimidazole ring towards the imine (**4.4**), probably due to the strongly de-activating effect of nitro group.



Scheme V. Coupling between imine **4.4** and 2-nitroimidazole, imidazole and piperidine.

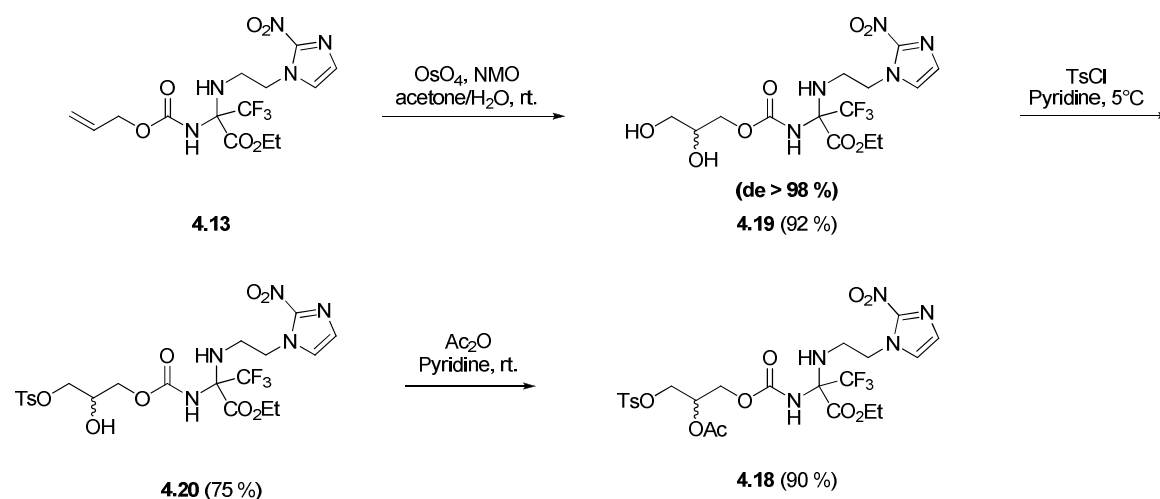
Although the direct coupling between azomycin (**3.8**) and imine (**4.4**) resulted in the exclusive formation of hydrate (**4.9a**), we assumed that the reaction of imine **4.4** with the more nucleophilic species 2-(*N*-aminoethyl)-2-nitroimidazole (**4.10**) could afford the desired nitroimidazole based compound (**4.13**).

As expected, the reaction of 1-(*N*-aminoethyl)-2-nitroimidazole (**4.10**) with the electrophilic imine (**4.4**) at rt. allowed to achieve the coupled product **4.13** with good yield (83%) [Scheme VI].



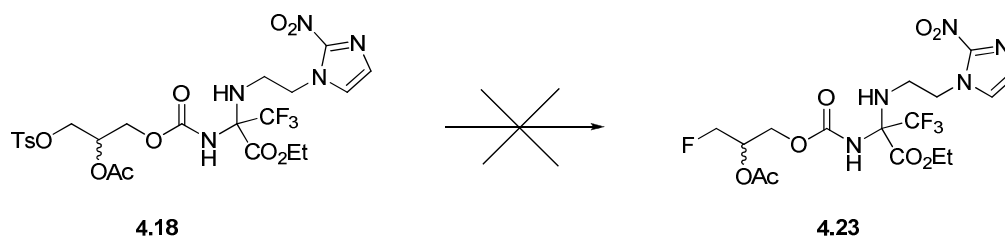
Scheme VI. Synthesis of coupled product **4.13**.

Oxidation of **4.13** with OsO_4 (catalytic amounts) and NMO afforded the corresponding *syn*-diol **4.19** with very good yield (92 %) and high diastereoselectivity ($de > 98$ %). The following protection of the primary alcohol of **4.19** with tosyl chloride and acetylation of the secondary hydroxyl group of **4.20** with acetic anhydride gave the precursor **4.18** with satisfactory yield (90%) [Scheme VII].



Scheme VII. Synthesis of the precursor **4.18** for ^{18}F -radiolabeling

The most challenging problem was the investigation of the optimal conditions for introducing the fluorine atom into the precursor molecule **4.18**, by using standard nucleophilic substitution conditions (a fluoride source and a polar aprotic solvent), before attempting the ^{18}F -radiolabelling procedure. Although we could easily achieve reasonable yields of the precursor compound **4.18**, the corresponding labelled molecule (**4.23**) could not be synthesised, as none of the “cold fluorination” conditions that were explored afforded the desired fluorinated derivative **4.23** [Scheme VIII, Table I]. Therefore, alternative conditions are currently under investigation.



Scheme VIII. The desired fluorinated product **4.23** could not be synthesised.

Table I. “Cold fluorination” conditions attempted.

MF	Solvent	Reaction temp (°C)	Yield (%)
KF/K 2.2.2.	dry MeCN	100	n.r. ^a
CsF	<i>t</i> -BuOH	80	n.r. ^a
CsF	<i>t</i> -amyl alcohol	80	n.r. ^a
CsF	<i>t</i> -amyl alcohol	rt	n.r. ^a
TBAF	dry THF	rt	n.r. ^a

^aNo reaction occurred: the starting material was consumed (TLC monitoring) and the non-tosylated product was formed (as evidenced by MS).

Alkylated sulfoxides as carbanion equivalents

Sulfoxides are an important class of organic compounds, which have been extensively used as chiral auxiliaries for the stereoselective synthesis of different compounds of biological interest, such as β -amino-alcohols, β -chloro-amines and aziridines^{X,XI}.

N-methyl *ortho*-carbamoylaryl benzyl sulfoxides (**5.1**) can be used as synthetic equivalents of α -hydroxy, α -chloro and α -acetamido benzyl carbanions [Figure IV] by means of a two-step sequence involving 1) highly diastereoselective α -C-alkylation with alkyl halides followed by 2) displacement of the sulfinyl residue by a hydroxyl, a chlorine or an acetamido group, respectively.

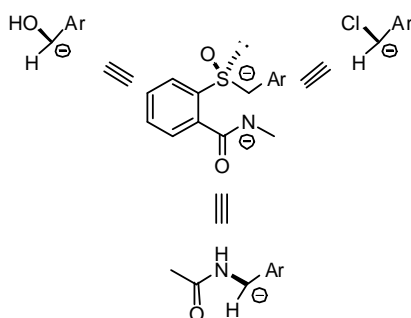
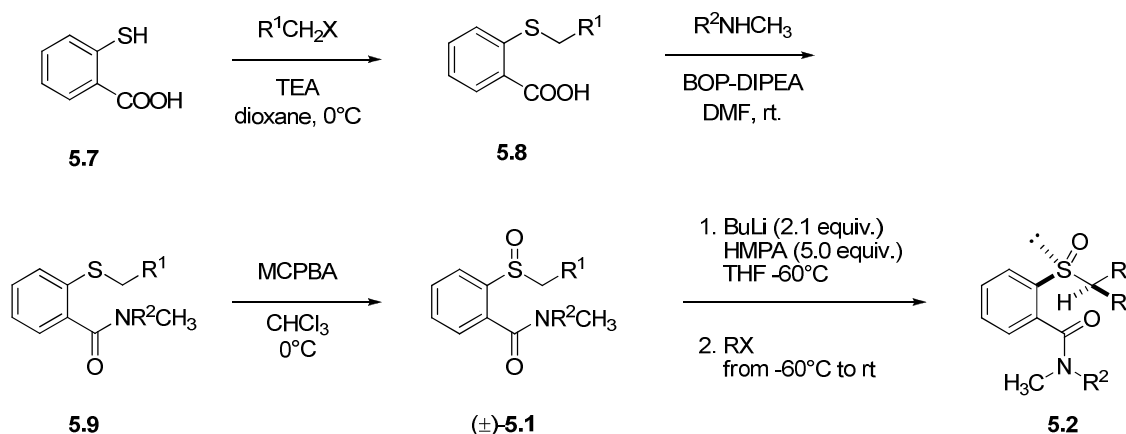


Figure IV. The new chiral umpolung synthon.

The starting sulfoxides (\pm)-**5.2** were prepared by *S*-alkylation of thiosalicylic acid (**5.7**) with alkyl halides, followed by conversion of **5.8** into amide with CH_3NH_2 and $(\text{CH}_3)_2\text{NH}$ and oxidation of sulfide **5.9** to (\pm)-**5.1** with MCPBA [Scheme IX]. The sulfoxides (\pm)-**5.1** were finally alkylated with different alkyl halides, after treatment with BuLi as deprotonating agent and HMPA as co-solvent.

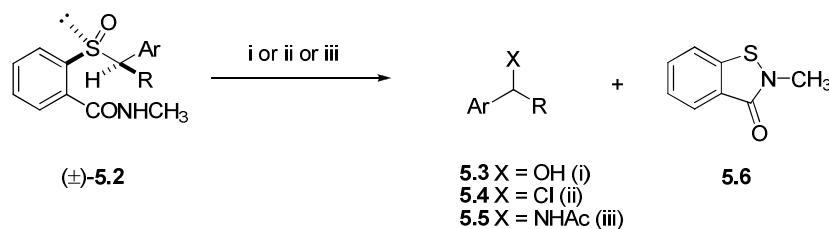


Scheme IX. Synthesis of sulfoxides **5.2**.

^X Volonterio, A., Bravo, P., Pesenti, C., Zanda, M. *Tetrahedron Lett.* **2001**, 42, 3985-3988.

^{XI} Volonterio, A., Bravo, P., Panzeri, W., Pesenti, C., Zanda, M. *Eur. J. Org. Chem.* **2002**, 3336-3340.

Alcohols **5.3**, chlorides **5.4** and acetamides **5.5** [Scheme X] were obtained, along with a co-product **5.6**, by submitting alkylated sulfoxides (\pm)-**5.2** to ‘non-oxidative Pummerer’ conditions [Scheme X, Table II].



i. TFAA, TMP, DCM, 0°C, then aq. NaHCO₃; ii. (COCl)₂, TMP, DCM, -50°C; iii. Tf₂O, TMP, CH₃CN, 0°C.

TFAA = Trifluoroacetic anhydride; TMP = 2,4,6-trimethyl pyridine; DCM = dichloromethane; Tf₂O = Trifluoromethanesulfonic anhydride.

Scheme X. Synthesis of alcohols **5.3**, chlorides **5.4** and acetamides **5.5**.

Table II. Synthesis of alcohols **5.3**, chlorides **5.4** and acetamides **5.5**.

Substrate	Ar	R	Product	X	Yield ^a (%)
(\pm)- 5.2e	Ph	Ph(CH ₂) ₃	(\pm)- 5.3e	OH	86
(\pm)- 5.2f	Ph	CH ₂ =CH(CH ₂) ₃	(\pm)- 5.3f	OH	72
(\pm)- 5.2i	4-MeO-Ph	Ph(CH ₂) ₃	(\pm)- 5.3i	OH	67
(\pm)- 5.2k	4-CF ₃ -Ph	Ph(CH ₂) ₃	(\pm)- 5.3k	OH	77
(\pm)- 5.2e	Ph	Ph(CH ₂) ₃	(\pm)- 5.4e	Cl	90
(\pm)- 5.2f	Ph	CH ₂ =CH(CH ₂) ₃	(\pm)- 5.4f	Cl	60
(\pm)- 5.2i	4-MeO-Ph	Ph(CH ₂) ₃	(\pm)- 5.4i	Cl	63
(\pm)- 5.2k	4-CF ₃ -Ph	Ph(CH ₂) ₃	(\pm)- 5.4k	Cl	78
(\pm)- 5.2g	Ph	CH ₃ (CH ₂) ₅	(\pm)- 5.5g	NHAc	62
(\pm)- 5.2h	Ph	CH ₃ (CH ₂) ₂	(\pm)- 5.5h	NHAc	67
(\pm)- 5.2j	4-MeO-Ph	3,4,5-TriMeO-Ph-(CH ₂) ₃	(\pm)- 5.5j	NHAc	48 ^b
(\pm)- 5.2k	4-CF ₃ -Ph	Ph(CH ₂) ₃	(\pm)- 5.5k	NHAc	57 ^b

^a Overall isolated yield.

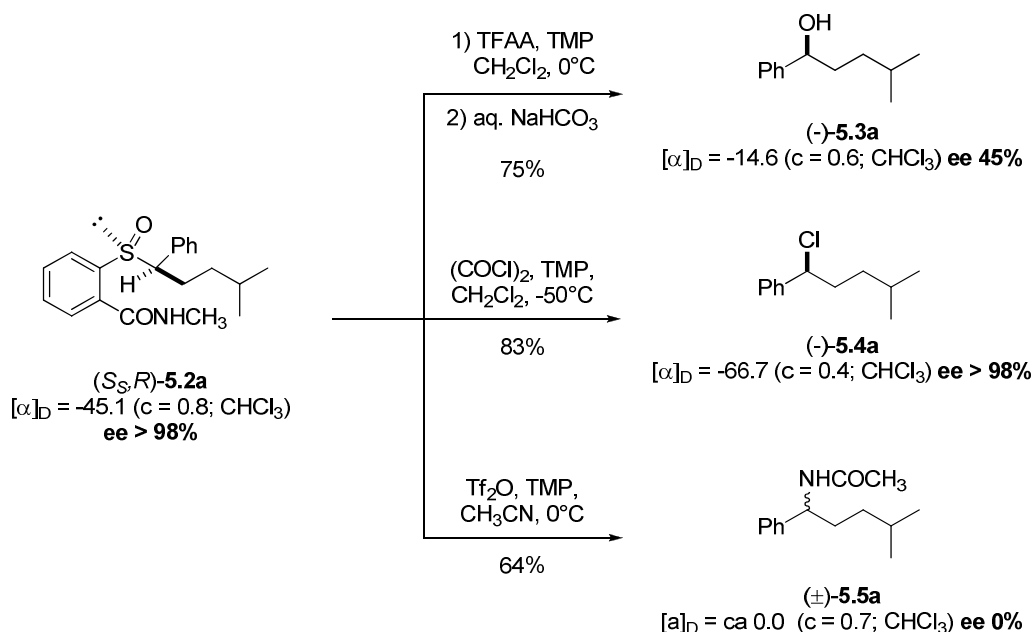
^b Formation of the corresponding tetralines as by-products was observed.

The reactions parameters for non-oxidative Pummerer reactions were investigated on an enantiomerically pure alkylated sulfoxide (*S*_S, *R*)-**5.2a**, in order to understand the mechanism by which the reaction took place, before extending the reactions to a wide library of alkylated sulfoxides (\pm)-**5.2**.

Although the NOPR (TFAA, TMP in DCM at 0°C, NaHCO₃) on enantiomerically pure (-)-**5.2a** [Scheme XI] afforded the alcohols (-)-**5.3a** with stereoinversion at benzylic carbon, a partial loss of enantiomeric purity was observed, thus suggesting that the reaction did not occur only through a S_N2 mechanism.

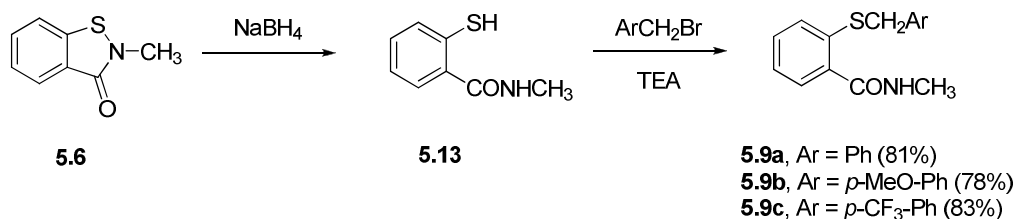
The NOCPR ((COCl)₂, TMP in DCM at -50°C) yielded the corresponding chlorides (-)-**5.4a** [Scheme XI] without loss of the starting enantiomeric excess (confirmed by chiral HPLC).

Surprisingly, when the sulfoxide (S_S , R)-**5.2a** was treated with Tf_2O , TMP in CH_3CN , the formation of racemic acetamides **5.5a** was observed [Scheme XI], thus confirming that the reaction proceeds through the formation of a carbocationic intermediate.



Scheme XI. Non-oxidative Pummerer reaction on sulfoxide (S_S , R)-**5.2a**

The benzothiazolone **5.6**, produced together with the NOPR-like outcomes, was converted to the sulfide **5.9** by regioselective reduction of N-S bond with NaBH_4 , followed by S-alkylation of **5.13** [Scheme XII].



Scheme XII. Regioselective reduction of N-S bond of **5.6**.

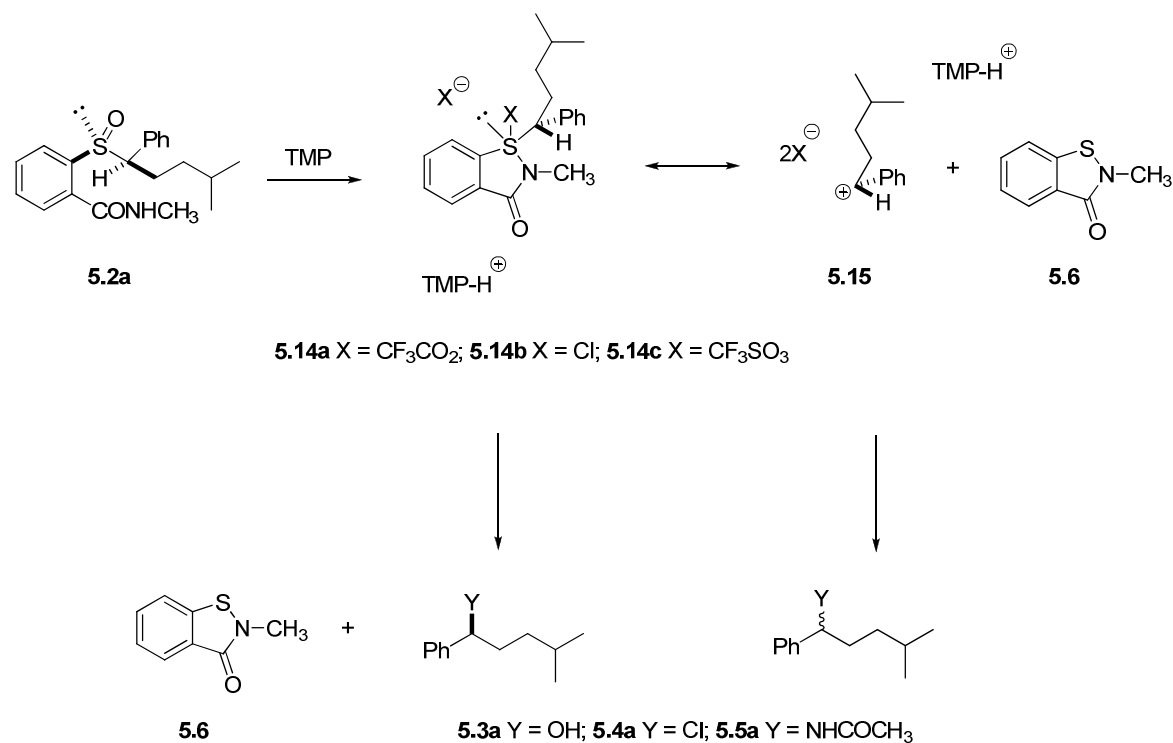
The mechanism of the reaction leading to the alcohols **5.3**, chlorides **5.4** and acetamides **5.5** is probably dependent on the nucleophilic species produced after acylation of sulfinyl moiety by different Pummerer reaction initiators, such as TFAA, $(\text{COCl})_2$, and Tf_2O .

The sulfoxide **5.2a** is activated by electrophilic addition to the Pummerer promoter and the following sulfur cation is attacked by the *ortho*-carbamoyl nitrogen, deprotonated by the TMP base, thus giving rise to the intermediate **5.14a-c** [Scheme XIII].

When the nucleophile X^- is sufficiently strong, such as Cl^- anion, the intermediate **5.14a-c** is supposed to undergo an internal rearrangement, involving a fragmentation of S-X and S-C bonds followed by formation of a new C-Cl bond *via* a $\text{S}_{\text{N}}2$ pathway.

On the other hand, when X^- is a poor nucleophile, such as TfO^- , this internal rearrangement cannot occur and the carbocationic species **5.15** is produced.

The latter can be attacked by the more nucleophilic solvent CH_3CN and give the corresponding acetamides **5.5a**, after hydrolysis [Scheme XIII]^{XII}.



Scheme XIII. Proposed mechanism for the Pummerer reactions.

Conclusions

In conclusion, we have:

1. Achieved an efficient and reproducible synthesis of the [^{18}F]FAZA precursor;
2. Performed the radiosynthesis of [^{18}F]FAZA and successfully accomplished a PET-hypoxia imaging experiment on hypoxic animal models;
3. Synthesised in good overall yields the precursor of a new potential hypoxia-PET radiotracer and tried different “cold fluorination” conditions, which have to be optimized.
4. Developed the synthesis of α -benzyl alcohols, chlorides and acetamides, by exploiting *N*-methyl *ortho*-carbamoylaryl benzyl sulfoxides as synthetic equivalents for α -hydroxyl, α -chloro and α -acetamido benzyl carbanions.

^{XII} Pinna, G., Bellucci, M. C., Malpezzi, L., Pisani, L., Superchi, S., Volonterio, A., Zanda, M. *Tetrahedron* **2011**, *67*, 5268-5281.

Chapter 1. Positron Emission Tomography

1.1 Introduction

Positron Emission Tomography (PET) is a molecular imaging technique which allows to visualize the human physiology by the detection of positron emitting radiopharmaceuticals¹. In the last decades, it has emerged as a powerful clinical diagnostic method for *in vivo* mapping of pathological processes occurring within the human body, thus allowing the real-time investigation of a disease and hence the study of a therapy, before that anatomical changes are visible.

Currently, a PET experiment can be applied for the following purposes:

- ✓ identification of a malignancy;
- ✓ measurement of tumour response to chemotherapy and radiotherapy;
- ✓ early detection of a pathology;
- ✓ assessment of molecular pathways such as metabolic activity, oxygen delivery, protein and DNA synthesis, cell proliferation, receptor binding and gene expression;
- ✓ design of new drugs, and study of their pharmacodynamics and pharmacokinetics;
- ✓ screening of tissues functionality and structural abnormalities.

The pharmaceuticals used for PET-imaging are labelled with radionuclides, which reach a stable lower energy state by emission of radiation (radioactive decay).

PET employs neutron deficient radionuclides, which decay *via* positron (β^+) emission, however a neutron deficient radionuclide can also decay *via* electron capture (EC):



The radioactive nuclides for the synthesis of the PET-tracers are produced with a particle accelerator (cyclotron) [Figure 1.1]. The cyclotron can generate beams of accelerated neutrons or charged particles, used for the irradiation of target materials (e.g. N₂, Ne, H₂¹⁸O, etc).

Irradiation by neutrons leads to neutron rich nuclides, whereas irradiation by charged particles like protons or deuterons leads to nuclear reactions giving rise to neutron deficient nuclides.

PET radionuclides have different physicochemical properties such as half-life ($t_{1/2}$), positron energy² and specific activity (SA), which have to be taken into account during the design and development of the radiopharmaceutical.

Half-life ($t_{1/2}$)

Half-life allows to measure the decay of a radioactive material.

It is the time taken for half of the radioactive sample to decay. It is measured in minutes (min).

A long half-life allows multiple step syntheses, the transport of radiotracer from radiochemistry laboratory to PET facilities and long *in vivo* investigations.

Positron (β^+) energy

Beta particles (β), as gamma (γ) and alpha (α), have an energy, which is measured in electron volts (eV).

The higher the particle energy, the more penetrating the particle.

Gamma particles are the more penetrating whereas beta particles have the least energy.

The positron energy is an important parameter that affects the spatial resolution during PET imaging. A low positron energy provides a high spatial resolution, hence a better quality of PET image.

Specific activity (SA)

The specific activity is a measure of the radioactivity per unit mass of the radiolabelled compound.

It is expressed in giga Becquerel per micromol (GBq μmol^{-1}) or Curies per micromol (Ci μmol^{-1}).

The radioactivity is the amount of radiation emitted by a sample or the number of atoms decaying per second. It is measured in Becquerel (1 Bq = 1 decay sec^{-1}).



Figure 1.1. Image of a commercial cyclotron.

PET mainly relies on the use of positron emitting radionuclides such as ^{11}C ($t_{1/2} = 20$ min), ^{13}N ($t_{1/2} = 10$ min), ^{15}O ($t_{1/2} = 2$ min) and ^{18}F , ($t_{1/2} = 110$ min).

However, other radionuclides are available for the production of labelled pharmaceuticals, namely ^{68}Ga ($t_{1/2} = 68.1$ min), ^{124}I ($t_{1/2} = 60$ 192 min), ^{64}Cu ($t_{1/2} = 762$ min), etc.

Amongst the radionuclides available for labelling procedures, fluorine-18 is the most widely used, because of its better physicochemical properties.

Given the surprising growth of PET as a diagnostic technique, the development of new PET tracers has been tremendously increased, leading to the necessity of automated systems that provide high amount of PET-probes and avoid an over exposure of operator to radiations.

The radiolabelling procedures are carried out inside “hot cells”, [Figure 1.2] which can be defined as lead-shielded automated fumehoods with lead glass windows many inches thick.

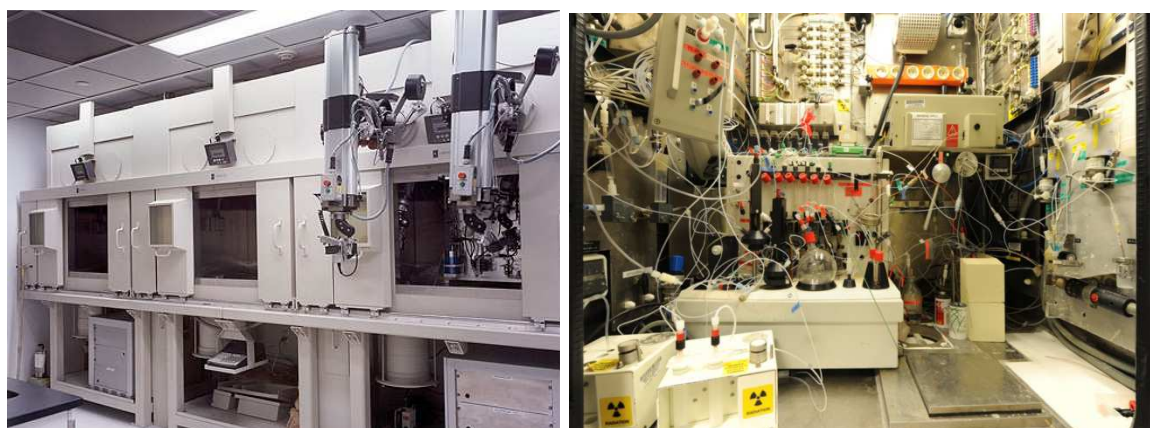


Figure 1.2. From left: hot cells for the production of radiopharmaceuticals and automated synthesizer.

After the radiosynthesis, the labelled compound has to be sequentially, purified, analyzed (commonly by HPLC) and then formulated to be administered (typically as a saline solution).

The PET probe is administered either *via* intravenous injection or inhalation by using a very small amount of radiopharmaceutical (typical range of $10^{-6} - 10^{-9}$ grams).

This implies that the behaviour of labelled compound can be studied *in vivo* without affecting the biological system being studied and, moreover demonstrates PET to be a very sensitive technique. However, the radiolabelled probe has to be synthesised, purified, analyzed and formulated within minutes, according to the half-life of the radionuclide used.

As a general rule of thumb, all the procedure must be completed within three half-lives of the radionuclide to ensure there is enough radioactivity to administer to the patient.

When finally a PET-imaging experiment is performed, 2D or 3D images of the area of the body where the radiotracer is localized are provided, thus allowing the assessment of biological mechanism occurring in the body [Figure 1.3].

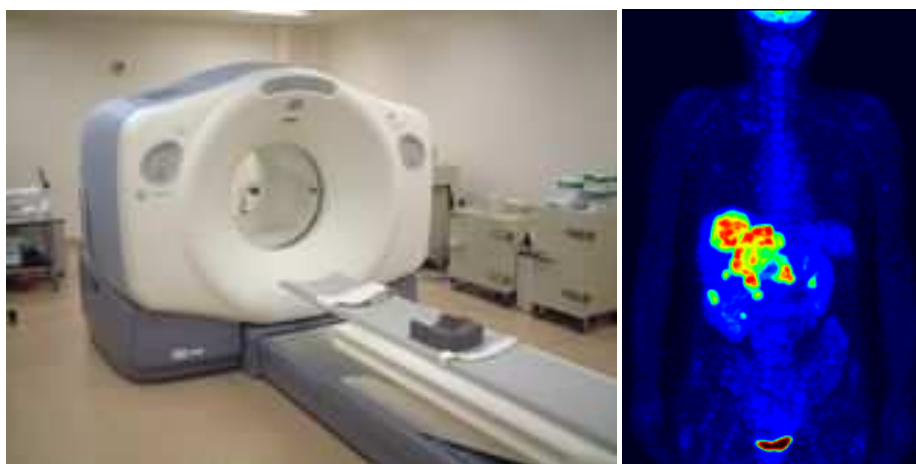


Figure 1.3 From left: a combined PET/CT scanner and a processed PET image of whole body.

1.2 Positron Emission Tomography principles

Positron Emission Tomography (PET) is a non-invasive and quantitative imaging method which allows for the *in vivo* measurement of biochemical processes by the detection of radiolabelled pharmaceuticals (picomolar concentrations of PET tracer can be detected).

PET employs mainly radiopharmaceuticals labelled with short-lived positron emitting radioisotopes such as ^{11}C ($t_{1/2} = 20$ min), ^{13}N ($t_{1/2} = 10$ min), ^{15}O ($t_{1/2} = 2$ min) and ^{18}F , ($t_{1/2} = 109.8$ min) [Table 1.1].

However a number of long-lived radionuclides such as ^{52}Fe , ^{55}Co , ^{75}Br , ^{124}I , ^{60}Cu are also used for the production of PET radiotracers (e.g. ^{60}Cu -ATSM, ^{124}I AZA).

The short-lived positron emitters ^{11}C , ^{13}N , ^{15}O are preferred to the long lived since C, N and O are normal constituents of biomolecules and their incorporation into a pharmaceutical molecule would allow to retain the same physicochemical and biochemical properties of the non-radiolabelled compound, thus avoiding undesired modifications of the drug behaviour.

Table 1.1. The most commonly used positron emitting radionuclides in PET.

Radionuclide	Half-life, $t_{1/2}$ (min)	Max. β^+ energy (MeV)	Nuclear reaction	Target	Product	Decay product
^{11}C	20.4	0.96	$^{14}\text{N}(\text{p}, \alpha)^{11}\text{C}$	$\text{N}_2 (+ \text{O}_2)$	$[^{11}\text{C}]\text{CO}_2$	^{11}B
				$\text{N}_2 (+ \text{H}_2)$	$[^{11}\text{C}]\text{CH}_4$	
^{13}N	9.97	1.19	$^{16}\text{O}(\text{p}, \alpha)^{13}\text{N}$	H_2O	$[^{13}\text{N}]\text{NO}_x$	^{13}C
				$\text{H}_2\text{O} + \text{EtOH}$	$[^{13}\text{N}]\text{NH}_3$	

^{15}O	2.04	1.72	$^{15}\text{N}(\text{d}, \text{n})^{15}\text{O}$	$\text{N}_2 (+ \text{O}_2)$	$[^{15}\text{O}]\text{O}_2$	^{15}N
^{18}F	109.8	0.64	$^{20}\text{Ne}(\text{d}, \alpha)^{18}\text{F}$	$\text{Ne} (+ \text{F}_2)$	$[^{18}\text{F}]\text{F}_2$	^{18}O
			$^{18}\text{O}(\text{p}, \text{n})^{18}\text{F}$	$[^{18}\text{O}]\text{H}_2\text{O}$	$^{18}\text{F}^-$	

The PET radionuclides decay in the body by emission of a positively charged particle, the positron (β^+) which, after travelling a short distance in the surrounding tissue, encounters an electron, giving rise to an annihilation event.

The annihilation results in the production of two gamma (γ) ray photons of 511 KeV of energy that travel at 180° each other [Figure 1.4].

The distance travelled by the positron in the matter (the positron range) before annihilation is different for each positron-emitting radionuclide and is dependent on the positron energy.

The positron energy affects the image quality, indeed the higher the positron energy, the larger the path travelled by positron, the greater the loss of spatial resolution.

The detection of a large number of annihilation events by an array of specific detectors allows to know the spatial distribution and location of a PET tracer in the body.

Finally, a two-dimensional or three-dimensional image is provided by using hardware and software for data acquisition, image reconstruction and manipulation.

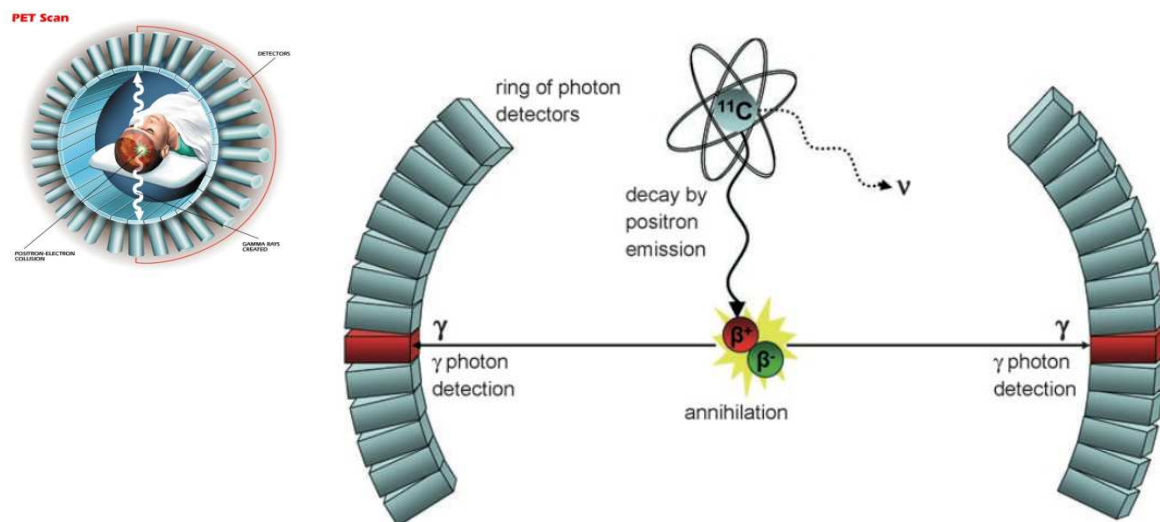


Figure 1.4. Schematic representation of annihilation event. The radioisotope emits a positron which after travelling a short distance within the body collides with a surrounding electron. This collision results in an annihilation, leading to two gamma (γ) ray photons detected by a PET scanner

1.3 PET radionuclide production

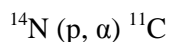
The radioactive isotopes for PET-imaging are produced in a particle accelerator, namely a cyclotron, where an appropriate target material is irradiated with either a beam of accelerated protons or deuterons, leading to a nuclear reaction [Table 1.1] which results in the production of a neutron deficient nuclide (from picomolar to nanomolar scale).

Nuclear Reaction: $^{18}\text{O} (p, n) ^{18}\text{F}$

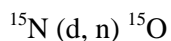
A nuclear reaction occurs when a target nucleus (^{18}O) is irradiated with an incident particle (a proton p), giving rise to another particle (a neutron n) emitted during the reaction, and the desired radionuclide (^{18}F).

The example reported above refers to the production of [^{18}F]fluoride, where ^{18}O -enriched water (H_2^{18}O) is irradiated with a beam of incident protons.

Other examples of nuclear reactions are the following:



this nuclear reaction allows either to produce [^{11}C]CO₂ by using nitrogen-14 mixed with a little (2%) oxygen as target material or [^{11}C]CH₄ by using nitrogen-14 mixed with hydrogen as target material;



$^{15}\text{O}_2$ is produced by irradiation of nitrogen-15 mixed with O₂.

1.3.1 Fluorine-18 radionuclide

At present, ^{18}F is by far the most used radionuclide for the synthesis of PET-pharmaceuticals.

Despite the other short-lived radioisotopes, fluorine-18 shows more favourable physicochemical properties.

Fluorine-18 has a relatively long half-life ($t_{1/2} = 109.8$ min) which allows for multistep labelling procedures, longer *in-vivo* investigation and distribution of the radiopharmaceutical to other clinical PET centres that lack of a radiochemistry laboratory

^{18}F PET-imaging provides good quality PET images, reflecting the low energy of positron emitted by fluorine-18 (0.64 MeV).

Furthermore, a number of ^{18}F labelling procedures are available, thus allowing easy and efficient production of a radiotracer.

Although fluorine atom is generally not a constituent of biomolecules, the substitution of a hydrogen atom or hydroxyl group by a fluorine atom is commonly applied, as the steric parameters for fluorine and hydrogen are similar (Van der Waals radii of fluorine and hydrogen are 1.35 Å and 1.20 Å respectively) and the replacement of hydrogen by fluorine does not imply significant steric perturbations³.

However, the strong electron-withdrawing character of fluorine may be responsible for altered electronic properties, leading to changes of lipophilicity and biological characteristics of the pharmaceuticals (e.g. distribution, metabolism, protein binding).

A fluorine substitution on an aryl ring generally increases the lipophilicity, while the replacement of a hydrogen atom by a fluorine atom in an alkyl chain decreases the lipophilicity⁴.

Although the carbon-fluorine bond is very strong, aliphatic bond is very often prone to enzymatic cleavage, whereas the aryl carbon-fluorine bond is more stable *in vivo*.

Thus the position to be labelled in the precursor molecule becomes crucial, also because it determines the metabolic fate of the radiotracer.

If the PET probe is highly metabolized in the body, undesired metabolites are produced and can accumulate or interact with other biomolecules, interfering with the detection of radiation emitted in the target tissue.

1.4 PET radiopharmaceuticals

An ideal radiopharmaceutical for PET-experiments should fulfil the following important requirements^{5,6}:

- 1) It should have high affinity for its biological target, thus preventing its nonspecific accumulation in other tissues and hence allowing to obtain high contrast PET images. A further interaction of the tracer with other types of molecules would interfere with the detection of the radioactivity of the tissue under investigation;
- 2) It should undergo a rapid metabolism. However metabolism may result in the production of metabolites which can take part in unknown biochemical processes and

accumulate. Therefore it is preferable that the radiolabelling of the selected molecule takes place in that part of the molecule which is easily cleared from the tissues;

- 3) It should be rapidly cleared from blood to reduce the time of exposure to radioactivity and hence provide a clear image of the tissue where it is localized;
- 4) It should be lipophilic to homogeneously distribute in all tissues but, at the same time, hydrophilic allowing a faster elimination *via* the renal pathway;

The lipophilicity determines the ability of the radiopharmaceutical to cross cell membranes and barriers like blood-brain-barrier (BBB). It is expressed as the logarithm of the *n*-octanol/water partition coefficient (logP). When the logP of a tracer is in the range 1.5-2, it can enter the lipid layers.

A large number of radiopharmaceuticals are available for PET-imaging experiments.

Although most of them are labelled with ^{18}F or ^{11}C nuclides, other several tracers labelled with radioisotopes such as ^{124}I , ^{60}Cu , ^{62}Cu or ^{68}Ga are used for detection of biochemical processes *via* PET.

It is fundamental that the half-life of the radioisotope used for labelling is commensurate with the timescale of the biological process to be studied.

The short half-lives of positron emitting nuclides such as ^{13}N ($t_{1/2} = 10$ min), ^{15}O ($t_{1/2} = 2$ min) avoid their use in PET imaging of biological processes occurring within a long time.

Thus, the PET-probes labelled with ^{13}N and ^{15}O have to be produced near the PET facilities.

Radiotracers as $^{13}\text{NH}_3$ and H_2^{15}O are commonly used to study blood flow, according to the short half-life of their radionuclides.

On the other hand, PET chemicals labelled with ^{11}C ($t_{1/2} = 20$ min) or ^{18}F ($t_{1/2} = 110$ min) (e.g. [^{18}F]FDG, [^{18}F]FLT, [^{11}C]Choline, [^{11}C]methionine) can be used to image long-time processes such as protein synthesis, DNA production, amino acids utilization.

The radiochemical yield (RCY) of the radiosynthesis and the specific activity of the radiolabelled compound (SA) are two other important characteristics associated to a PET pharmaceutical.

The RCY is related to both chemical yield and half-life of the isotope. It is expressed as a fraction of radioactivity originally present in the sample after a radiochemical separation. The RCY should be preferably high, thus allowing to measure the efficiency of radiolabeling procedure.

The specific activity (SA) indicates the activity per amount of the radiolabelled compound and it is commonly measured in giga Becquerel per micromol ($\text{GBq } \mu\text{mol}^{-1}$) or Curies per micromol ($\text{Ci } \mu\text{mol}^{-1}$).

However, the theoretical values of specific activity calculated for a radiolabelled compound are never reached because of the natural presence of the stable isotope of radionuclide during the labelling procedure, which results in an isotopic dilution. This dilution is more obvious when the stable isotope (called carrier) of the nuclide is added by the operator during the production of the radioisotope (e.g. addition of the stable isotope of fluorine during the production of [^{18}F]F $_2$).

When the cold material (i.e. the non radioactive material) of the same chemical identity is not added on purpose by the investigator during the preparation of the radiopharmaceutical, the production of the radiopharmaceutical is called *non-carrier added* (NCA).

PET radiotracers can be classified by radionuclide, uptake mechanism (receptor binding, metabolic trapping, etc.) or fields of applications (cardiology, oncology, neurology).

Presently, cardiology, oncology⁷ and neurology are the three major areas of PET application.

Radiopharmaceuticals such as [^{13}N]ammonia or [^{15}O]water are used for the assessment of myocardial blood flow in cardiology.

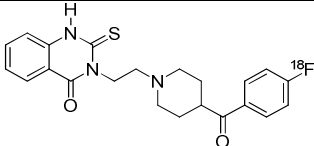
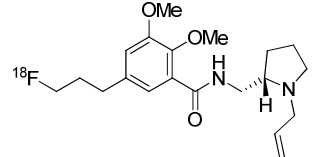
PET is furthermore applied for detecting hypoxia (an imbalance between oxygen consumption and oxygen supply) associated to heart diseases or malignancies by using radiotracers as [^{18}F]FMISO, [^{18}F]FAZA, both nitroimidazole compounds.

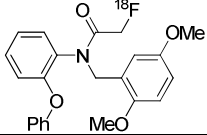
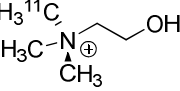
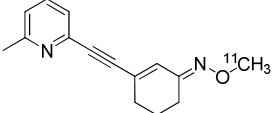
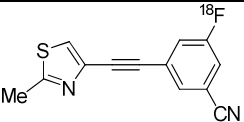
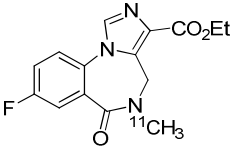
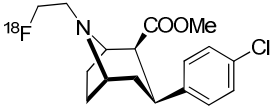
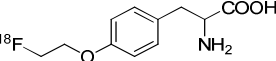
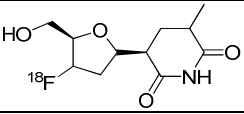
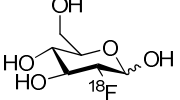
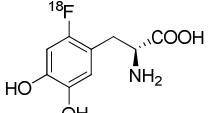
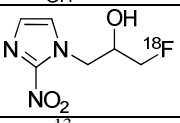
[^{18}F]Fluorodeoxyglucose ([^{18}F]FDG), a sugar derivative, is used for PET imaging of glucose metabolism in tumors and metabolic disfunctions.

PET radiopharmaceuticals are widely used in neurology⁸ for imaging the central nervous system (CNS) function, namely the neurotransmission regulated by dopamine, acetylcholine, serotonin or glutamate, thus allowing the detection and investigation of neurological disorders associated to altered concentration of these neurotransmitters, such as Parkinson's (L-DOPA) and Alzheimer's (acetylcholine) diseases.

To date, most of the PET radiotracers are labelled with fluorine-18 radioisotope, according with its better properties, as aforesaid⁹.

Table 1.2. Some PET-radiopharmaceuticals and their application.

Radiotracer	Chemical structure	Target
[^{18}F]Altanserin		Brain 5-HT ₂ Receptors
[^{18}F]Fallypride		Brain D ₂ receptors

[¹⁸ F]FBR		Brain benzodiazepine receptors
[¹³ C]Choline		Cell membranes
[¹³ C]ABP688		Brain mGlu5 receptors
[¹⁸ F]FMTEB		Brain mGlu5 receptors
[¹³ C]Flumazenil		Brain benzodiazepine receptors
[¹⁸ F]FECNT		Brain dopamine transporters
[¹⁸ F]FET		Tumor location
[¹⁸ F]FLT		Cellular proliferation
[¹⁸ F]FDG		Glucose metabolism
[¹⁸ F]FDOPA		Brain dopamine metabolism
[¹⁸ F]FMISO		Hypoxic cells
[¹³ N]Ammonia	¹³ NH ₃	Blood
[¹⁵ O]Water	H ₂ ¹⁵ O	Blood

1.4.1 2[¹⁸F]fluoro-2-D-deoxyglucose ([¹⁸F]FDG)

[¹⁸F]FDG (**1.3**) is currently the most widely used PET radiotracer, which allows for the assessment of several pathological conditions, but it is mainly used in oncology for the evaluation of chemo- and radio-therapy.

It represents the fluorinated-derivative of 2-deoxy-D-glucose (DG) (**1.1**), a chemotherapeutic agent used to study the glycolytic rate in malignancies^{10,11} [Figure 1.5].

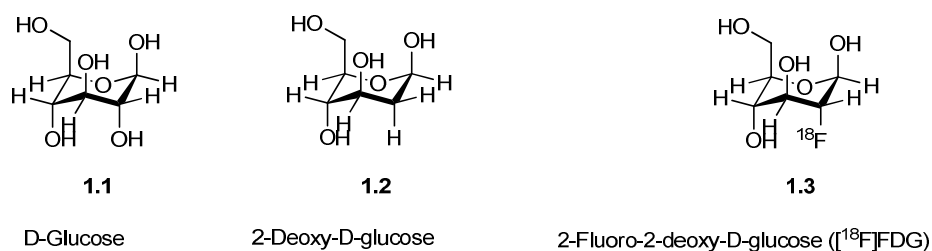


Figure 1.5 Glucose and its analogs: 2-deoxyglucose (DG) and fluorodeoxyglucose (FDG).

It is well known that a tumor tissue consists of rapidly growing cells, where the glucose metabolism is enhanced. Indeed, an over expression of enzymes, (e.g. Hexokinases, HKs), and transmembrane transporters (e.g. Glucose transmembrane transporters, GLUT-1 and GLUT-3), involved in glycolysis, is observed.

2-Deoxy-D-glucose is transported into the cancer cell by the glucose transporter (GLUT) and is phosphorylated by the enzyme Hexokinase, which converts DG to 2-deoxy-glucose-6-phosphate. The subsequent isomerisation of the gluco-pyranose to fructo-furanose by Glucose-phosphate isomerase can not take place as it needs the presence of the hydroxylic function in position 2, which is missing in 2-deoxy-D-glucose. Therefore, 2-deoxy-glucose-6-phosphate is not further metabolised and, because of the negative charge of phosphate group, it can not penetrate the cell membrane, thus accumulating within the tumor cell.

The ^{18}F labelled 2-deoxy-D-glucose (FDG) behaves the same manner as DG when it enters the cancer cells via the glucose transporter (GLUT) [Figure 1.6]. Therefore, the glycolytic pathway of the cancer cells can be monitored by detection of the ^{18}F nuclide radiation through PET-imaging methods.

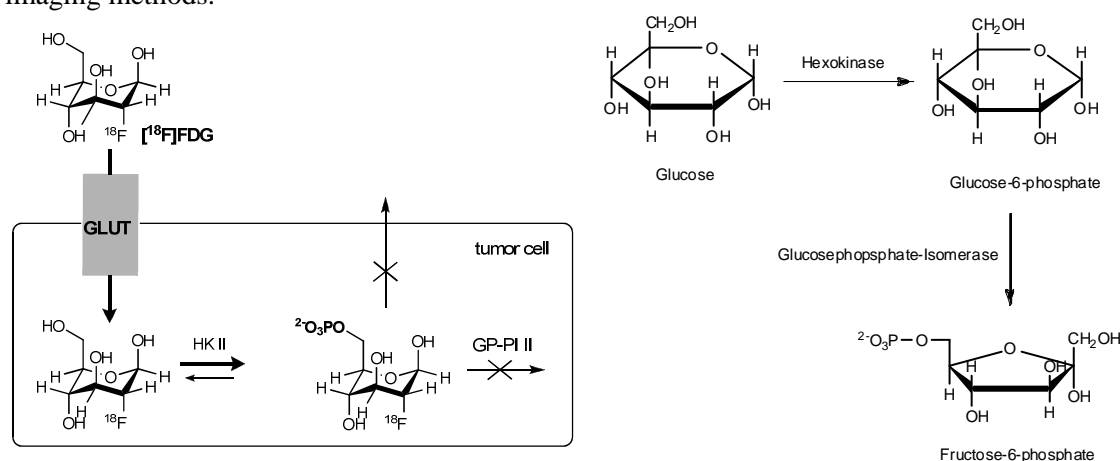


Figure 1.6. Metabolic trapping of ^{18}F -fluorodeoxyglucose and catabolic path of glucose metabolism.

1.4.2 6- ^{18}F fluoro-L-dihydroxyphenyl alanine (^{18}F L-DOPA)

^{18}F 6-Fluoro-L-DOPA (**1.7**) has been extensively used as a PET-tracer to visualize the functionality of dopaminergic neurons, specifically their capacity to synthesise dopamine (DA) during neurological disorders as Parkinson's disease, associated with a degeneration of dopaminergic neurotransmission.

Moreover ^{18}F 6-fluoro-L-DOPA-PET-imaging can be used to investigate the status of tumor growth by measuring the increasing availability of this amino-acid inside the tumor cells.

Indeed, the tumor cells show a high metabolic activity, leading also to an increasing demand of amino-acids.

Therefore an high rate of protein synthesis and an over-expression of amino-acid transporters are observed in the tumor cells.

Dopamine, a neurotransmitter involved in several cerebral mechanisms, is synthesised from the amino acid L-tyrosine, which is first hydroxylated and then decarboxylated before giving rise to the amino acid [**Figure 1.7**].

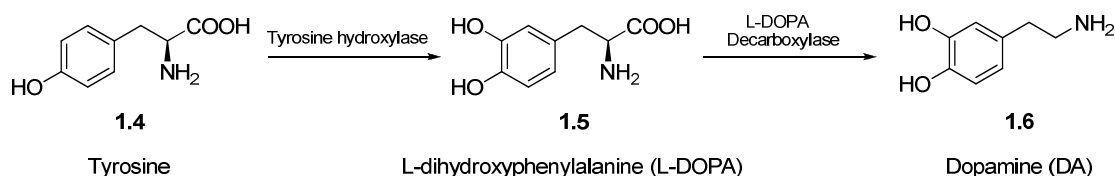


Figure 1.7. Intracellular synthesis of dopamine from L-tyrosine.

If dopamine is labelled with the ^{18}F -radionuclide, it can be detected by means of PET, thus allowing the measurement of dopamine use by the neuronal cells.

Since dopamine is not able to cross the blood-brain-barrier (BBB), its ^{18}F -labelled derivative can not be directly used for PET-imaging, thereby it has to be produced *in situ*, starting from a precursor.

The synthetic precursor of ^{18}F 6-fluorodopamine, namely ^{18}F 6-fluoro-L-DOPA (**1.7**), is able to cross the blood-brain-barrier (BBB) *via* an active transport system and is then transformed by a decarboxylase enzyme into ^{18}F 6-fluoro-dopamine (**1.8**), which can be visualized by PET [**Figure 1.8**].

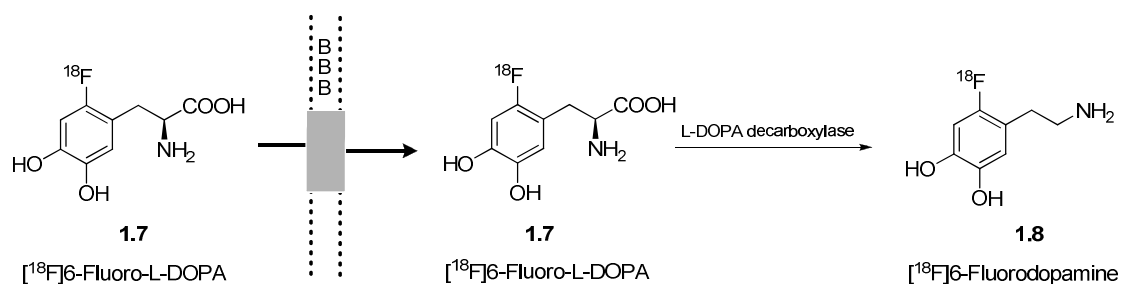


Figure 1.8. Transport and decarboxylation of $[^{18}\text{F}]6\text{-Fluoro-L-DOPA}$ to $[^{18}\text{F}]6\text{-Fluorodopamine}$ in the CNS.

1.4.3 3'-Deoxy-3'- $[^{18}\text{F}]$ fluorothymidine ($[^{18}\text{F}]$ FLT)

Amongst the biochemical changes occurring in cancer cells, the increased DNA synthesis is the essential hallmark that reflects the proliferation rate of malignancy.

Consequently a great availability of nucleosides is dictated and satisfied by an increased uptake of cytosine, guanine, adenine and thymidine.

Unlike the other nucleosides, thymidine is the only one exclusively incorporated into DNA and not RNA, therefore the radiolabelled derivative of thymidine has been evaluated as a potential PET-tracer for tumor detection and for early assessment of tumor response to chemo- and radiotherapy.

First attempts to image the cell proliferation via radiolabelled thymidine used the ^{11}C -labelled compound, which resulted not particularly suitable for PET-imaging of DNA synthesis because of its rapid *in vivo* metabolism and the short half-life of carbon-11 nuclide, thereby ^{11}C -thymidine (**1.10**) was replaced by the ^{18}F -labeled derivative.

3'-Deoxy-3'- $[^{18}\text{F}]$ fluorothymidine (**1.9**) is a nucleoside labelled at the 3' position of the sugar ring with ^{18}F and was demonstrated to be a valuable PET tracer since it exhibited a higher resistance to metabolic breakdown than ^{11}C -thymidine [**Figure 1.9**].

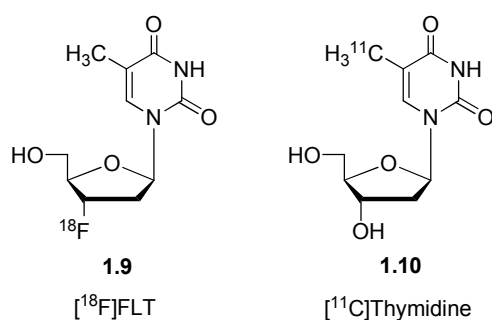


Figure 1.9. Chemical structures of thymidine radiolabeled with ^{18}F (1.9) and ^{11}C (1.10).

After entering the cell via nucleoside transporter, [^{18}F]fluorothymidine is converted by kinases to [^{18}F]fluorothymidine triphosphate (FLT-TP), which is not incorporated into DNA since the ^{18}F -atom at the 3' position of deoxyribose in place of the hydroxyl group prevents further metabolism. Nevertheless, due to the negative charge of the phosphate, [^{18}F]thymidine-triphosphate is not able to cross the cell membrane and thus becomes trapped intracellularly [Figure 1.10].

Hence, PET-detection of [^{18}F]thymidine-triphosphate allows the evaluation of the cell proliferation by measuring its increasing uptake in the cell.

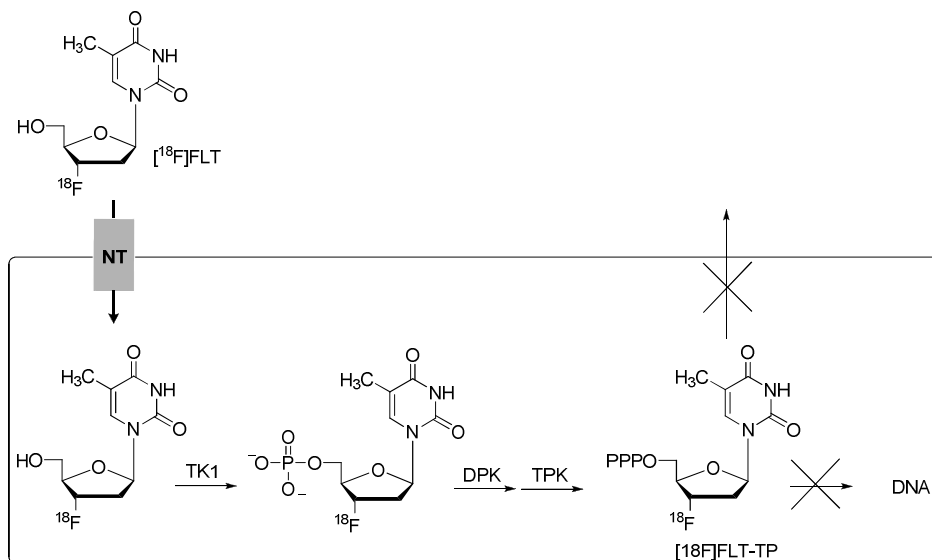


Figure 1.10. Metabolic trapping of [^{18}F]fluorothymidine.

[^{18}F]Fluorothymidine is transported into the cell by a nucleoside transporter (NT) and then phosphorylated by a thymidine kinase enzyme (TK) to [^{18}F]fluorothymidine monophosphate, subsequently converted to [^{18}F]fluorothymidine triphosphate, which is not incorporated into DNA and can not penetrate the cell membrane because of the negative charge of phosphate, thus it is trapped into the cell.

1.4.4 [^{18}F]Fluoromisonidazole ([^{18}F]FMISO)

[^{18}F]Fluoromisonidazole PET-imaging is used for quantitative assessment of hypoxia, defined as an imbalance between oxygen consumption and oxygen supply.

Hypoxia was found to be an important hallmark of several solid tumors, where the low oxygen partial pressure has been recognised to be responsible for tumor progression and resistance to both chemo- and radiotherapy.

Therefore the early detection of hypoxia would allow the real time monitoring and evaluation of tumor response to treatment.

PET hypoxia imaging with [^{18}F]FMISO (**1.11**) is the most widely used method for measurement of tumor oxygenation, however different hypoxia PET-tracers are available, such as [^{18}F]FAZA (**1.12**) and [^{64}Cu]ATSM (**1.13**) [Figure 1.11].

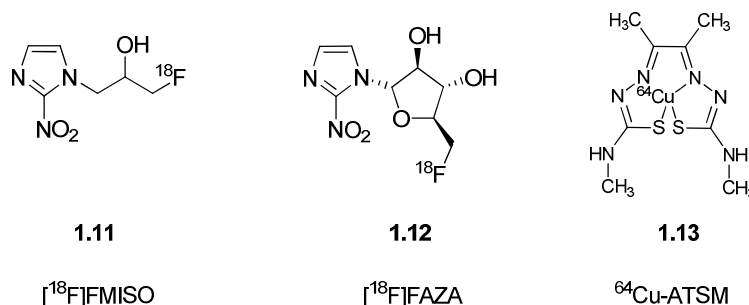


Figure 1.11. Chemical structures of [^{18}F]Fluoromisonidazole (1.11), [^{18}F]fluoroarabinofuranosylnitroimidazole (1.12) and [^{64}Cu]copper-diacetyl-bis-methylthiosemicarbazone (1.13).

[^{18}F]FMISO is a 18-fluorine labelled nitroimidazole which allows the detection of hypoxic tissues once it is trapped inside the tumor cells via a mechanism strictly correlated to the oxygen level of cancer cells

The nitroimidazole function plays a key role in the trapping mechanism of [^{18}F]FMISO.

Intracellularly, the nitro group (NO_2) undergoes a single electron reduction mediated by nitro reductase enzymes, giving an intermediate which, if oxygen is abundant, is reoxidized to the original state.

However, when oxygen is deficient a further reduction of the nitroimidazole occurs, thus forming a highly reactive species which covalently binds to intracellular biomolecules, thus accumulating within the cell [Figure 1.12].

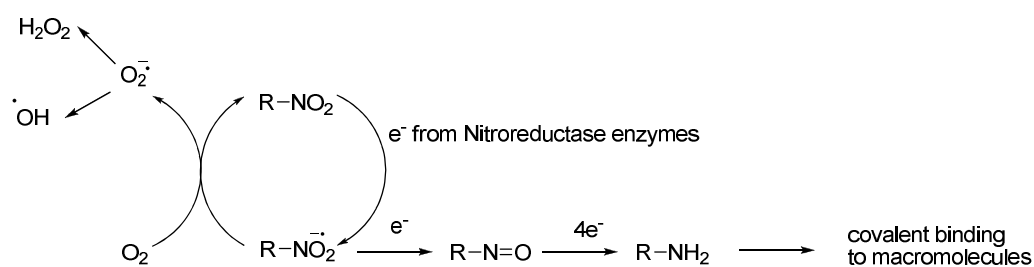


Figure 1.12. Intracellular mechanism of nitroimidazole compounds trapping.

1.4.5 [^{11}C]choline and [^{18}F]Fluorocholine ([^{18}F]FCH)

A number of biochemical changes are associated with cancers, such as increased DNA and protein synthesis, increased metabolic activity, low oxygen levels, etc.

A high production of phospholipids is another hallmark of many cancers, reflecting the tumor growth rate.

Considerable amounts of the phospholipid phosphatidylcholine (lecithin) have been found in rapidly proliferating tumors¹².

Lecithin is produced intracellularly, starting from choline, a quaternary ammonium base, which is transported into the cell by a specific sodium-independent transporter. Choline is also the precursor for the synthesis of the neurotransmitter acetylcholine.

Inside the cell, choline is initially submitted to phosphorylation, catalyzed by the enzyme choline kinase¹³, leading to phosphorylcholine¹⁴, which is further transformed into phosphatidylcholine [Figure 1.13].

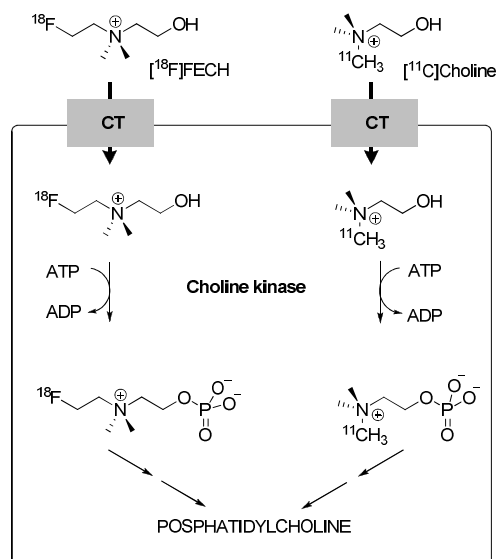


Figure 1.13. [^{18}F]FECH and [^{11}C]Choline uptake mechanism. Both tracers are transported into the cell via choline transporters (CT). In the cell, they undergo phosphorylation by the enzyme choline kinase and, after several biosynthetic processes, become integrated into phosphatidylcholine, hence into the cell membrane.

Hence, in tumor cells, high levels of lecithin are correlated with an increased enzymatic activity of choline kinase and an increased uptake of choline.

Thus, radiolabelled choline was predicted to be a potential PET-probe for imaging of phospholipids synthesis in cancer cells.

The first attempt to image the membrane lipid synthesis via PET was performed with ^{11}C -labelled choline (1.14) [Figure 1.14] in brain and prostate cancers¹⁵.

Because of the rapid *in vivo* metabolism, [^{11}C]choline was replaced with ^{18}F -labelled derivatives of choline, namely [^{18}F]fluorocholine ([^{18}F]FCH) (**1.15**) and [^{18}F]fluoroethylcholine ([^{18}F]FECH) (**1.16**) [Figure 1.14].

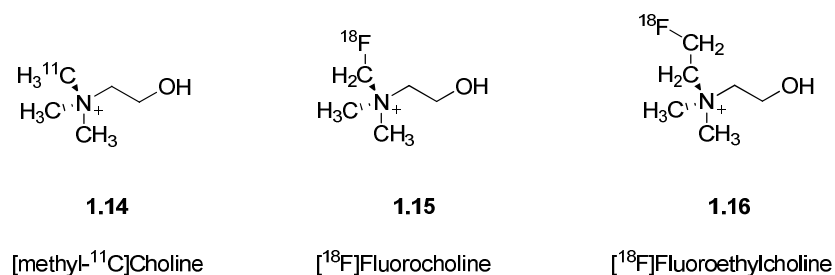


Figure 1.14. Radiolabelled choline derivatives.

1.5 Synthetic strategies for radiolabelling with fluorine-18

As stated above fluorine-18 is, along with carbon-11, the most used radioisotope for PET radiochemistry, given its suitable physicochemical properties, namely relatively long half-life and low positron energy.

To date several chemical methods may be applied to achieve reasonable radiochemical yields (RCYs) of ^{18}F -labelled pharmaceuticals with high specific activity (SA).

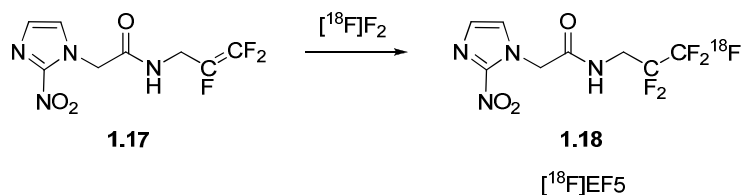
Although new ^{18}F -labelling strategies, such as enzyme-catalyzed [^{18}F]fluorination, microwave-enhanced reactions, polymer supported reagents¹⁶, have been developed, two main chemical approaches are exploited in PET radiochemistry, namely 1) the direct fluorination of a suitable precursor molecule, where the radionuclide is introduced in one synthetic step and 2) the indirect fluorination, where the radioisotope is incorporated into the target molecule by reaction with a so called prosthetic group, which is commonly an aryl or alkyl group bearing a reactive functionality. The latter is indicated when the selected precursor molecule is not able to tolerate the quite harsh reaction conditions used for direct methods (typically, polar aprotic solvents and high reaction temperatures).

Direct fluorinating methods involve two specific classes of chemical reactions: nucleophilic reactions and electrophilic reactions. Currently, nucleophilic reactions have found large applicability in PET radiochemistry, given their selectivity and their high RCYs in comparison with electrophilic reactions, which, however, have represented in the past years the method of choice for introducing ^{18}F -isotope.

1.5.1 Electrophilic fluorination

The electrophilic fluorination is commonly performed by using $[^{18}\text{F}]\text{F}_2$, which is obtained from the nuclear reactions $^{20}\text{Ne}(\text{d}, \alpha)^{18}\text{F}$ or $^{18}\text{O}(\text{p}, \text{n})^{18}\text{F}$.

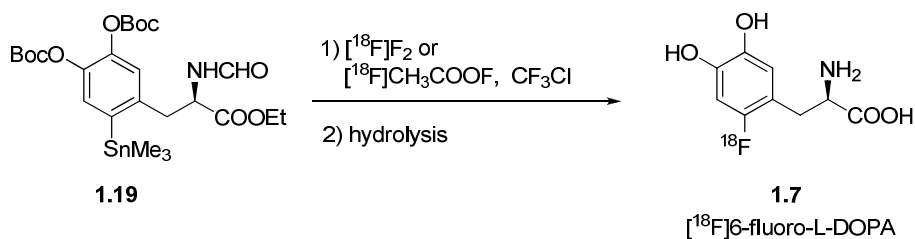
A recent example of PET-tracer synthesised by direct fluorination with $[^{18}\text{F}]\text{F}_2$ is EF5 (2-(2-nitro-1*H*-imidazol-1-yl)-*N*-(2,2,3,3,3-pentafluoropropyl)acetamide (**1.18**) [Scheme 1.1], a 2-nitroimidazole based compound used for PET-imaging of tumor hypoxia (see chapter 2).



Scheme 1.1. Synthesis of EF5 by direct electrophilic fluorination with $[^{18}\text{F}]\text{F}_2$.

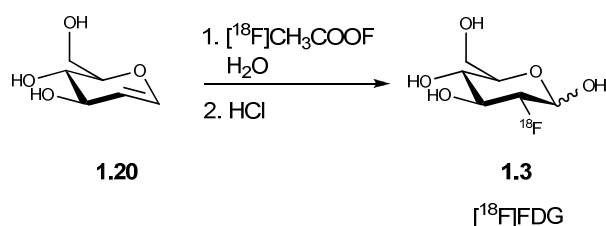
Demetalation of an organotin precursors is another type of electrophilic reaction where $[^{18}\text{F}]\text{F}_2$ or acetyl hypofluorite ($\text{CH}_3\text{COO}[^{18}\text{F}]\text{F}$) are used as fluorinating agents. The synthesis of $[^{18}\text{F}]6$ -fluoro-L-DOPA is an example of application of this synthetic approach [Scheme 1.2].

The first synthesis of $[^{18}\text{F}]\text{L-DOPA}$ was first performed in 1984 by Kieseveiter and coworkers¹⁷. Currently, the electrophilic fluorination is the method of choice for the synthesis of $[^{18}\text{F}]\text{fluoro-L-DOPA}$, performed starting from the treatment of an organotin Boc-protected precursor (**1.19**) either with $[^{18}\text{F}]\text{F}_2$ or $[^{18}\text{F}]\text{CH}_3\text{COOF}$, followed by hydrolysis under acidic conditions [Scheme 1.2].



Scheme 1.2. Electrophilic synthesis of $[^{18}\text{F}]\text{fluoro-L-DOPA}$, starting from an organotin precursor.

Among the synthetic routes to 2- $[^{18}\text{F}]\text{fluoro-2-deoxy-D-glucose}$ ($[^{18}\text{F}]\text{FDG}$) (**1.3**), the electrophilic fluorination with acetyl hypofluorite ($\text{CH}_3\text{COO}[^{18}\text{F}]\text{F}$) as fluorinating reagent represents a suitable method, although $[^{18}\text{F}]\text{FDG}$ can be obtained also by nucleophilic fluorination. $[^{18}\text{F}]\text{fluoro-2-D-deoxyglucose}$ ($[^{18}\text{F}]\text{FDG}$) (**1.3**) was first synthesised in 1976 by Dr. Wolf and co-workers at Brookhaven National Laboratory¹⁸.



Scheme 1.3. Synthesis of [^{18}F]FDG via electrophilic fluorination by using [^{18}F]acetyl hypofluorite.

1.5.2 Nucleophilic fluorination

Nucleophilic fluorination is the most common synthetic strategy performed to produce ^{18}F -labelled compounds for PET imaging, and involves the direct introduction of ^{18}F -radionuclide into the target molecule.

Two classes of nucleophilic reactions can be applied for the synthesis of ^{18}F -labelled PET-tracers, namely aliphatic and aromatic nucleophilic substitutions.

Typically, these reactions are performed by using [^{18}F]-fluoride sources such as potassium fluoride (KF), cesium fluoride (CsF) or tetrabutylammonium fluoride (TBAF), in aprotic polar media such as acetonitrile, THF, DMF or DMSO at high reaction temperatures.

The degree of solvation of [^{18}F]fluoride ion is a limiting factor as it decreases the nucleophilicity and the products rate. Indeed, the reactions with KF as the fluorinating agent are conducted in the presence of the phase transfer reagent Kryptofix 2.2.2, which forms a strong complex with the potassium cation, thus increasing the nucleophilicity of [^{18}F]fluoride ion.

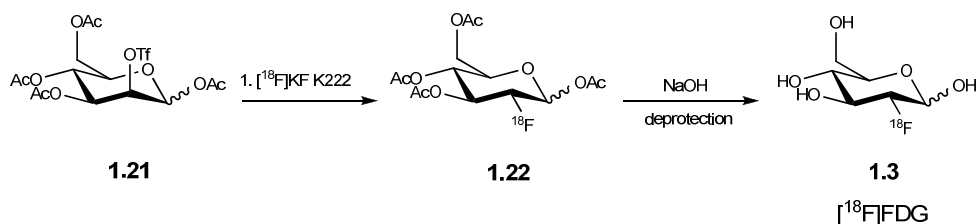
Aliphatic nucleophilic fluorination

The important requirement for aliphatic nucleophilic fluorination is the presence on the precursor molecule of a suitable leaving group such as mesylate, tosylate, triflate, iodo or bromo. Moreover, when other potentially competing groups (acid, alcohol or amine group) are present on the precursor molecule, they need to be protected from reacting, thus avoiding the production of by-products.

The syntheses of [^{18}F]FDG and [^{18}F]fluoroethylcholine are achieved by aliphatic nucleophilic fluorination, where the leaving group triflate (TfO) is displaced by the [^{18}F]fluoride ion.

As aforementioned [^{18}F]FDG can be also synthesised by aliphatic nucleophilic substitution reaction, which involves the treatment of the acetyl-protected sugar tetra-*O*-acetyl-2-triflate- β -

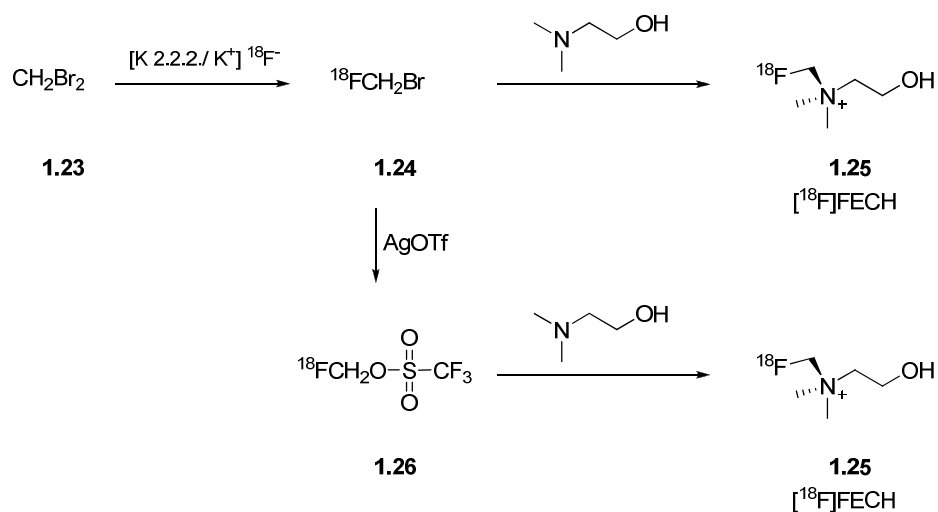
mannose (**1.21**) with a [^{18}F]fluoride source. The subsequent deprotection of the intermediate **1.22** completes the synthesis of [^{18}F]FDG [**Scheme 1.4**].



Scheme 1.4. Synthesis of [^{18}F]FDG through aliphatic nucleophilic reaction and deprotection.

The synthesis of [^{18}F]fluoroethylcholine is an example of indirect fluorination, involving a prosthetic group labelled with ^{18}F -radionuclide.

Fluoroethylcholine ([^{18}F]FECH) is produced starting from monofluorination of dibromomethane (**1.23**) under nucleophilic substitution conditions with ^{18}F -fluoride, followed by reaction with dimethylethanolamine¹⁹. In another procedure, the intermediate fluorobromomethane (**1.24**) is converted to [^{18}F]fluoromethyltriflate (**1.26**) and then reacted with dimethylethanolamine [**Scheme 1.5**].

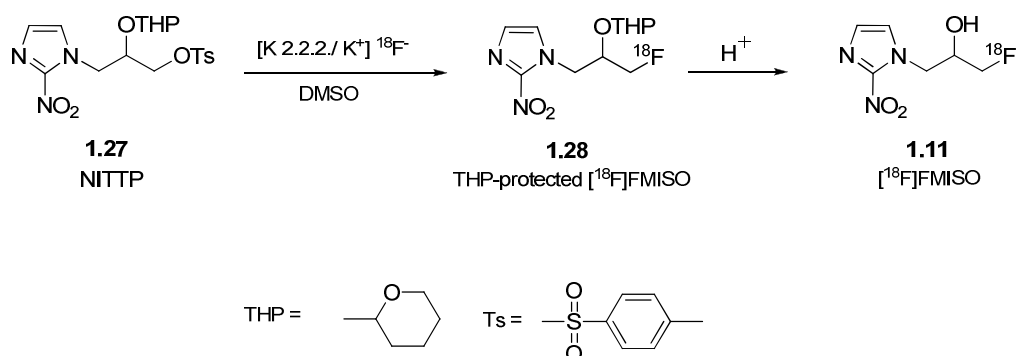


Scheme 1.5. Synthetic routes to [^{18}F]fluoroethylcholine.

The synthesis of ^{18}F -fluoromisonidazole²⁰ ([^{18}F]FMISO) (**1.11**) is another classical example of aliphatic nucleophilic fluorination,.

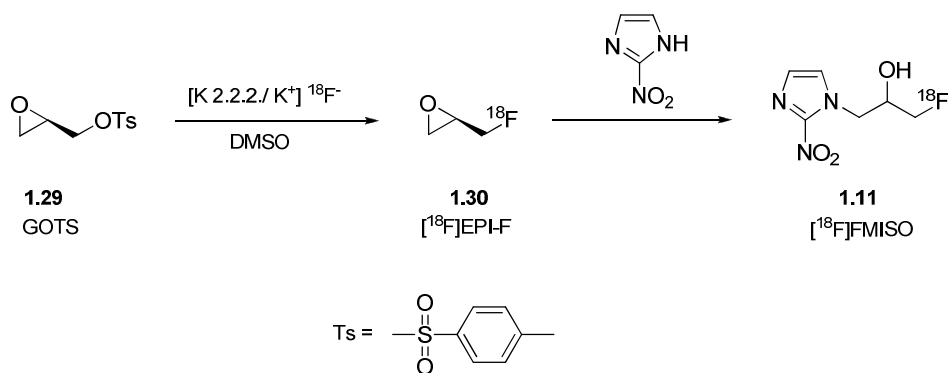
^{18}F -radiolabelled FMISO can be generally afforded by means of two different synthetic strategies. The first synthetic approach consists of ^{18}F -fluorination of a tetrahydropyranyl-protected precursor 1-(2'-nitro-1'-imidazolyl)-2-*O*-tetrahydropyranyl-3-*O*-toluenesulfonylpropanediol

(NITTP) (**1.27**), followed by hydrolysis of the protecting group of **1.28** to afford the desired [^{18}F]FMISO, as reported by Lim and Berridge²¹ [Scheme 1.6].



Scheme 1.6. Reaction scheme for the synthesis of [^{18}F]FMISO: ^{18}F -fluorination of NITTP precursor and subsequent removal of the THP protecting group under acidic conditions.

Alternatively, Grierson *et al*²² have proposed another route where [^{18}F]FMISO is produced in two steps: ^{18}F -fluoride displacement of (2*R*)-(-)glycidyl tosylate (GOTS) (**1.29**) to give [^{18}F]epifluorohydrin (EPI-F) (**1.30**) and subsequent coupling with the 2-nitroimidazole moiety (2-NIM) under basic conditions [Scheme 1.7].



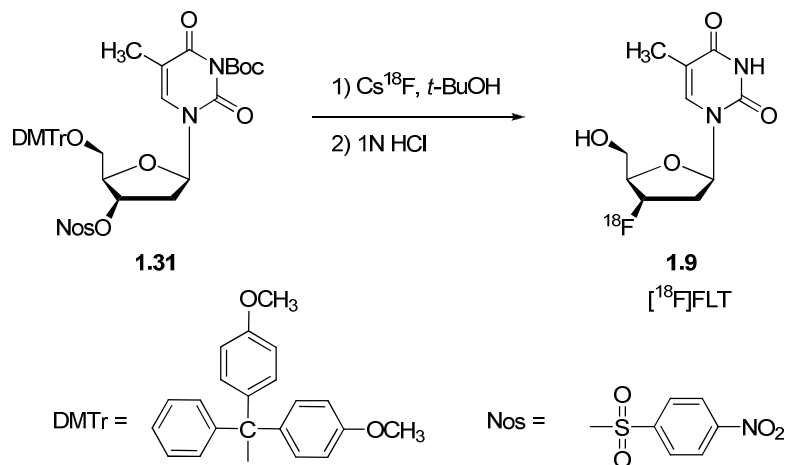
Scheme 1.7. Synthesis of [^{18}F]FMISO via the [^{18}F]EPI-F intermediate: nucleophilic displacement of GOTS precursor with ^{18}F -fluoride and epoxide ring opening by coupling with 2-NIM.

Although protic solvents are not generally indicated for $\text{S}_{\text{N}}2$ reactions, given their capacity to solvate the nucleophile and hence reduce its reactivity, recent studies^{23,24} have reported the use of protic solvents as reaction media for nucleophilic fluorination reactions with alkali metal fluoride.

Sterically hindered alcohols such as *tert*-butyl alcohol and *tert*-amyl alcohol have been described to be useful in the application of aliphatic nucleophilic reactions where the precursor protected with sulfonates is reacted with fluoride sources such as CsF and TBAF.

This conditions have been applied in the synthesis of ^{18}F -labelled thymidine (^{18}F FLT).

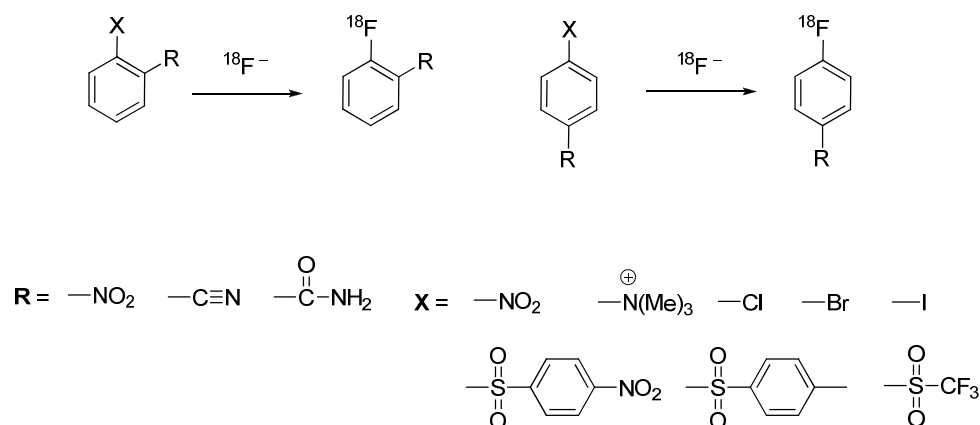
^{18}F Fluorothymidine can be synthesised by reacting a protected nosylate precursor, namely 3-*N*-Boc-5'-*O*-dimethoxytrityl-3'-*O*-nosyl-thymidine (**1.31**), with ^{18}F CsF in *t*-BuOH to give the corresponding ^{18}F -labelled intermediate, subsequently deprotected under acidic conditions [Scheme 1.8].



Scheme 1.8. Radiosynthesis of ^{18}F Fluorothymidine starting from protected precursor (**1.31**), then sequentially submitted to ^{18}F labeling and hydrolysis.

Aromatic nucleophilic fluorination

Aromatic ^{18}F fluorinations require the presence of a suitable electron-withdrawing group (nitro, cyano, acyl) on the aryl ring at the *ortho* or *para* positions with respect to a good leaving group (nitro, trialkylamine, halogen, nosylate, tosylate or triflate) [Scheme 1.9].



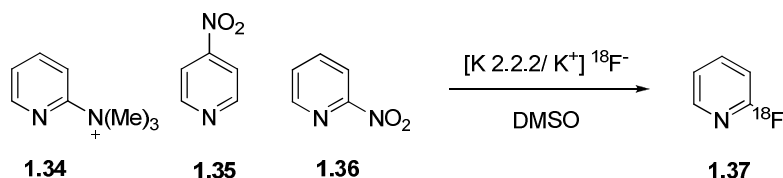
Scheme 1.9. General scheme of aromatic nucleophilic fluorinations.

The use of nitro group (NO_2) as both leaving group and electron-withdrawing group is widely exploited in the synthesis of ^{18}F -radiolabelled compounds. The radiosynthesis of [^{18}F]flumazenil (**1.33**) [Scheme 1.10], a PET radioligand for imaging the benzodiazepine receptor, is a good example of aromatic nucleophilic substitution involving the displacement of the nitro group by the [^{18}F]fluoride/ $\text{K} 2.2.2$.

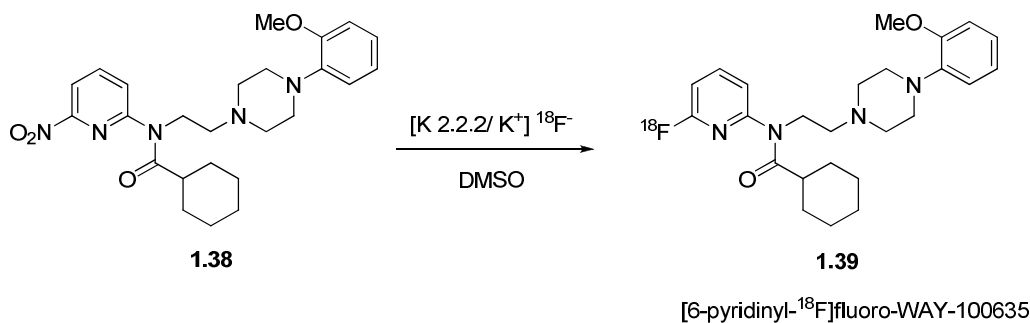


Scheme 1.10. Radiosynthesis of [^{18}F]flumazenil.

Nucleophilic aromatic reactions may be also exploited for the introduction of [^{18}F]radioisotope on pyridinyl rings, with good radiochemical yields (RCYs), when the leaving group is on the electron-deficient positions (2- 4- and 6-positions)²⁵ [Scheme .11]. This strategy has been exploited for the synthesis of a number of radioligands of several receptors (nicotinic, 5-HT_{1A} mGluR5)^{26, 27}.

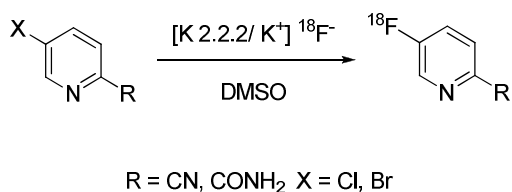


Scheme 1.11. Aromatic nucleophilic fluorinations on pyridinyl rings.



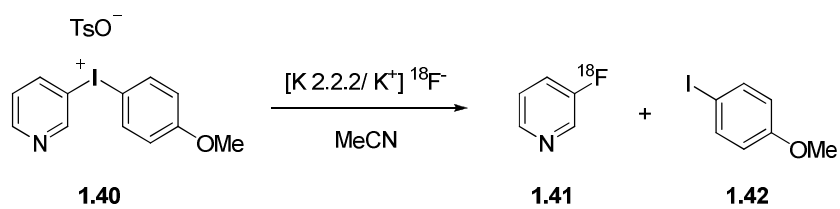
Scheme 1.12 Synthesis of the PET radioligand for imaging the 5-HT_{1A} receptor ([6-pyridinyl-¹⁸F]fluoro-WAY-100635).

Furthermore, when an electron-withdrawing group such as cyano (CN) or amido (CONH₂) is on the *ortho* position of the pyridinyl ring, the [¹⁸F]fluoride ion can be also incorporated on the 3-position in place of a leaving group such as chloro (Cl) or bromo (Br) [Scheme 1.13]²⁸.



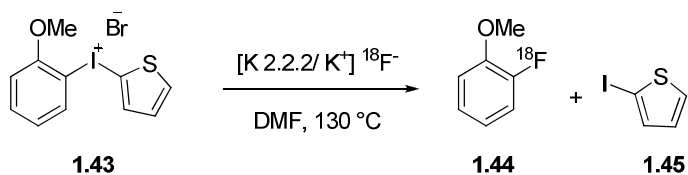
Scheme 1.13. ¹⁸F-labelling of the meta position of pyridines.

However, the introduction of the [¹⁸F]fluoride ion into the 3-position can be efficiently achieved even without the presence of an electron-withdrawing group, when the reaction is carried out on diaryl-iodonium salts as precursors. The presence of an electron-rich ring on the diaryl-iodonium salt directs the fluorination to the pyridinyl ring at the 3-position [Scheme 1.14]²⁹.



Scheme 1.14. ¹⁸F-fluorination of 3-[¹⁸F]fluoropyridine starting from a diaryl-iodonium salt.

Diaryl-iodonium salts as synthetic precursors are also used for directing ¹⁸F-fluoride ion to electron-rich arenes. When the salt contains two electron-rich arenes, the fluorination takes place on the less electron rich ring [**Scheme 1.15**]^{30, 31, 32}.



Scheme 1.15. Nucleophilic fluorination of an electron-rich arene.

Chapter 2. PET-Imaging of Hypoxia

2.1 What is Hypoxia?

Hypoxia results from an inadequate oxygen (O_2) supply to body tissues and is proved to be responsible for physiological changes occurring in the region of the body where it is localized^{33,34}.

Hypoxia can be also defined as a state of reduced O_2 availability or decreased O_2 partial pressure (lower than 25-30 mmHg), which affects the biological functions of organs, tissues or cells.

A number of factors have been recognised to be causes of hypoxia, such as 1) low O_2 partial pressure in arterial blood due to, e.g., pulmonary diseases or high altitude (hypoxemic hypoxia); 2) reduced ability of blood to carry O_2 as a result of anemia, methemoglobin formation, or carbon monoxide poisoning (anemic hypoxia); 3) reduced tissue perfusion, generalized or local (circulatory or ischemic hypoxia); 4) deterioration of the diffusion geometry, e.g., increased diffusion distances, concurrent versus countercurrent blood flow within microvessels (diffusional hypoxia); or 5) inability of cells to use O_2 because of intoxication, as in cyanide poisoning (histotoxic or cytotoxic hypoxia).

The prevalence of hypoxic areas is a characteristic feature of locally advanced solid tumors and has been described in a wide range of human malignancies, including cancer of the breast, uterine cervix, vulva, head and neck, prostate, rectum, pancreas, as well as brain tumors, soft tissue sarcomas, and malignant melanomas.

2.2 Physiological changes related to hypoxia

A large body of evidence has proven tumor hypoxia to be strictly associated with tumor propagation, malignant progression, and resistance to both radiotherapy and chemotherapy.

These conditions are due to biological changes occurring inside hypoxic tumor cells at the molecular level, involving the proteome (i.e., the complete set of proteins within a cell at a certain time) and the genome of neoplastic cells.

With regard to hypoxia-induced proteome changes, it is well established that tumor hypoxia may lead to neoplastic growth arrest or neoplastic growth impairment, resulting in apoptosis, differentiation, necrosis and cellular quiescence.

Furthermore, hypoxia is responsible for tumor propagation, as well as malignant progression of a neoplasm, which may refer to local spread (through direct invasion of neighbouring tissues and organs), perifocal spread (through migration of single neoplastic cells and microfoci into the interstitial space, lymphatic space involvement, and perineural invasion), regional spread (through metastases to the lymph nodes), and distant spread (through metastases or dissemination into body cavities, such as the peritoneum and pleura).

It is worth noting that hypoxia also promotes changes in the genome of hypoxic cancer cells, such as mutations, gene amplification, and chromosomal rearrangements.

Among the multiple changes involved in a low oxygen state, the hypoxia-induced chemo- and radiotherapy represents a severe problem, as it strongly influences the efficacy of anticancer treatment.

The resistance of hypoxic tumor cells to chemotherapeutic agents is related to several mechanisms, including tissue acidosis (which is commonly observed in hypoxic tumors with a high glycolytic rate), inhibition of cell proliferation and decreased cytotoxicity of some agents. The sensitivity of tumor cells towards radiation therapy (x- and γ radiation) is progressively reduced when the O_2 partial pressure in a tumor is less than 25-30 mmHg.

During the treatment of a cancer by using ionizing radiations, the interaction of the intracellular water with the radiations results in the production of highly reactive oxygen free radicals that cause the damage of the DNA of cells. In the presence of molecular oxygen the damage of DNA is even increased, while when there is inadequate oxygen supply to the cells, the efficacy of radiation treatment is reduced and a higher dose of radiation is required to achieve the same biological effect obtained in presence of normal oxygen levels.

2.3 Tumour hypoxia measurement

As hypoxia plays a fundamental role in determining the response of solid tumors to therapy, in the last decades its accurate measurement has been considered a crucial target to be achieved.

The oxygenation status of tumour tissues can be assessed either by invasive or non-invasive procedures, which mainly provide information regarding the oxygen partial pressure within the tumor.

Among the invasive methods, the use of polarographic O_2 electrodes has represented for years the standard procedure for the detection of tumor hypoxia.

However, as the oxygen electrode system (or Eppendorf electrode) is applicable only to easily accessible tumors, it can not distinguish between a necrotic or anoxic tissue and, moreover it is

technically difficult to perform, hence molecular imaging methods, such as PET (Positron Emission Tomography) (non-invasive method), have been extensively studied.

2.3.1 Molecular imaging of hypoxia with PET

As already mentioned, Positron Emission Tomography (PET) relies on the use of radiolabeled chemicals^{35,36} to account for either pathological or physiological processes occurring in the cells at the molecular level.

With regard to hypoxia, a large number of tracers have been investigated and rapidly developed, allowing the specific assessment of oxygen deficit in tumor tissues.

As reported by Mees *et al.*³⁷, the development of a hypoxia tracer needs to take into account an array of important criteria, which require the ideal PET-hypoxia marker to be (1) exclusively hypoxia-sensitive and thus differentiating hypoxia, normoxia, anoxia and necrosis.

The ideal hypoxia tracer should be (2) capable to image and distinguish acute hypoxia from chronic hypoxia, it should be (3) easily available, non-toxic, fast, easy to perform and guarantee repeated measurements. Furthermore it should be (4) lipophilic to maintain a homogeneous distribution in all tissues including tumours and, at the same time hydrophilic, allowing its faster elimination. (5) It should have little hypoxia-independent degradation *in vivo* leading to non-specific tracer metabolites and/or little non specific tissue binding, so that only oxygen-specific retention mechanism determines the amount of tracer that is temporarily or permanently trapped. (6) It should be sensitive at intracellular pO₂ levels rather than at blood flow pO₂, thus reflecting the tumor response to therapy and, finally (7) it should offer the ability to quantify. Unfortunately, at present none of these requirements is completely possessed by the currently available PET-markers.

2-Nitroimidazole compounds

A number of studies have investigated the feasibility of several 2-nitroimidazole compounds for the *in vivo* PET-imaging of tumor hypoxia, and their evaluation, as well as their radiosynthesis currently represent a critical target to be achieved.

The prognostic role of nitroimidazole derivatives in early response to the radiotherapy was suggested by the work of Chapman *et al.*^{38,39}, who were the first to propose the 2-nitroimidazole as biomarker of hypoxia in 1979.

2-Nitromidazole tracers are able to detect tumor hypoxia once they accumulate within the hypoxic cells. After diffusion into hypoxic cells, 2-nitroimidazole compounds are reduced into highly reactive intermediaries by intracellular reductases in a process that is directly related to the level

of oxygenation. These metabolites covalently bind to thiol groups of intracellular molecules and thereby they are trapped in the hypoxic cells.

The retention of 2-nitroimidazoles in hypoxic tissues is possible because of the presence of nitro-group in the tracer molecular structure.

Given that the nitro group has a high affinity for electrons, it binds an electron formed during the respiratory cycle of the cell, giving rise to a radical anion $-\text{NO}_2^{\cdot-}$.

If oxygen (O_2) is present in the cell in a sufficient concentration, it can accept the electron from the nitro radical, forming reduction products and subsequently returning the nitro group to its parent state, allowing the marker to diffuse out from the cell.

On the other hand, in hypoxic conditions, the nitro-radical accepts another electron and forms a 2-electron reduction product which can not be returned to its original state but is further reduced to highly reactive alkylating agent, which strongly binds to intracellular molecules and, hence, is irreversibly trapped [Figure 2.1].

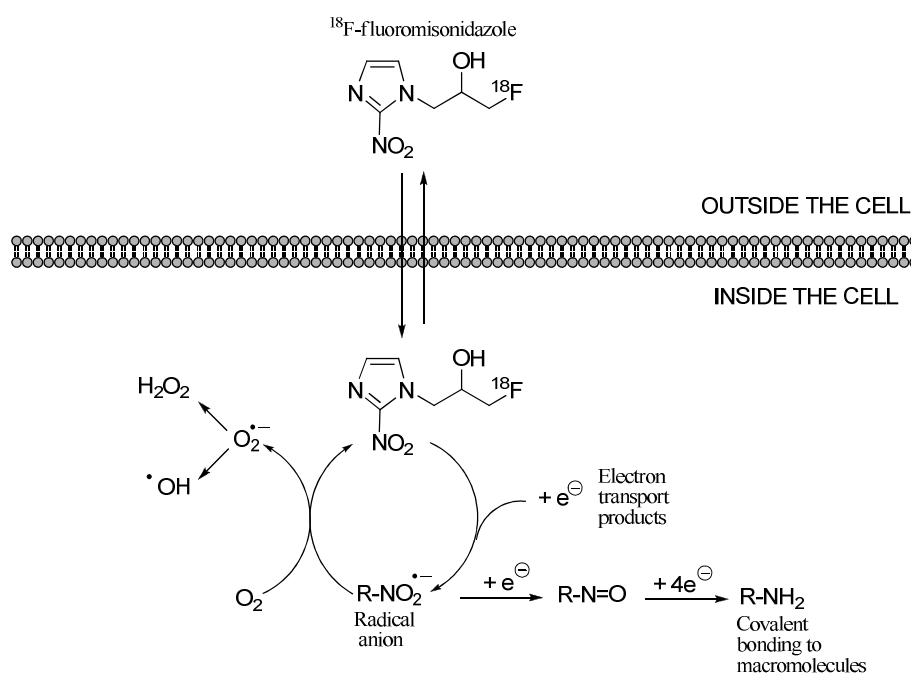


Figure 2.1. Mechanism of intracellular trapping of nitroimidazoles under hypoxic conditions, example of $[^{18}\text{F}]$ -Fluoromisonidazole ($[^{18}\text{F}]$ -FMISO).

When tagged with an appropriate radioactive isotope, 2-nitroimidazole compounds can be detected using PET imaging methods.

Most of hypoxia nitroimidazole imaging agents, as well as the radiotracers used in PET-imaging experiments, are labelled with the radioisotope fluorine-18, as it provides high quality PET images of the region of the body where it is localized and has a long half-life (109.7 min), which

allows reasonable reaction time and delivery of tracer to PET facilities when it is not possible to perform the imaging experiment immediately after that the radio-synthesis is completed.

A great variety of hypoxia 2-nitroimidazole PET probes has been largely investigated and evaluated in the past several decades, therefore, nowadays a considerable library of hypoxia tracers is available for *in vivo* PET-imaging. Some important hypoxia PET tracers are summarized in **Figure 2.2**.

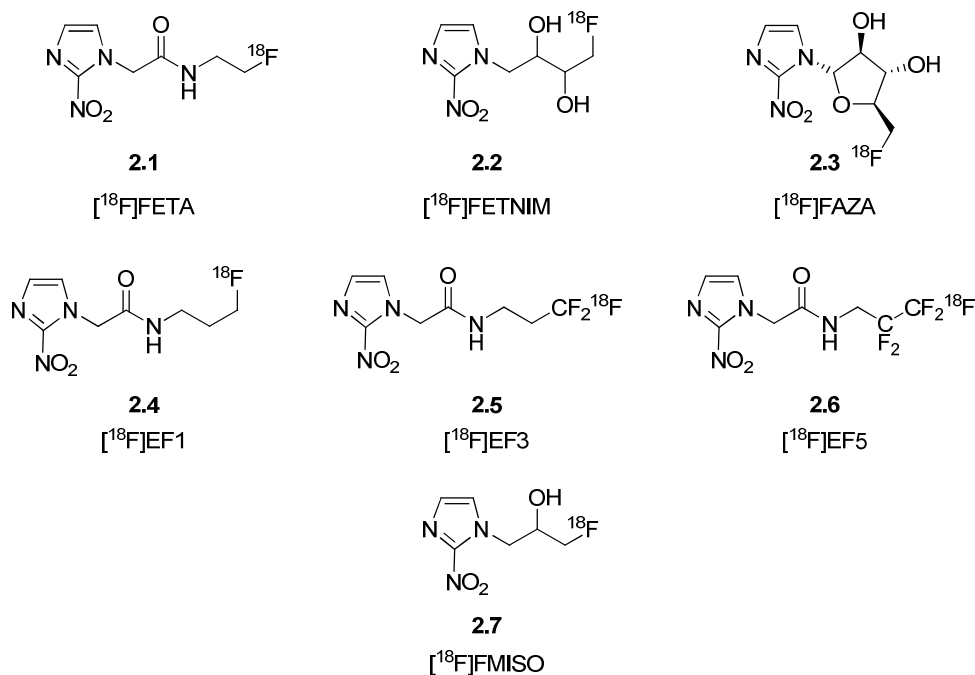
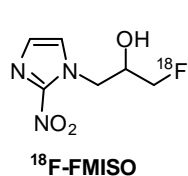


Figure 2.2. Nitroimidazole agents for tumor hypoxia PET imaging: ^{18}F -fluoroetanidazole (**2.1**), ^{18}F -fluoroerythronitroimidazole (**2.2**), ^{18}F -fluoroazomycin arabinoside (**2.3**), ^{18}F -monofluoropropyl acetamide of etanidazole (**2.4**), ^{18}F -trifluoropropyl acetamide of etanidazole (**2.5**), ^{18}F -pentafluoropropyl acetamide of etanidazole (**2.6**).

^{18}F Fluoromisonidazole (^{18}F FMISO)



1-(2'-nitro-1'-imidazolyl)-3-fluoro-2-propanol, FMISO, labelled with the short-lived positron-emitter fluorine-18, was suggested as a tracer for the determination of hypoxic tissue *in vivo* with PET in 1984⁴⁰.

Among the nitroimidazole hypoxia radiosensitizers, ^{18}F -labeled 1-(2-nitroimidazolyl)-3-fluoro-2-propanol (^{18}F -Fluoromisonidazole (^{18}F FMISO)) has been regarded as a prognostic probe suitable for predicting the tumor response to radiation treatment for thirty years. According to its high lipophilicity ($\log P = 0.45$), ^{18}F -FMISO uptake in all organs has been demonstrated to be considerable, allowing its free penetration into the hypoxic cells through a

diffusion process. Moreover, ^{18}F -FMISO has shown an appropriate reduction potential ($E = -389$ mV), which reflects its trapping in hypoxic cells via the oxygen-dependent reduction of the nitro ($-\text{NO}_2$) group. Additionally, ^{18}F -FMISO is capable of differentiating hypoxia from necrosis, as it is not retained in necrotic cells, therefore its cellular uptake is solely related to the O_2 partial pressure of the hypoxic cells.

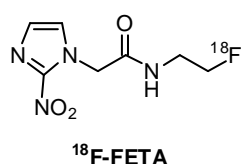
Although during the last decades ^{18}F -FMISO has been considered as the gold standard for detecting tumor oxygenation *via* PET, important disadvantages have been reported.

A harsh limitation is the low clearance of ^{18}F -FMISO from the body, due to its high lipophilicity, resulting in longer waiting times after tracer application and a higher radiation exposure.

In addition, ^{18}F -FMISO displays a significant non-oxygen dependent metabolism leading to a considerable amount of radioactive metabolite products.

Unlike other hypoxia PET-radiotracers which are mostly eliminated via the renal system (e.g. [^{18}F]FAZA, [^{18}F]FETA), according to their better pharmacokinetics, ^{18}F -FMISO is cleared not only via the renal system, but also via the biliary system, reflecting its low hydrophilicity.

[^{18}F] Fluoroetanidazole ([^{18}F]FETA)



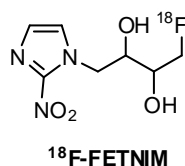
Given the main disadvantages of [^{18}F]FMISO in terms of pharmacokinetics, namely high metabolism and slow clearance, both dependent on its high lipophilicity, more hydrophilic nitroimidazole tracers have been developed and investigated.

Certainly, they were required to retain the oxygen dependent binding of the lead compound ([^{18}F]FMISO), allowing to be suitable for the sole detection of tumor hypoxia, distinguishing normoxia and necrosis.

[^{18}F]FETA (*N*-(2-fluoroethyl)-2-(2-nitroimidazole-1-yl)-acetamide), the monofluorinated derivative of etanidazole appeared to be a suitable PET hypoxia marker as *in vitro* studies has demonstrated that its tumor retention was related to the low O_2 partial pressure and it was similar to that for [^{18}F]FMISO.

It is remarkable that [^{18}F]FETA has shown fewer metabolites *in vivo* and less retention in liver than [^{18}F]FMISO, being excreted through the renal system, according to its better physicochemical properties. Moreover [^{18}F]FETA has been able to readily cross the blood-brain-barrier, proving to be suitable for detecting hypoxia brain tumor.

[¹⁸F] Fluoroerythronitroimidazole (¹⁸F]FETNIM)



4-[¹⁸F]Fluoro-2,3-dihydroxy-1-(2'-nitro-1'-imidazolyl) butane
 [¹⁸F]Fluoroerythronitroimidazole or (¹⁸F]FETNIM) is a potential nitroimidazole derivative currently to be demonstrated as a suitable PET hypoxia radiosensitizer.

However, preliminary studies have already shown [¹⁸F]FETNIM to be able to detect the low oxygenation status in tumors and to accumulate in hypoxic cells through the bioreductive mechanism.

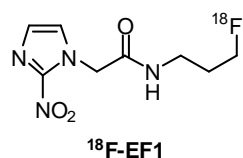
The presence of two hydroxyl functionalities in its molecular structure confers a high hydrophilic character, which is demonstrated by its lower uptake in the fat, cerebellum and liver of rats and by its faster excretion through the kidneys.

Furthermore it has a low uptake in lungs, as it should be in well-oxygenated organs.

Therefore, [¹⁸F]FETNIM pharmacokinetics can be summarized by low peripheral metabolism, little defluorination, metabolic trapping in hypoxic tissues and rapid elimination from well-oxygenated tissues, in accordance to its higher hydrophilicity than [¹⁸F]FMISO.

These findings, together with its easy preparation suggest [¹⁸F]FETNIM may offer advantages for PET imaging of hypoxic tumors *in vivo*.

[¹⁸F]EF derivatives: [¹⁸F]EF1



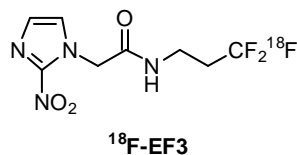
[¹⁸F]EF compounds are fluorinated derivatives of etanidazole with one or more hydrogen atoms substituted by fluorine in the propyl chain. Several extensive studies evaluated their potential as PET hypoxia tracers.

The pharmacokinetics profile of 2-(2-nitroimidazole-1-yl)-*N*-monofluoropropyl acetamide (¹⁸F]EF1) was assessed in tumor bearing rats⁴¹.

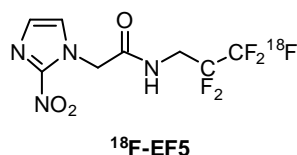
[¹⁸F]EF1 was found to heterogeneously diffuse throughout all tissues, with exception of central nervous system (CNS), where its concentration was not optimal, reflecting its high hydrophilicity in comparison with other ¹⁸F-EF compounds, i.e. [¹⁸F]EF5.

This finding was consistent with the predominant elimination of [¹⁸F]EF1 through the renal pathway, although excretion through the gastrointestinal tract was also observed.

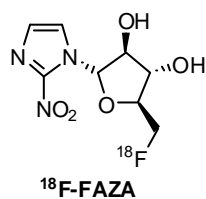
Worth of note was, certainly, [¹⁸F]EF1 unique accumulation inside hypoxic tissues rather than necrotic, thus demonstrating its potential of being a better alternative for [¹⁸F]FMISO.

[¹⁸F]EF3

2-(2-nitroimidazole-1-yl)-*N*-(3,3,3-trifluoropropyl) acetamide is another 2-nitroimidazole compound that belongs to the group of PET-labeled nitroimidazole compounds. It has shown promising pharmacokinetics, biodistribution and high uptake in hypoxic tumors⁴². Furthermore it is predominantly excreted via the kidneys, and it is not extensively metabolised.

[¹⁸F]EF5

2-(2-nitroimidazol-1-yl)-*N*-(2,2,3,3,3-pentafluoropropyl)-acetamide labelled with fluorine-18 ([¹⁸F]EF5) has been studied in rodent and human tumors⁴³ to assess its potential to detect hypoxia, giving encouraging results, such as uniform diffusion in all tissues, main elimination through the renal system, and no detectable metabolism. Moreover, as required for hypoxia marker, its tumor uptake was found to be inversely proportional to the O₂ partial pressure of tumor tissues⁴⁴. Nevertheless, more extensive *in vivo* studies are needed to evaluate the role of [¹⁸F]EF5 in hypoxia PET imaging.

[¹⁸F] Fluoroazomycin arabinoside ([¹⁸F]FAZA)

1- α -D-(5-deoxy-5-[¹⁸F]-fluoroarabinofuranosyl)-2-nitroimidazole ([¹⁸F]FAZA) is a 2-nitroimidazole-based molecule with a sugar addition, invented and developed at the Cross Cancer Institute in Edmonton, Alberta in 1999⁴⁵.

[¹⁸F]FAZA is currently being used as an *in vivo* marker to noninvasively assess hypoxia in several human malignancies, such as squamous cell carcinoma of the head and neck (HNSCC), small-cell lung cancer (SCLC) or non-small-cell lung cancer (NSCLC), malignant lymphoma, and high-grade gliomas.

As for all nitroimidazole compounds, its uptake is regulated by O₂ partial pressure, moreover it is hypoxia-sensitive and can distinguish normoxic and necrotic tissues.

Clearly, in presence of hypoxic conditions, [¹⁸F]FAZA undergoes reductive metabolism, forming highly reactive intermediates that strongly bind to intracellular molecules.

In the last decades, [¹⁸F]FAZA has represented a good alternative to the use of [¹⁸F]FMISO for PET tumor hypoxia detection as it shows considerable advantages in comparison to its congener.

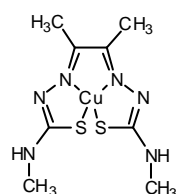
Unlike [^{18}F]FMISO, [^{18}F]-fluoroazomycin arabinoside shows better biokinetics, that allows its faster clearance from the body, resulting in shorter waiting times after tracer application and a lower radiation exposure.

As demonstrated in a number of *in vivo* studies, [^{18}F]FAZA and its metabolites exhibit a more rapid elimination from blood and non-target tissues mainly via renal pathway in comparison to [^{18}F]FMISO, which requires longer times to be cleared through both hepatobiliary and renal systems.

Given that [^{18}F]FAZA has a lower hydrophobicity than [^{18}F]FMISO, PET experiments performed using this sugar derivative afford a better quality image of the region of interest, in contrast to [^{18}F]-fluoromisonidazole, which undergoes non-specific lipoidal uptake in the brain, liver and other organs, thereby interfering with the image quality.

All these drawbacks have questioned the [^{18}F]FMISO suitability as a PET hypoxia tracer, therefore dictating the extensive investigation of [^{18}F]FAZA as a potential PET hypoxia marker.

^{60}Cu -ATSM: a non-nitroimidazole PET hypoxia agent



Copper(II)-diacetyl-2,3-*bis*(N^4 -methyl-3-thiosemicarbazone) labeled with ^{60}Cu (^{60}Cu -ATSM) is a novel PET hypoxia radiopharmaceutical, that has demonstrated to be predictive of prognosis in patients with uterine cervix, lung, rectum, head and neck cancers.

Cu^{2+} -ATSM ^{60}Cu -ATSM represents a very promising PET hypoxia-imaging agent, as extensive *in vivo* studies have shown ^{60}Cu -ATSM to accumulate selectively in hypoxic cells and to clear rapidly from normoxic cells^{46,47}. As for nitroimidazole agents, ^{60}Cu -ATSM is retained in hypoxic cells through a bioreductive process dependent on the low O_2 partial pressure.

Because of its high cell membrane permeability, ^{60}Cu -ATSM easily enters the intracellular environment, and it is subsequently reduced from Cu^{2+} -ATSM to $[\text{Cu-ATSM}]^+$, which is reversibly trapped within the hypoxic cell [**Figure 2.3**].

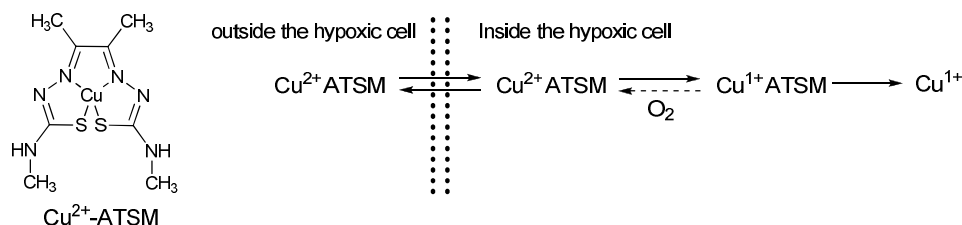


Figure 2.3. Chemical structure of Cu^{2+} -ATSM and mechanism of retention in hypoxic tissues.

Although ^{60}Cu -ATSM has demonstrated favourable properties for PET hypoxia detection besides an easy production, the short half-life of the copper radionuclide ^{60}Cu (half-life, 0.395 hours) is not a negligible factor.

Indeed, a major problem during a PET experiment is the time-consumption required for shipping the radiopharmaceutical from the production site to PET facilities, as most of the PET centres do not have an in house cyclotron.

This limitation has been overcome by replacement of ^{60}Cu with the long-lived radionuclide ^{64}Cu (half-life, 12.7 hours).

Interestingly, the image quality of hypoxic region provided by ^{64}Cu -ATSM PET imaging is better than that obtained by using ^{60}Cu -ATSM, in accordance with the ^{64}Cu positron energy of 0.66 MeV, similar to that of ^{18}F radionuclide, which is known to provide good quality PET images.

Chapter 3. Synthesis of [¹⁸F]FAZA

3.1 Introduction

Hypoxia is the result of an inadequate oxygen supply to the body tissues. It has been found in several solid tumors and is responsible for multiple molecular changes occurring inside the tumor tissues, thus leading to resistance to both chemo- and radiotherapy.

Therefore, the early detection and measurement of tumor oxygenation allow the real-time monitoring of malignancy and evaluation of its response to treatment.

Radiolabelled 2-nitroimidazoles are a class of PET-tracers used for the *in vivo* assessment of hypoxia. Their use as PET-probes was first suggested by Chapman in 1979⁴⁸.

The nitroimidazole functionality of these compounds has been proved to undergo an initial single electron reduction of the nitro group, when the tracer penetrates the cell membrane. The reduction intermediate can be converted to the original state and diffuse out of the cell when there is enough oxygen inside the cell, otherwise it is submitted to a further reduction, thus forming a highly reactive derivative, which is trapped within the cell by formation of covalent bonding with the intracellular macromolecules.

Although [¹⁸F]FMISO is the most widely used 2-nitroimidazole compound for the hypoxia assessment *via* PET in a variety of solid tumours, it has shown different drawbacks compared to other new developed PET hypoxia markers.

Amongst these, [¹⁸F]FAZA displayed significant advantages over [¹⁸F]FMISO such as a faster elimination from blood and non target tissues, leading to a lower radiation burden and a high diffusion capability, together with a selective uptake in hypoxic tissues, inversely proportional to the oxygen level.

Therefore, the clinical use [¹⁸F]FAZA in hypoxia PET-imaging has incredibly arisen, leading to an increasing demand of [¹⁸F]FAZA availability. With this regard, a project aimed at providing reasonable amounts of [¹⁸F]FAZA for clinical application was commenced at the University of Aberdeen.

An optimized and reproducible chemical synthesis of the [¹⁸F]FAZA precursor (DAcTs-AZA) along with [¹⁸F]FAZA radiosynthesis and PET imaging on hypoxic animal models are herein described.

The chemical synthesis of [^{18}F]FAZA precursor was performed manually at the Institute of Medical Sciences at the University of Aberdeen, while the radiosynthesis, purification and *in vivo* evaluation of [^{18}F]FAZA were conducted at John Mallard Scottish PET centre at the Aberdeen Royal Infirmary.

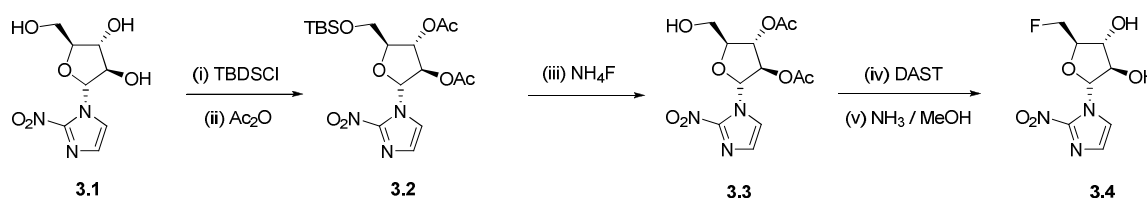
3.2 State of the art on FAZA synthesis

1- α -D-(5-Fluoro-5-deoxyarabinofuranosyl)-2-nitroimidazole (FAZA) was first synthesised in 1999 by Kumar and co-workers⁴⁹, who furthermore synthesised the ^2H and ^3H labelled FAZA derivatives and conducted a preliminary study of their biological properties.

The cold FAZA was synthesised starting from 1- α -D-arabinofuranosyl-2-nitroimidazole (α -AZA) (**3.1**), which was selectively protected at the primary C-5' hydroxyl group with *tert*-butyldiphenylsilyl chloride (TBDSCI) and subsequently reacted with acetic anhydride, giving the derivative 1- α -D-(5-*O-tert*-butyldiphenylsilyl-2,3-di-*O*-acetylarabinofuranosyl)-2-nitroimidazole (**3.2**).

The following treatment of **3.2** with ammonium fluoride afforded the corresponding di-acetylated α -AZA (**3.3**), deprotected at C-5'.

The desired 1- α -D-(5-fluoro-5-deoxyarabinofuranosyl)-2-nitroimidazole (**3.4**) was accomplished by reaction of 1- α -D-(2,3-di-*O*-acetylarabinofuranosyl)-2-nitroimidazole (**3.3**) with diethyl aminosulfurtrifluoride (DAST), followed by deprotection with ammonia in methanol. [Scheme 3.1].



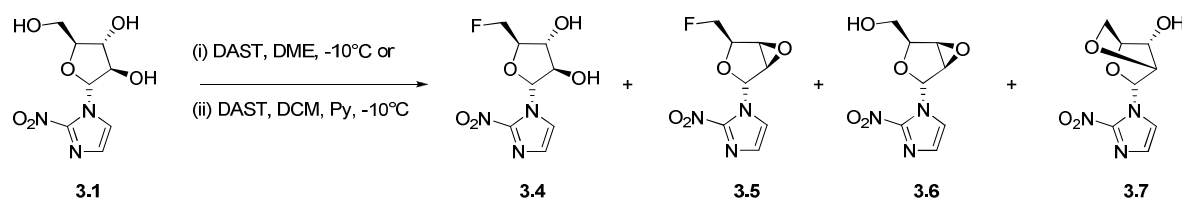
Scheme 3.1. Synthesis of FAZA by Kumar.

Since the original synthesis of FAZA involved multiple synthetic steps along with the use of expensive reagents and a low yield (~ 12%), Kumar *et al.* proposed an alternative synthetic route⁵⁰, which provided reasonable yields (12% to 25%) of FAZA in a single step and shorter time (3h).

FAZA was synthesised by reacting 1- α -D-arabinofuranosyl-2-nitroimidazole (AZA) (**3.1**) with diethylaminosulfurtrifluoride (DAST), in either anhydrous dimethoxyethane (DME) or anhydrous dichloromethane (DCM) as a solvent, at -10°C .

Both reaction conditions afforded dehydration products (**3.5-3.7**), competing with the formation of the desired FAZA (**3.4**).

However FAZA was obtained as the major product (25%) by using anhydrous DME at -10°C, whereas the use of anhydrous DCM, in the presence of catalytic amount of pyridine, at -10°C, afforded predominantly the fluorinated side product **3.5** (20.5%) [Scheme 3.2].



Scheme 3.2. Alternative route to FAZA.

Several recent works on the literature reported the synthesis of 1- α -D-2,3,5-tri-*O*-benzoylarabinofuranosyl)-2-nitroimidazole (α -tribenzoyl-AZA) (**3.10**), which was achieved by coupling 1-*N*-trimethylsilyl-2-nitroimidazole with the corresponding protected α -arabinofuranose, in the presence of mercuric cyanide.

The benzoyl protective group at the C-2' plays an important role in determining the formation of the coupled product, as its electronical interaction with the halogen at the C-1' allows the retention of configuration and the exclusive formation of α -tribenzoyl-AZA.

The alternate use of protective groups such as benzyl or silyl in place of benzoyl at C-1' position, is not efficient, as they are cleaved under the acidic conditions due to the displacement of the C-1' halogen, suggesting that the nucleosidic bond between azomycin and sugar is weak under acidic conditions.

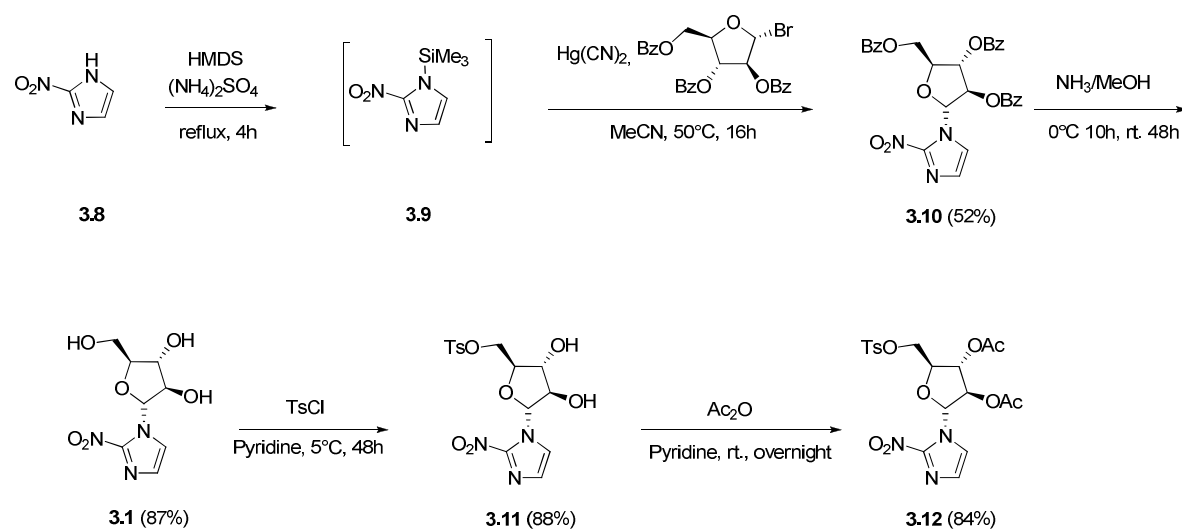
3.3 Results and discussion

3.3.1 Chemical synthesis of [¹⁸F]FAZA precursor

The synthesis of [¹⁸F]FAZA precursor started with the initial treatment of azomycin (**3.8**) with hexamethyldisilazane (HMDS), in the presence of a catalytic amount of ammonium sulphate ((NH₄)₂SO₄), giving the corresponding intermediate 1-*N*-trimethylsilyl-2-nitroimidazole (**3.9**), which upon coupling to the commercially available 2,3,5-Tri-*O*-benzoyl- α -D-arabinofuranosyl bromide, in the presence of mercuric cyanide ((Hg)CN₂), afforded reasonable yields of 1- α -D-2,3,5-Tri-*O*-benzoylarabinofuranosyl)-2-nitroimidazole (tribenzoyl AZA) (**3.10**).

The following deprotection of **3.10** to α -D-arabinofuranosyl-2-nitroimidazole (**3.1**) was achieved with ammonia in methanol at 0 °C for 10h, then at r.t. for 2 days in very good yields.

Further reaction of the primary alcohol at C-5' of **3.1** with tosyl chloride yielded the corresponding tosylated derivative (**3.11**) which after treatment with an excess of acetic anhydride gave the desired [18 F]FAZA precursor **3.12** in satisfactory yields [Scheme 3.3].



Scheme 3.3. [18 F]FAZA precursor synthesis.

3.3.2 Radiosynthesis of [18 F]FAZA

[18 F]FAZA was synthesised by standard nucleophilic substitution conditions, involving the displacement of the tosyl protecting group on the precursor molecule **3.12** by the no-carrier-added (NCA) [18 F]fluoride ion [Scheme 3.4], followed by hydrolysis of the protective acetyl groups [Scheme 3.5].

Labelling with [18 F]fluoride ion

[18 F]Fluoride is commonly produced through a cyclotron by proton irradiation of an 18 O-enriched water ([18 O]H₂O) target, according to the nuclear reaction $^{18}\text{O}(p,n)^{18}\text{F}$.

It is obtained as a solution of [18 F]fluoride ion in the irradiated target water, and has a high specific activity since it is produced “no-carrier-added” (NCA), without adding cold fluorine to the target (the ratio [18 F]fluoride ion radioactivity to mass of total fluoride ion is high).

The aqueous [18 F]fluoride ion obtained is a poor nucleophile, given its high degree of solvation in the target [18 O]water. Hence, the bulk [18 O]water must be removed by passing the [18 O]H₂O

containing [^{18}F]F $^-$ through an ion-exchange resin, where the [^{18}F]fluoride ion is trapped, thus allowing the recovery of the expensive [^{18}O]water.

The trapped [^{18}F]fluoride is then eluted with a mixture of an aqueous weak base such as potassium carbonate (K_2CO_3) and Kryptofix 2.2.2 in anhydrous acetonitrile.

The potassium carbonate allows to elute the [^{18}F]fluoride as [^{18}F]KF, while the phase transfer reagent Kryptofix 2.2.2 improves the nucleophilicity of [^{18}F]fluoride ion, forming a strong complex with the potassium cation and leaving the [^{18}F]fluoride ion “naked”. Moreover, Kryptofix 2.2.2 enables the [^{18}F]fluoride ion to be solubilised in a polar aprotic solvent such as acetonitrile, DMSO or DMF. The nucleophilicity of [^{18}F]fluoride is further enhanced by azeotropic evaporation of the residual water with acetonitrile.

Alternatively, ^{18}F -tetrabutylammonium fluoride ([^{18}F]TBAF) or ^{18}F -cesium fluoride ([^{18}F]CsF) can be used in place of [^{18}F]KF/K 2.2.2 for fluorination reactions. [^{18}F]TBAF is obtained by eluting the [^{18}F]fluoride trapped on ion exchange resin with tetrabutylammonium hydrogencarbonate.

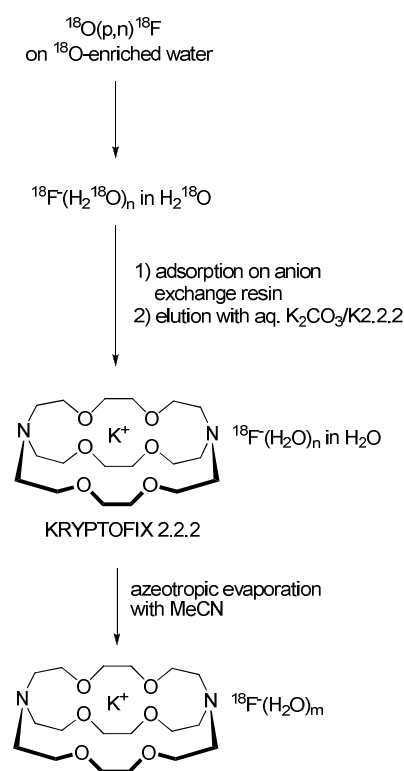


Figure 3.1. Schematic representation of the production and preparation of “naked” [^{18}F]fluoride with Kryptofix 2.2.2. and by azeotropic evaporation.

Automated synthesis of diacetyl[^{18}F]FAZA

K_2CO_3 (1.8 mg, 130 μmol) in H_2O for irrigation (0.5 ml), Kryptofix 2.2.2 (10.7 mg, 28 μmol) in anhydrous MeCN (1 ml), and the precursor (**3.12**) (5 mg, 10 μmol) in anhydrous DMSO

(0.5 ml) were loaded (injected) into the vials 7, 8 and 9, respectively, of the synthesis automated module (TRACERlab FX_{FDG}), routinely used for the clinical production of [¹⁸F]FDG [Figure 3.2]. The precursor molecule (Ts-diAc-AZA) (3.12) was previously purified by HPLC (semipreparative column: Phenomenex Luna C₁₈, 10 mm x 250 mm, 5 μ, 100 Å, mobile phase: ACN/H₂O= 50/50 to 100% ACN in 18 min, flow rate: 5.0 ml/min, wavelength: 300 nm, FAZA prec. retention time= 9,5 min) and dried over P₂O₅ under vacuum in a desiccator overnight.

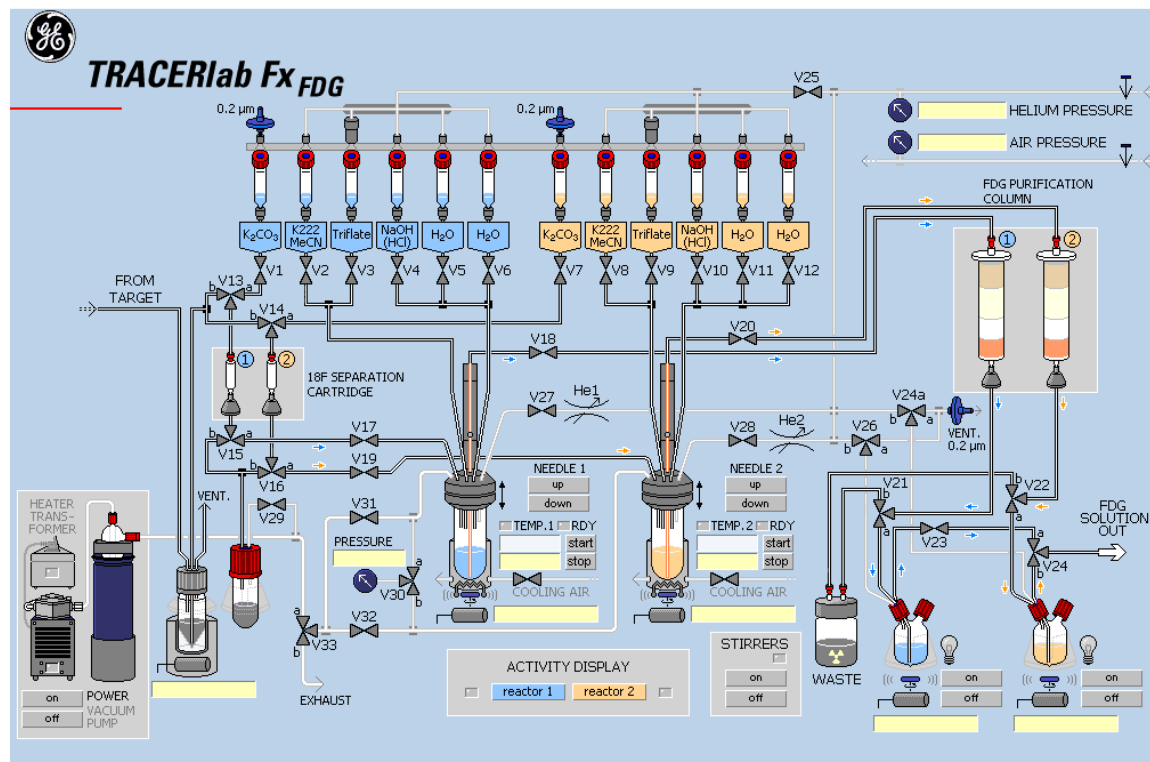
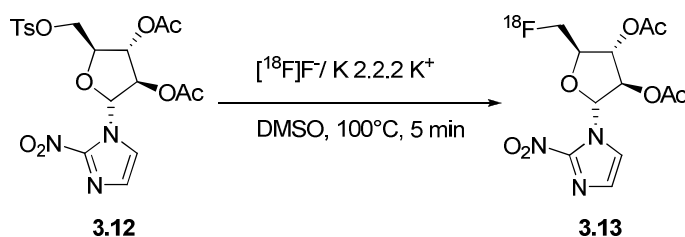


Figure 3.2. Scheme of the TRACERlab FX_{FDG} for the automated production of precursor 3.12.

At the end of 25 min bombardment (EOB), 7 GBq of activity of [¹⁸F]fluoride ([¹⁸F]F⁻) were trapped on a ChromaFix anion exchange cartridge, then washed with water and eluted with the K₂CO₃ solution into the reaction vessel.

Afterwards, K 2.2.2 in anhydrous MeCN was added, then the [¹⁸F]F⁻ solution was evaporated under a He gas stream and dried by azeotropic evaporation with anhydrous MeCN at a range temperature of 60-80°C.

Ts-diAc-AZA (3.12) in anhydrous DMSO was then added to dry ¹⁸F-fluoride (5 MBq) and the resulting mixture was heated at 100 °C for 5 min [Scheme 3.4].



Scheme 3.4. [¹⁸F]Fluorination of [¹⁸F]FAZA precursor.

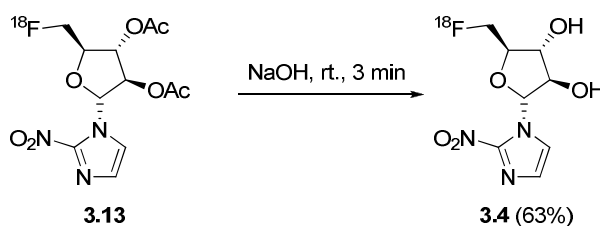
Finally, the reaction mixture was cooled to 30-35°C and transferred via a Lite Alumina N cartridge to the reception vessel, and reactor and lines were washed with 0.5 ml of DMSO to collect the remaining radioactivity.

At the end of radiolabeling procedure 2.62 GBq of activity (unreacted ¹⁸F-fluoride and generated ¹⁸F-diAc-AZA) were retained on the cartridge and 1.312 GBq of ¹⁸F-diAc-AZA were collected.

[¹⁸F]FAZA production

The final removal of acetyl protective groups under basic conditions afforded the desired [¹⁸F]FAZA (**3.4**) [Scheme 3.5].

The reaction mixture containing the crude ¹⁸F-diAc-AZA (0.5 mL) was treated with a 0.1 N NaOH solution (0.5 mL) and stirred at room temperature (25°C) for 3 min. Afterwards, the solution was neutralized with 0.2 N HCl (0.5 mL).



Scheme 3.5. Hydrolysis of diacetyl[¹⁸F]FAZA.

The mixture was purified via HPLC (semipreparative column: Phenomenex Luna C₁₈, 10 mm x 250 mm, 5 μ, 100 Å, mobile phase: MeOH/H₂O, gradient from 15% to 90% MeOH in 25 min, flow rate 4.0 ml/min, UV detector, 300 nm, and radioactivity detector) and the resulting fractions were collected.

The isolated fraction containing [¹⁸F]FAZA (198 MBq, ret. time 14-18 min) was then diluted with 30 ml of water of injection and passed through an Oasis C-18 Plus cartridge, where the

[¹⁸F]FAZA was trapped. The cartridge was then washed with 25 ml of water for irrigation and dried (5.2 MBq of non retained activity were detected).

The retained [¹⁸F]FAZA was eluted with EtOH (4 ml), which was evaporated under reduced pressure, to give 130.9 MBq of product.

The latter was redissolved in 1 ml of 10% EtOH and filtered through a 0.22 µm Millex-GV filter to give 99.8 MBq of sterile [¹⁸F]FAZA.

The non-decay-corrected radiochemical yield (RCY) of [¹⁸F]FAZA was 12%, 90 min after the EOB.

Table 3.1. Flow chart of [¹⁸F]FAZA radiosynthesis scheme.

Step I: Nucleophilic fluorination of the FAZA precursor

- (i) [¹⁸F]fluoride trapped on a ChromaFix anion exchange cartridge
- (ii) [¹⁸F]fluoride eluted from the column using K₂CO₃ solution to the reaction vessel
- (iii) Potassium fluoride [¹⁸F] dried by azeotropic distillation with acetonitrile (1 ml)
- (iv) FAZA precursor (5 mg) dissolved in DMSO (0.5 ml) and added to the reaction vessel
- (v) S_N2 fluorination reaction carried out at 100°C for 5 min

Step II: Deprotection

- (i) The reaction mixture was cooled to 30-35°C
- (ii) 0.1 N NaOH (0.5 ml) was added to the reaction vessel
- (iii) Hydrolysis carried out at rt for 3 min
- (iv) Quenching of reaction with 0.2 N HCl (0.5 ml)

Step III: Purification

- (i) The [¹⁸F]FAZA was isolated through HPLC
 - (ii) The [¹⁸F]FAZA fraction was passed through an Oasis C-18 Plus cartridge
 - (iii) [¹⁸F]FAZA was collected by flushing with EtOH and filtered through a 0.22 µm Millex-GV filter
-

Analytical control of di-acetyl[¹⁸F]FAZA and [¹⁸F]FAZA

The radiolabelling procedure was monitored by radio-TLC of the reaction mixture after fluorination and after hydrolysis. The radio-TLC chromatogram after fluorination evidenced two peaks corresponding to the ¹⁸F-labelled intermediate (di-acetyl[¹⁸F]FAZA) and to ¹⁸F-fluoride in traces, respectively [Figure 3.3a]. The radio-TLC of the peak isolated after hydrolysis and HPLC purification confirmed the formation of [¹⁸F]FAZA [Figure 3.3b]. A further evidence is provided by the HPLC chromatogram of [¹⁸F]FAZA after co-elution with commercial “cold” FAZA [Figure 3.4].

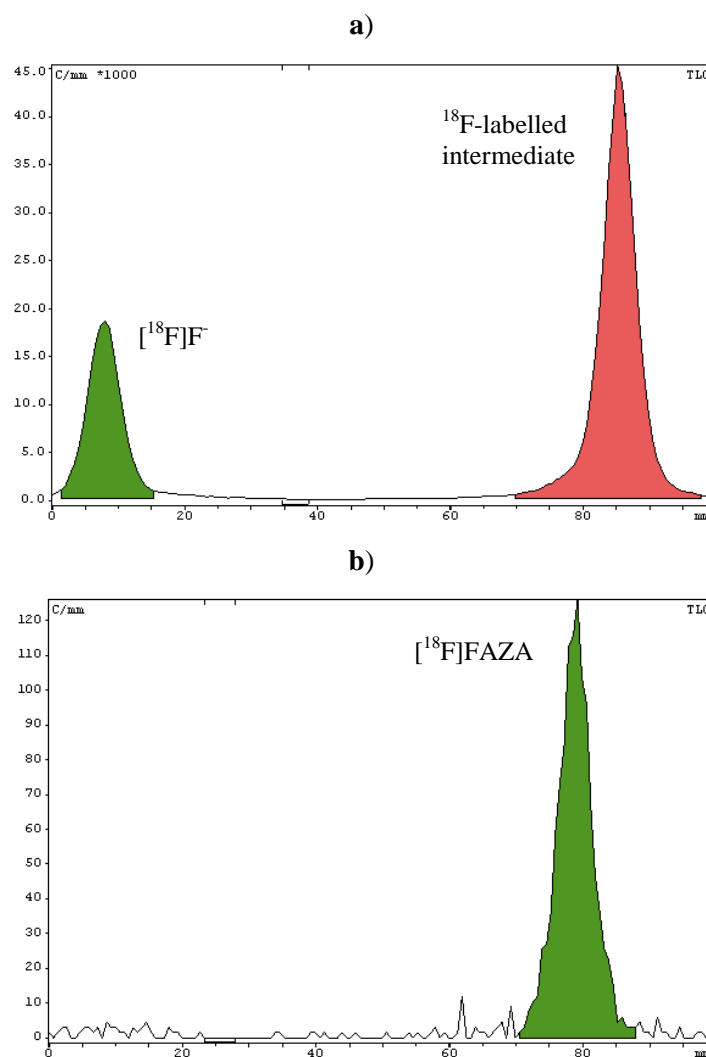


Figure 3.3. Radio-TLC chromatograms: (a) after fluorination (^{18}F -labelled intermediate: $R_f = 0.86$) and (b) after hydrolysis (^{18}F]FAZA: $R_f = 0.80$). mobile phase: ACN/ H_2O 95:5.

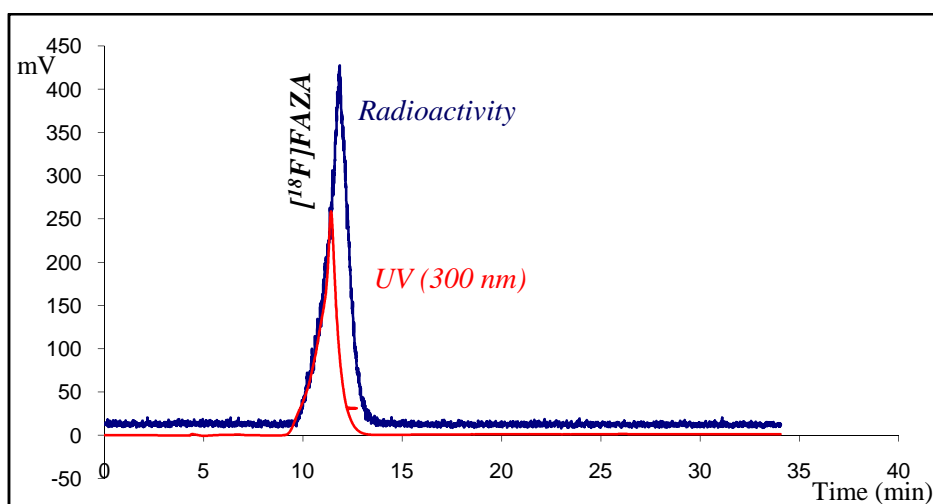


Figure 3.4. HPLC analysis of [^{18}F]FAZA co-eluted with cold FAZA. (analytical column: Phenomenex Luna C_{18} , 4.6 mm x 250 mm, 5 μ , 100 \AA ; mobile phase: MeOH/ H_2O from 15% to 90% MeOH in 30 min; flow rate: 4 mL/min; wavelength: 300 nm). [^{18}F]FAZA retention time = 11.4 min.

3.3.3 [^{18}F]FAZA hypoxia PET imaging

For PET study, 2 transgenic hypoxic mice (PTP1B) (weight: 28-35 g) were injected intravenously with [^{18}F]FAZA tracer (0.30 mL, 21.05 and 27.43 MBq) while sedated with isoflurane. PET studies were performed on anesthetized animals 131 and 247 min after tracer injection. Tracer uptake was clearly visible in the fat of mice [**Figure 3.5**].

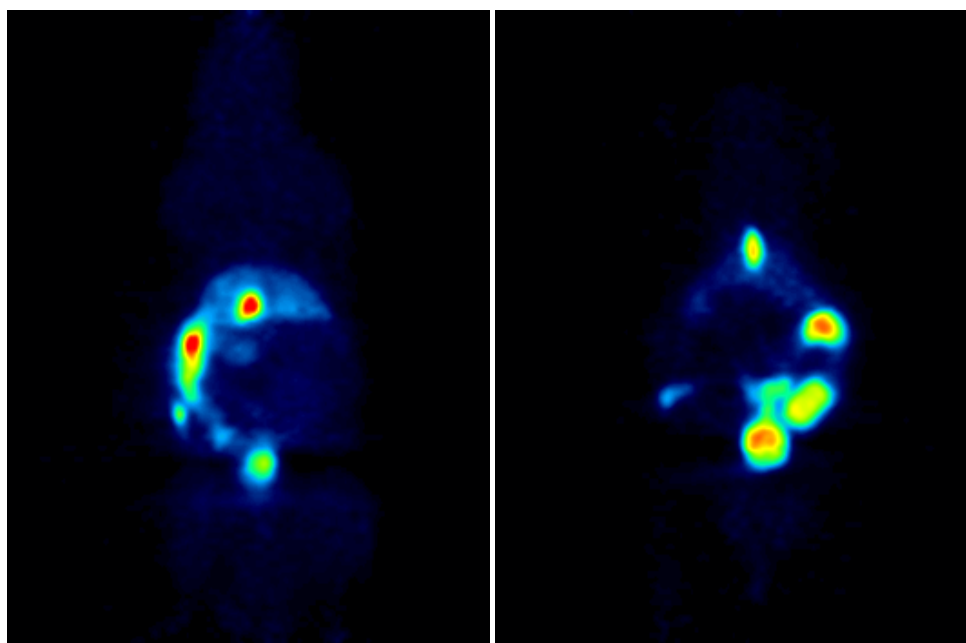


Figure 3.5. PET images of two transgenic hypoxic mice (PTP1B) after PET imaging with [^{18}F]FAZA. The images evidence focal areas of [^{18}F]FAZA uptake in the fat of mice.

3.4 Conclusions

We have developed and achieved an efficient synthesis of the [^{18}F]FAZA precursor and carried out the [^{18}F]FAZA radiosynthesis with a good overall yield.

We conducted a pre-clinical imaging experiment on hypoxic animal models, which showed the [^{18}F]FAZA selective uptake in the fat (the area affected by hypoxia).

Nevertheless further imaging experiments on animal models are required to implement treatment planning of hypoxic tumor tissues in order to be able to assess hypoxia in tumor human patients.

We aim at providing reasonable amounts of [^{18}F]FAZA to be routinely used for detecting hypoxic tumor and evaluating the tumor response to chemo- and radiotherapy in human patients by means of PET.

Chapter 4. Synthesis of a novel potential PET radioligand for hypoxia imaging

4.1 Aim of the project

The aim of the project herein described was to develop an efficient synthesis of a new potential PET tracer for the detection of hypoxia *via* PET methods. Provided that the azomycin moiety is a key structural hallmark which allows for the tracer trapping under hypoxic conditions, and that the radioisotope is essential to image the hypoxic tissue, we aimed at achieving a new 2-nitroimidazole derivative, radiolabelled with a positron emitting radionuclide.

The rationale of this work was the introduction of a peptidomimetic scaffold within a 2-nitroimidazole based structure, to be radiolabelled with the radioisotope fluorine-18 in the final synthetic step, as it is commonly required for all ^{18}F -labeled PET radiotracers, because of the short half life of the radionuclide ($t_{1/2} = 110$ min).

The positron-emitting isotope fluorine-18 could be introduced *via* nucleophilic substitution conditions, involving the displacement of a suitable leaving group by the non-carrier-added ^{18}F -fluoride ion, produced through a cyclotron [Figure 4.1].

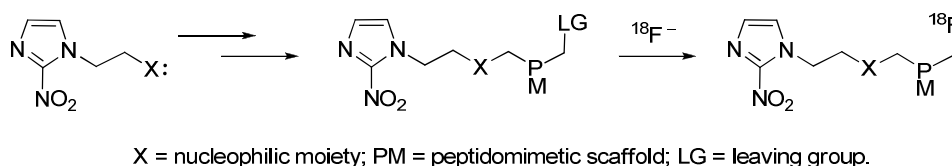
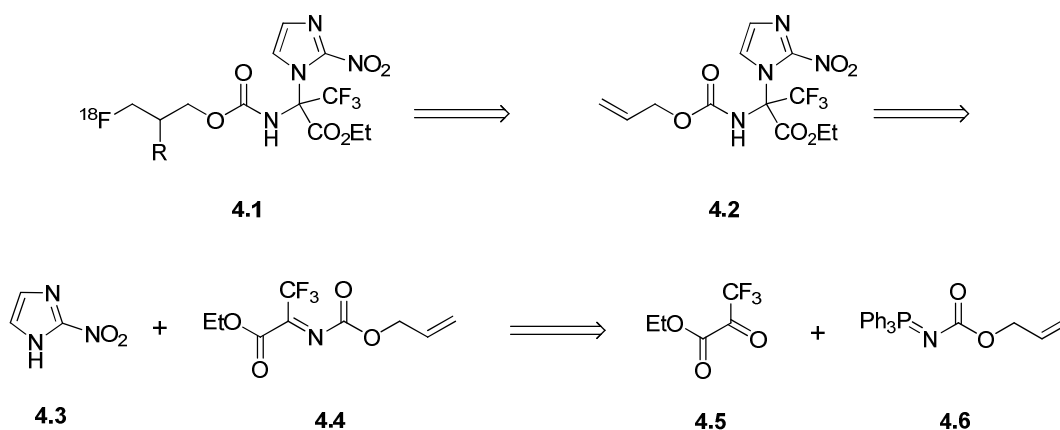


Figure 4.1. General synthetic route to the new potential hypoxia tracer.

We initially aimed at obtaining the peptidomimetic intermediate **4.2** from the reaction of 2-nitroimidazole **4.3** with a suitable electrophile, such as the aza-Wittig product **4.4**.

Afterwards, the intermediate **4.2** could be sequentially modified at the allyl terminal function in order to introduce a good leaving group and, finally, the radionuclide fluorine-18 by a radiolabelling procedure [Scheme 4.1].



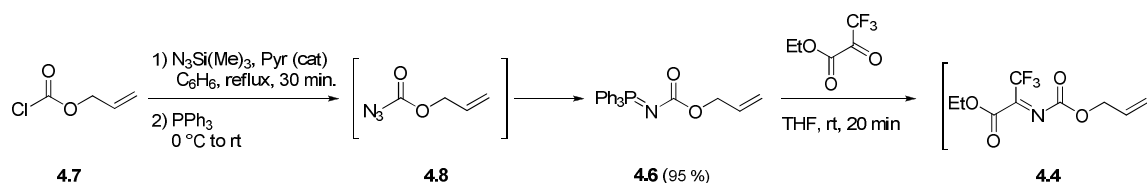
Scheme 4.1. Retrosynthetic pathway for the new PET hypoxia radiopharmaceutical.

4.2 Results and discussion

4.2.1 Synthesis of trifluoro-*N*-alcoxy carbonylimino intermediate

The trifluoro-*N*-alcoxy carbonylimino intermediate **4.4** was easily synthesised by reacting the phospho- λ^5 -azene **4.6** with highly electrophilic 3,3,3-trifluoroethyl pyruvate **4.5**, under anhydrous conditions.

Treatment of the commercially available allyl chloroformate (**4.7**) with trimethylsilylazide ($\text{N}_3\text{Si}(\text{Me})_3$), in the presence of a catalytic amount of pyridine, followed by reaction of the resulting intermediary azide (**4.8**) with triphenylphosphine, allowed to achieve the iminophosphorane **4.6** [Scheme 4.2], according to a Staudinger-reaction mechanism.



Scheme 4.2. Synthesis of trifluoro-*N*-alcoxy carbonylimino intermediate (**4.4**).

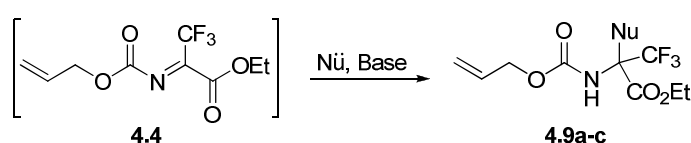
The azomycin **4.3** was thought to be reactive towards strong electrophiles, given the presence of the nitrogen atom at the 3 position, therefore we argued that its treatment with **4.4** could give rise to the coupling product **4.2**. Surprisingly, we observed that the only product we could isolate was the hydrate of the intermediate **4.4**.

However, we expected the trifluoro-*N*-alkoxycarbonylimino derivative **4.4** to be strongly reactive, as several works in literature described the wide application of aza-Wittig reaction products in the synthesis of optically pure fluorinated molecules⁵¹.

We assumed that the strong electron-withdrawing capacity of the nitro-group decreased the reactivity of the imidazole ring, thus preventing the reaction product to take place.

The hydrated product was also isolated when stoichiometric amounts of deprotonating bases such as NaH and DIPEA were used in order to increase the nitroimidazole ring reactivity [Table 4.1].

We obtained the formation of the desired coupling product when we performed the reaction between **4.4** and more nucleophilic species such as imidazole and piperidine [Table 4.1], thus demonstrating that the nitro-group played a strongly de-activating role during the reaction.



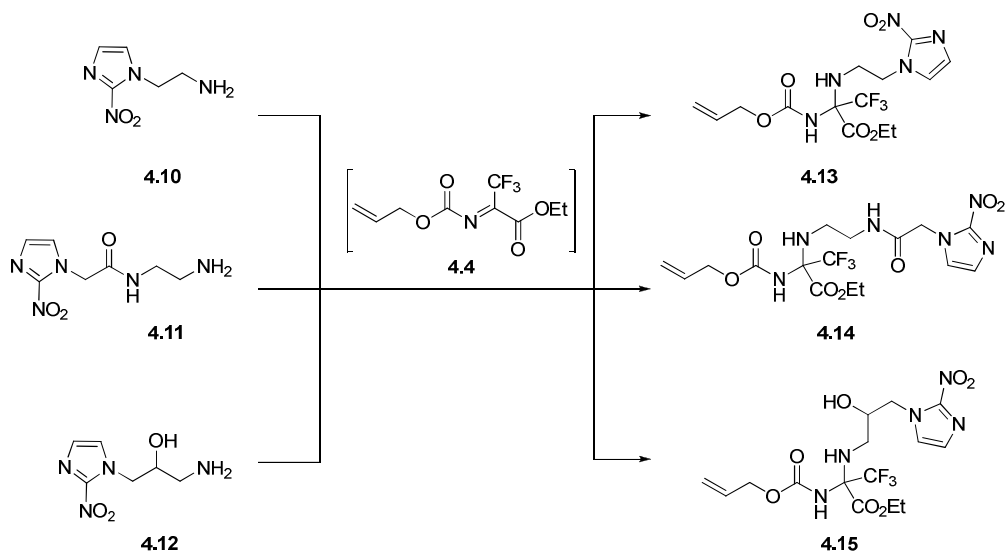
Scheme 4.3. Planned introduction of nitroimidazole by using a base.

Table 4.1. Attempts to introduce 2-nitroimidazole, and introduction of imidazole and piperidine

Entry	Nu:	Base	Solvent	Temperature	Product	Yield %
1		NaH	dry THF	0°C to r.t.		36
2			dry THF	r.t.		28
3		none	dry THF	r.t.		quant.
4		none	dry THF	r.t.		55
5		none	dry THF	r.t.		25

Given the lack of reactivity by 2-nitroimidazole, we tried a different synthetic step aimed at introducing a nucleophilic moiety at the 1 nitrogen of 2-nitroimidazole, namely an aminoalkyl-chain, which could be more nucleophilic towards the imine **4.4**, affording the corresponding derivatives **4.13**, **4.14**, and **4.15**.

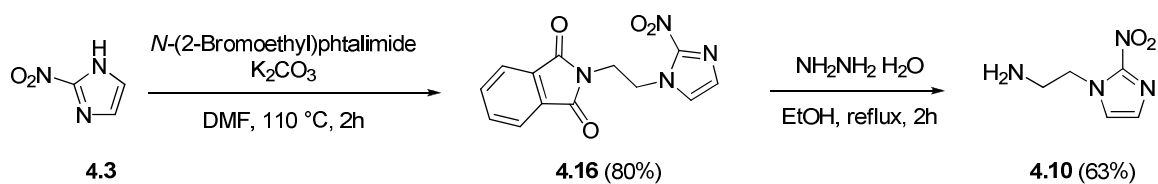
Amongst the possible aminoalkyl-nitroimidazole candidates, we focused on the one bearing an aminoethyl function on the nitrogen at 1 position (**4.10**) [Scheme 4.4].



Scheme 4.4. Alternative synthetic route to different nitroimidazole compounds.

4.2.2 Synthesis of *N*-ethylamino-2-nitroimidazole

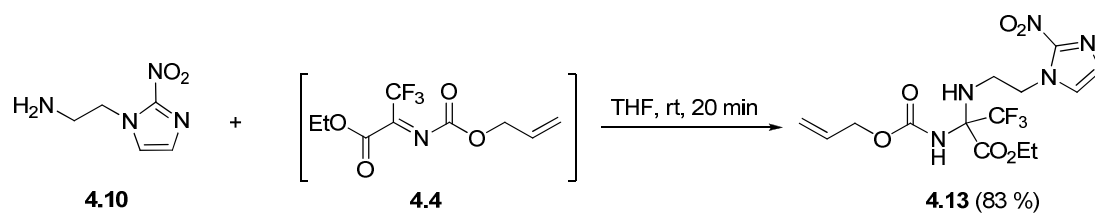
The preparation of *N*-ethylamino-2-nitroimidazole **4.10** started with the alkylation of 2-nitroimidazole **4.3** with the commercially available (2-bromoethyl)phthalimide, producing the corresponding phthalimide **4.16**, which was subsequently deprotected by treatment with hydrazine monohydrate to afford the desired amine intermediate in satisfactory yields [Scheme 4.5].



Scheme 4.5. Synthesis of 2-(2-nitro-1H-imidazolyl)ethylamine (4.8).

4.2.3 Introduction of 2-nitroimidazole functionality

The preparation of racemic nitroimidazole derivative (**4.13**) was obtained in very good yields by reaction between the imine **4.4** formed *in situ* and the nucleophilic aminoethyl-2-nitroimidazole (**4.10**), under dry conditions, in order to avoid the possible formation of the hydrate (**4.9 a**) [Scheme 4.6].



Scheme 4.6. Synthesis of nitroimidazole peptidomimetic derivative **4.13**.

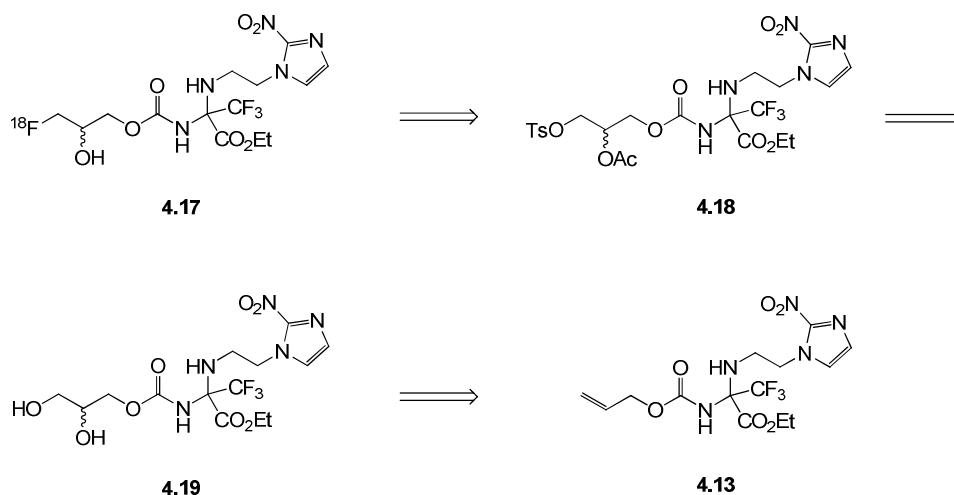
4.2.4 Synthesis of the precursor for ^{18}F -radiolabelling

In our retrosynthetic strategy the oxidation of the olefinic bond of **4.13** under Upjohn conditions⁵² would give rise to the corresponding *syn*-1,2-diol (**4.19**).

Selective tosylation of the primary hydroxyl group in **4.19**, followed by the protection of the secondary alcohol moiety with acetic anhydride were planned to give the corresponding protected diol (**4.18**).

The latter, sequentially submitted to nucleophilic substitution and basic hydrolysis, would be converted into the desired fluorinated derivative (**4.17**).

The fluorination reaction was expected to be easily performed, given the ability of the tosyl group to work as a good leaving group, which allows its wide use in ^{18}F -radiolabelling chemistry [Scheme 4.7].



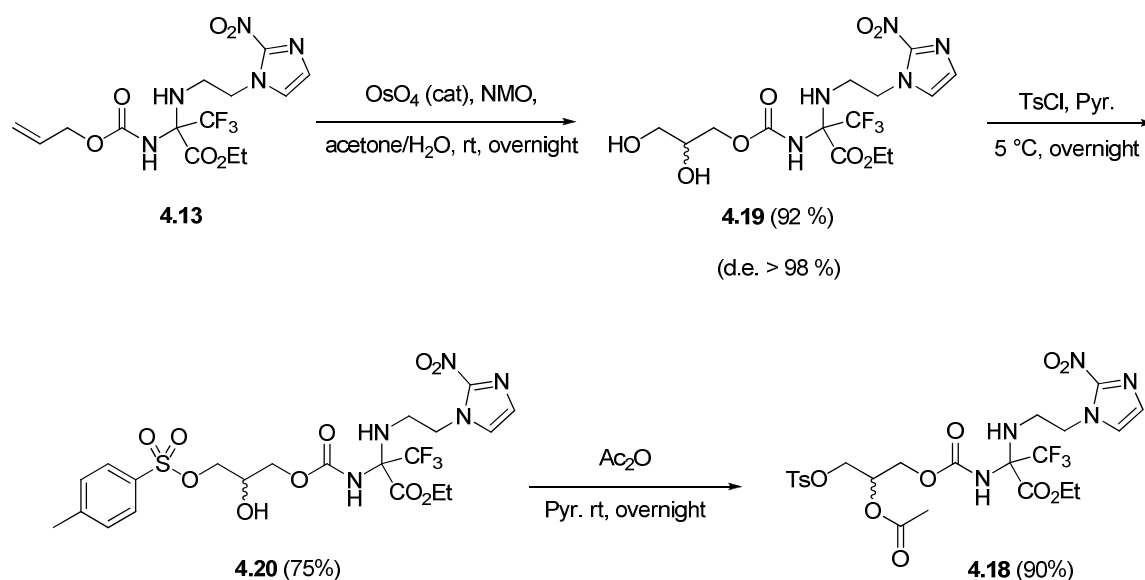
Scheme 4.7. Retrosynthetic approach towards the new potential fluorinated 2-nitroimidazole tracer.

Results and discussion

Oxidation of the olefinic bond of **4.13** was performed with stoichiometric amounts of *N*-methylmorpholine-*N*-oxide (NMO) in the presence of 5 mol % osmium tetroxide, according to the Upjohn procedure [Scheme 4.8]. Surprisingly we achieved the desired *syn*-diol (**4.19**) with de > 98%. We assumed that this result arose from the ability of 2-nitroimidazole ring to work similarly to chiral amines involved in the Sharpless dihydroxylation, namely coordinating the osmium atom and directing the oxidation in an intramolecular manner.

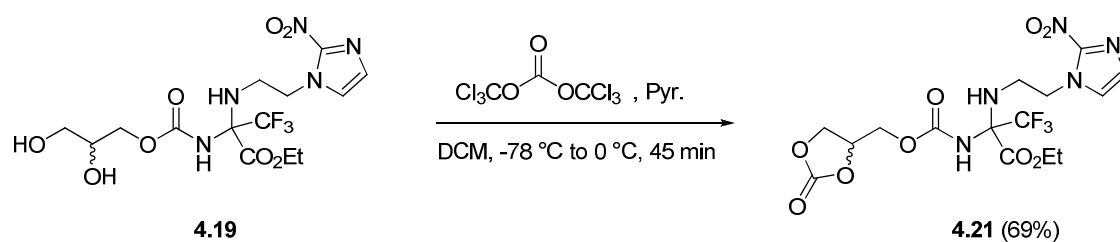
We then performed the tosylation of the *syn*-1,2-diol **4.19** at 5°C using pyridine both as a solvent and base, achieving reasonable yields of the corresponding protected primary alcohol (**4.20**).

The final acetylation of the secondary alcohol moiety in **4.20** by a large excess (8 eq.) of acetic anhydride afforded the protected precursor **4.18** in 90 % yield [Scheme 4.8].



Scheme 4.8. Synthesis of the precursor for [^{18}F]-radiolabelling; NMO = *N*-Methylmorpholine-*N*-oxide, TsCl = Tosyl chloride, Py = pyridine, Ac_2O = acetic anhydride.

In order to achieve a crystalline compound and assess its stereochemistry, (\pm)-**4.19** was converted into the cyclic carbonate derivative (**4.21**), after treatment with pyridine and triphosgene in CH_2Cl_2 , at -78 °C to 0 °C [Scheme 4.9].



Scheme 4.9. Derivatization of *syn*-1,2-diol (4.19) into cyclic carbonate (4.21).

The crystallization of the carbonate derivative (4.21) either with diisopropyl ether or hexane/EtOAc was unsuccessful in affording suitable crystals and further attempts of derivatization and crystallization are currently in progress.

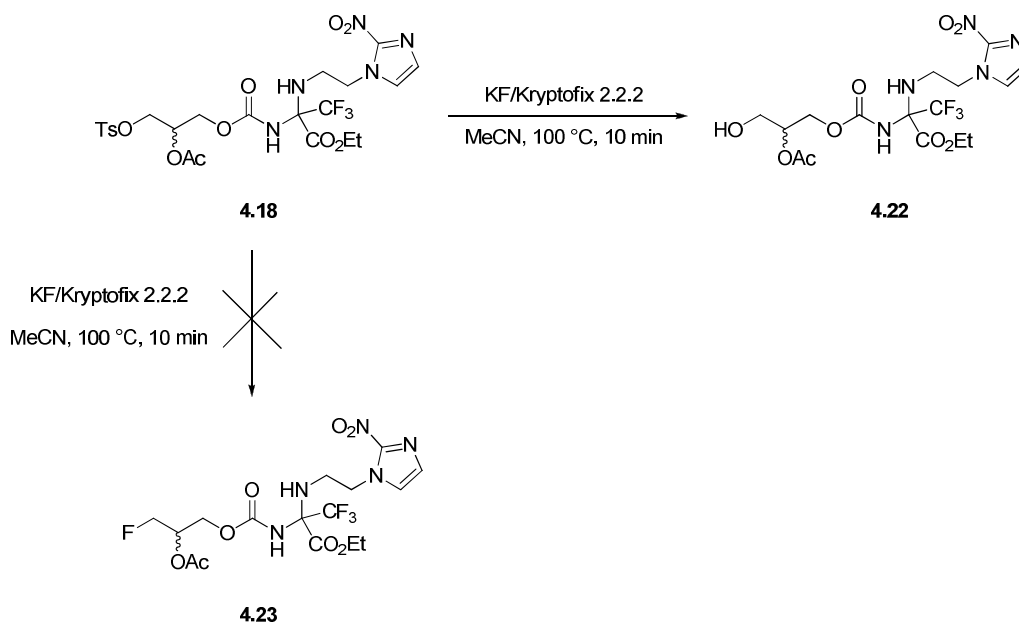
4.2.5 Introduction of ^{18}F -radionuclide

In order to introduce a ^{18}F -radionuclide into the precursor 4.18 in the hot cell, we first attempted the cold fluorination by using KF in the presence of the phase-transfer reagent Kryptofix-222 (K_{222}) in a dry polar aprotic solvent such as acetonitrile, at $100\text{ }^\circ\text{C}$, as this is a suitable and feasible procedure commonly adopted in the production of a large number of PET-tracers.

As already mentioned, K-2.2.2 plays a crucial role during fluorination, since it improves the reactivity of fluoride ion by forming a strong complex with the potassium cation, thus leaving the fluoride ion naked and highly nucleophilic.

However, in our case the fluorinated derivative (4.23) could not be isolated, and the product deprotected at the primary carbon (4.22) was formed instead (TLC monitoring and MS analysis) [Scheme 4.10].

Conceivably, this result was related to the harsh reaction conditions ($100\text{ }^\circ\text{C}$ temperature), leading both to the degradation of the starting material and formation of the undesired deprotected product (4.22).



Scheme 4.10. Cold fluorination with KF/Kryptofix 2.2.2.

According to several works reported in literature^{53,54}, the use of a polar solvent as a reaction medium along with a cesium halide in S_N2 reactions enhances the nucleophilicity of fluoride anion and the rate of substitution, reflecting the ability of nonpolar protic solvent to form a strong hydrogen bonding with the fluoride ion of the CsF salt, thus weakening the ionic bond of the salt. However, treatment of the 2-nitroimidazole precursor **4.18** with CsF, using both *t*-BuOH and *t*-amyl alcohol as polar solvents at 80°C resulted in the formation of detosylated product (**4.22**) (assessed by MS), and the same outcome was achieved by using CsF in *t*-amyl alcohol at rt.

A further fluorination attempt involving TBAF (1 M THF solution) as fluoride source instead of CsF and dry THF as polar aprotic solvent failed in giving the expected product **4.23**.

Nevertheless, an ongoing work is focused on the achievement of the best “cold” reaction conditions in order to introduce the fluorine atom into the synthesised precursor.

All the previous attempts to introduce the fluorine atom are listed in the following table [Table 4.2].

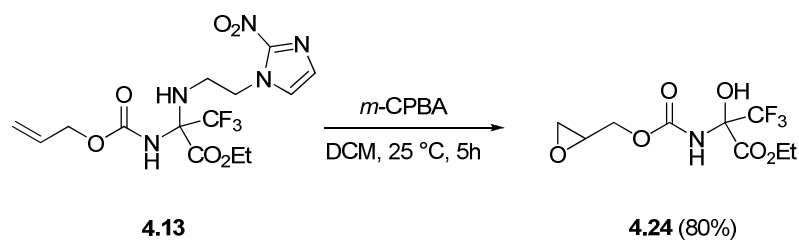
Table 4.2. “Cold” fluorination conditions.

MF	Solvent	Reaction temp (°C)	Yield
KF/K 2.2.2.	dry MeCN	100	n.r. ^a
CsF	<i>t</i> -BuOH	80	n.r. ^a
CsF	<i>t</i> -amyl alcohol	80	n.r. ^a
CsF	<i>t</i> -amyl alcohol	rt	n.r. ^a
TBAF	dry THF	rt	n.r. ^a

^aNo reaction occurred: the starting material was consumed (TLC monitoring) and the non-tosylated product was formed (MS assessment).

An alternative route to the synthesis of the final fluorinated 2-nitroimidazole compound **4.17** consisted in the epoxidation of double bond in **4.13** followed by the epoxide ring opening by fluoride.

The oxidation of **4.13** with *m*-CPBA afforded the desired epoxide at the allylic portion, however the strongly acidic conditions, due to the *in situ* formation of *m*-chloro benzoic acid as by-product, we isolated the hydrolysis product missing the amino ethylimidazole function (**4.24**) [Scheme 4.11].



Scheme 4.11. Epoxidation of alkene function of 4.13.

4.3 Conclusions

We developed an efficient and reproducible synthesis of the precursor of a new potential PET hypoxia radiotracer from satisfactory to very good overall yields.

The rationale was the construction of a 2-nitroimidazole ^{18}F -radiolabelled compound with a peptidomimetic building block in its structure.

Different fluorinating procedures were attempted without success and a number of synthetic routes to the ^{18}F -fluorinated compound are currently under investigation and evaluation.

However the radiolabelling procedure involving the nucleophilic displacement of a good leaving group on the precursor molecule by ^{18}F -fluoride ion is still thought to represent the method of choice.

Furthermore we observed a diastereoselective (de > 98%) synthesis of a *syn*-1,2-diol (**4.19**), which was presumably formed through a Sharpless-like mechanism, involving the intramolecular participation of 2-nitroimidazole ring as a ligand, which could enable osmium tetroxide (OsO_4) to selectively oxidize one face of the alkene (**4.13**) over the other.

This hypothesis has to be further investigated by assessing the stereochemistry of the diol through single crystal X-ray diffraction and NMR analysis of reaction mechanism.

The Ts-Ac-nitroimidazole precursor (**4.18**) resulted chemically labile under strong acidic conditions and unstable at high temperatures (over 80 °C).

Chapter 5. Sulfoxides as carbanion equivalents

5.1 Introduction

The concept of polarity inversion of functional groups has been extensively exploited in organic synthesis for the production of several synthetic synthons, since it was introduced in the mid 1960 by Corey and Seebach⁵⁵, who defined *umpolung* as ‘any process by which donor and acceptor reactivity of an atom are interchanged’⁵⁶. In their pioneering work they converted an electrophilic acyl carbon into a nucleophilic acylating agent by protecting the carbonyl group of an aldehyde as dithioacetal.

The idea of polarity inversion was then applied in organic synthesis to achieve a number of different substrates, involved in organometallic chemistry, aromatic chemistry and peptide chemistry.

Importantly, the polarity reversal has been extensively studied also in the field of sulfoxide chemistry.

Sulfoxides are a class of organic compounds which have found a large use as chiral auxiliaries, for the stereoselective synthesis of biologically important compounds, such as β -amino-alcohols, β -chloroamines and aziridines^{57,58}.

α -sulfinyl carbanions have demonstrated to be suitable chiral intermediates to perform stereoselective C-C bond forming reactions, by alkylating with proper electrophiles, Michael addition to α,β -unsaturated systems, addition to C=O bonds of aldehydes and ketones and addition to C=N bonds of imines.

Enantiomerically pure α -Li sulfoxides have been used as chiral α -hydroxy, α -chloro carbanion equivalents with alkyl and aryl imines in a two-step procedure, involving 1) a C-C bond forming reaction leading to β -sulfinyl amines and a 2) ‘non-oxidative’ Pummerer reaction (NOPR) or chloro-Pummerer reaction (NOCPR), which allow for replacing the sulfinyl auxiliary by an OH or a Cl atom, respectively, with an S_N2-like pathway (stereoinversion at carbon).

In this chapter a new application of α -Li sulfoxides as α -acetamido benzyl carbanion equivalents for the synthesis of acetamido derivatives is described, together with their use for the production of α -benzyl alcohols and chlorides.

5.2 Results and discussion

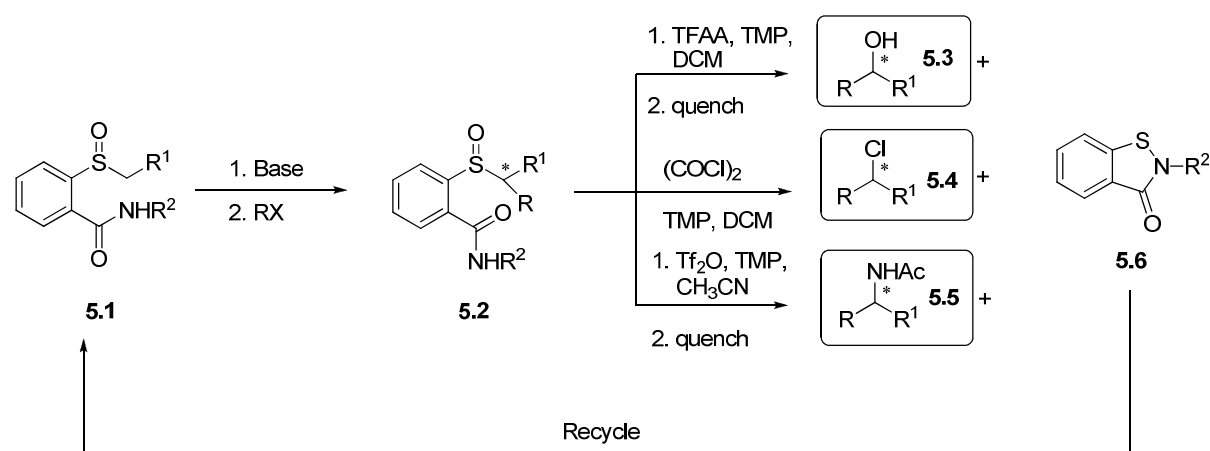
The C-alkylation of racemic *ortho*-[(*N*-alkyl)carbamoyl]phenylsulfoxide **5.1** with a suitable halide, in the presence of a base, was planned to afford the α -alkylsulfoxide **5.2**. The latter, after treatment with trifluoroacetic anhydride (TFAA) or oxalyl chloride, in the presence of *sym*-collidine (TMP) in DCM, was expected to give rise to NOPR and NOCPR-like outcomes, namely the alcohol **5.3** and the chloride **5.4**, respectively.

The acetamide **5.5** could be achieved by using trifluoromethanesulfonic anhydride (Tf₂O) in the presence of TMP and MeCN.

Acetonitrile was thought to play both the role of solvent and nucleophile, as we assumed that the reaction product **5.5** could take place through the formation of a carbocationic intermediate.

When Tf₂O is used as a promoter of the Pummerer reaction, the poor nucleophilic TfO⁻, formed after sulfinyl addition of **5.2** to Tf₂O, should not attack the carbocationic species, which should be trapped by the more nucleophilic acetonitrile instead.

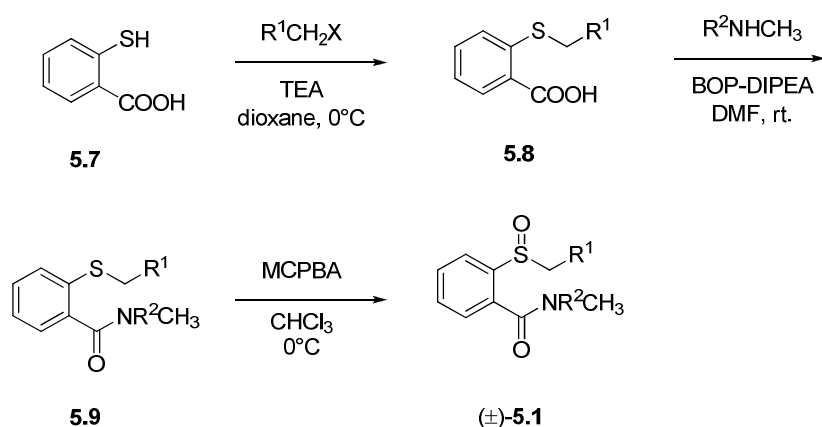
The synthetic pathway proposed in the scheme **5.1** below leads to the formation of benzoisothiazolone **5.6** as the co-product. The latter could be converted to the starting sulfoxide **5.1** by regioselective reduction of the N-S bond, followed by S-alkylation of thiophenol and oxidation of the resulting sulfide.



Scheme 5.1. Planned synthetic strategy.

5.2.1 Synthesis of sulfoxides **5.1**

The synthesis of racemic sulfoxides (\pm)-**5.1** started with S-alkylation of commercially available thiosalicylic acid with alkyl halides, affording the *ortho*-carboxy sulfides (**5.8**), which were transformed into amides by coupling with CH₃NH₂ and (CH₃)₂NH, and oxidized with MCPBA to (\pm)-**5.1a-g** in good overall yields [Scheme 5.2, Table 5.1].



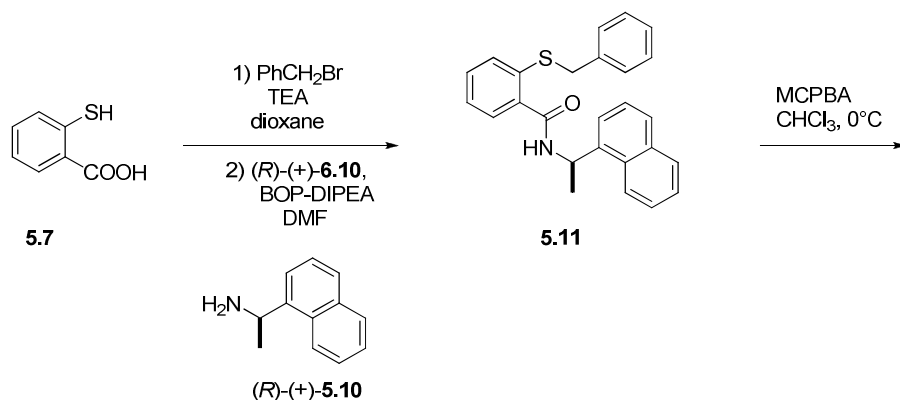
Scheme 5.2. Synthesis of racemic sulfoxides (±)-5.1.

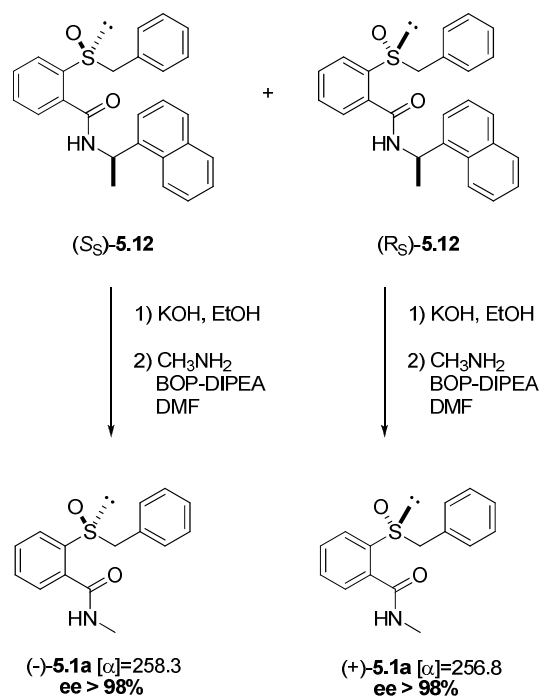
Table 5.1. Synthesis of sulfoxides (±)-5.1.

Entry	Prod.	X	R ¹	R ²	Yield ^a (%)
1	5.1a	Br	C ₆ H ₅	H	82
2	5.1b	Br	4-MeO-C ₆ H ₄	H	78
3	5.1c	Br	4-CF ₃ -C ₆ H ₄	H	68
4	5.1d	Br	4-NO ₂ -C ₆ H ₄	H	75
5	5.1e	Br	Et	H	81
6	5.1f	I	H	H	77
7	5.1g	Br	Ph	Me	84

^a Overall isolated yield from thiosalicylic acid.

Enantiomerically pure sulfoxides (+)-**5.1a** and (-)-**5.1a** were synthesised starting by S-alkylation of thiosalicylic acid (**5.7**) with benzyl bromide followed by coupling with enantiomerically pure (+)-2-β-naphthyl-ethylamine. Oxidation of sulphide **5.11** with MCPBA afforded an equimolar ratio of the two diastereoisomers (*S_S*)- and (*R_S*)-**5.12**, which were separated by flash chromatography. The following hydrolysis with KOH in refluxing ethanol and coupling with CH₃NH₂ yielded the products (+)-**5.1a** and (-)-**5.1a** with ee > 98% [**Scheme 5.3**].





Scheme 5.3. Preparation of enantiomerically pure sulfoxides $(+)$ -**5.1a** and $(-)$ -**5.1a**.

5.2.2 Alkylation of sulfoxides **5.1**

Several reaction conditions for alkylation of (\pm) -**5.1** were investigated, in order to optimize yield and diastereoselectivity, by modifying different reaction parameters, such as base, co-solvents and reagents equivalents [Table 5.2].

Table 5.2. Reaction conditions for alkylation of (\pm) -**5.1a**.

Entry	Base (equiv)	Co-solvent (equiv)	de ^a (%)	Yield ^b (%)
1	LDA (2.1)	None		n.r. ^c
2	LDA (1.05) BuLi (1.05)	None	<5	11
3	BuLi (2.1)	None	<5	32
4	BuLi (2.1)	HMPA (2.4)	94	19 ^d
5	BuLi (2.1)	HMPA (2.4)	94	55 ^e
6	BuLi (2.1)	TMEDA (2.4)		n.r. ^{c,e}
7	BuLi (2.1)	HMPA (5.0)	94	92 ^e

^a Measured by HPLC/¹H-NMR

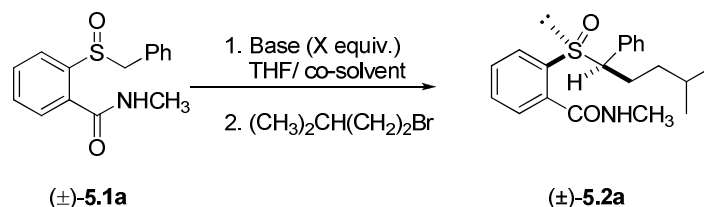
^b Overall isolated yield.

^c No reaction occurred and the starting sulfoxide was almost completely recovered.

^d HMPA was added after deprotonation with BuLi.

^e Co-solvent was added before BuLi.

The sulfoxide (\pm)-**5.1** and 1-Br-3-methylbutane were selected as reaction partners for alkylation, before proceeding to the preparation of a library of alkylated sulfoxides (\pm)-**5.1** [Scheme 5.4].



Scheme 5.4. Alkylation of (\pm)-**5.1a** with 1-Br-3-methylbutane.

Since lithium amides and alkyl lithium reagents are commonly used for deprotonating the α -proton of a sulfoxide, we first treated benzyl sulfoxide (\pm)-**5.1a** with 2.1 equiv. of LDA (the first equivalent is quenched by the amidic proton) before adding the halide. However, the desired product was not formed, and the starting material was recovered almost quantitatively [entry 1, Table 5.2].

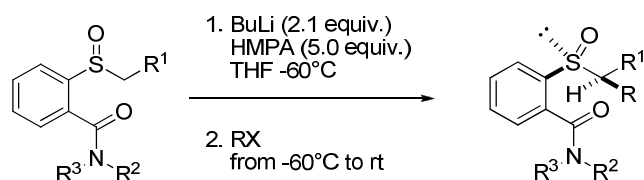
When both LDA (1.05 equiv.) and BuLi (1.05 equiv.) were used as deprotonating agents, only small amounts of product were formed (11% yield) and an almost equimolar diastereomeric ratio was assessed [entry 2, Table 5.2]. The same diastereomeric ratio was obtained by using 2.1 equiv. of BuLi, however the yield was increased (32%) [entry 3, Table 5.2].

The addition of a co-solvent such as HMPA was thought to increase both yield and diastereoselectivity, given the ability of HMPA to sequester the lithium ion, thus rendering the C-N-bis anion more reactive. Interestingly, the diastereomeric excess was increased up to 94%, when 2.4 equiv. of HMPA were added after deprotonation with BuLi (2.1 equiv.) even if the yield was still too low (19%) [entry 4, Table 5.2].

However, it was possible to raise the yield (55%) by adding the co-solvent (2.4 equiv.) before the deprotonation with BuLi, and the same diastereomeric excess (94%) was obtained [entry 5, Table 5.2].

Finally, the use of 5 equiv. of HMPA and 2.1 equiv. of BuLi allowed to give high yields (92%) of alkylated sulfoxide (\pm)-**5.2a** along with a high diastereoselectivity [94%, entry 7, Table 5.2].

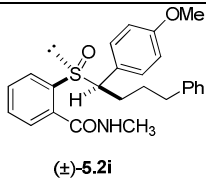
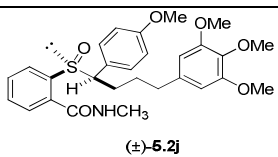
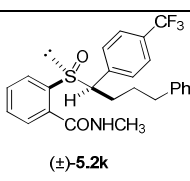
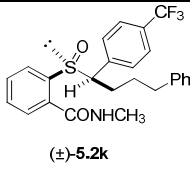
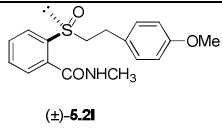
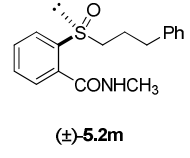
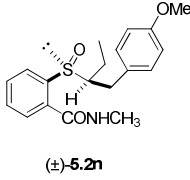
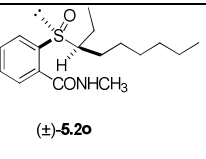
The optimized conditions thus obtained were then applied to the synthesis of different alkylated sulfoxides (\pm)-**5.2**, achieved by reacting *ortho*-[(*N*-alkyl)carbamoyl]phenyl sulfoxides **5.1** with different alkyl halides [Scheme 5.5, Table 5.3].

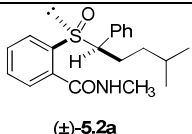


Scheme 5.5. Alkylation of ortho-[(N-alkyl)carbamoyl]phenyl sulfoxides.

Table 5.3. Alkylation of ortho-[(N-alkyl)carbamoyl]phenyl sulfoxide.

Entry	Substrate	R ¹	R ²	R ³	Alkyl halide	Product	d.e. ^a	Yield % ^b
1	(±)- 5.1a	Ph	Me	H	PhCH ₂ Br		58	96
2	(±)- 5.1a	Ph	Me	H	(E)-CH ₃ CH=CHCH ₂ Br		66	79
3	(±)- 5.1a	Ph	Me	H	CH ₃ I		50	48 ^c
4	(±)- 5.1a	Ph	Me	H	Ph(CH ₂) ₃ Br		94	74
5	(±)- 5.1a	Ph	Me	H	CH ₂ =CH(CH ₂) ₃ Br		92	95
6	(±)- 5.1a	Ph	Me	H	CH ₃ (CH ₂) ₄ Br		88	69
7	(±)- 5.1a	Ph	Me	H	CH ₃ (CH ₂) ₄ I		86	65
8	(±)- 5.1a	Ph	Me	H	CH ₃ (CH ₂) ₂ I		92	74

9	(±)- 5.1b	4-MeO-Ph	Me	H	Ph(CH ₂) ₃ Br	 (±)- 5.2i	86	78
10	(±)- 5.1b	4-MeO-Ph	Me	H	(3,4,5-triMeO-C ₆ H ₂)-(CH ₂) ₃ Br	 (±)- 5.2j	96	88
11	(±)- 5.1c	4-CF ₃ -Ph	Me	H	Ph(CH ₂) ₃ Br	 (±)- 5.2k	78	51
12	(±)- 5.1c	4-CF ₃ -Ph	Me	H	Ph(CH ₂) ₃ Br	 (±)- 5.2k	42 ^e	65 ^d
13	(±)- 5.1d	4-NO ₂ -Ph	Me	H	Ph(CH ₂) ₃ Br	–	–	n.r. ^e
14	(±)- 5.1f	H	Me	H	(4-MeO-C ₆ H ₄)CH ₂ Cl	 (±)- 5.2l	–	62
15	(±)- 5.1f	H	Me	H	Ph(CH ₂) ₃ Br	 (±)- 5.2m	–	85
16	(±)- 5.1e	Et	Me	H	(4-MeO-C ₆ H ₄)CH ₂ Cl	 (±)- 5.2n	32	70
17	(±)- 5.1e	Et	Me	H	CH ₃ (CH ₂) ₅ Br	 (±)- 5.2o	< 5	60
18	(±)- 5.1g	Ph	Me	Me	PhCH ₂ Br	–	–	n.r. ^e
19	(+)- 5.1l	Ph	(<i>S</i>)-(1-C ₁₀ H ₇)C H(CH ₃)	H	PhCH ₂ Br	–	–	n.r. ^e

20	(S)(-)- 5.1a	Ph	Me	H	(CH ₃) ₂ CH(CH ₂) ₂ Br	 (±)- 5.2a	94	92 ^f
----	---------------------	----	----	---	--	--	----	-----------------

^a Measured by HPLC/¹H NMR..

^b Overall isolated yield.

^c A 34% of the corresponding *C,N*-dimethylated product was recovered.

^d Reaction stopped after 330 min (-70 °C → rt).

^e No reaction occurred.

^f No epimerization at sulfur occurred.

^g Reversal of diastereoselectivity was obtained

The reaction of sulfoxide (±)-**5.1a** with benzyl bromide and crotyl bromide afforded the desired products (±)-**5.2b,c**, respectively, with high yield and good diastereoselectivity [entries **1 and 2**, Table **5.3**]. When the sulfoxide (±)-**5.1a** was treated with the less hindered and highly reactive methyl iodide, we observed the formation of the corresponding methylated product (±)-**5.2d**, however both yield and diastereocontrol were low, because of the concomitant formation of the *C,N*-dimethylated product [entry **3**, Table **5.3**].

Bromides, such as 1-Br-3-Ph-propane, 1-Br-4-pentene, and 1-Br-pentane reacted smoothly with sulfoxide (±)-**5.1a**, leading to the formation of alkylated sulfoxides (±)-**5.2e-g**, respectively, with good yields and high diastereoselectivities [entries **4-6**, Table **5.3**]. 1-I-pentane reacted with sulfoxide (±)-**5.1a** affording the corresponding product (±)-**5.2g** with yield and diastereocontrol similar to those obtained with the brominated derivative [entry **7**, Table **5.3**]. Also the reaction of 1-I-propane with (±)-**5.1a** produced the desired (±)-**5.2h** with high yield and diastereoselectivity [entry **8**, Table **5.3**].

The alkylation of the electron-rich substrate (±)-**5.1b** with 1-Br-3-Ph-propane and 1-Br-3-(3,4,5-triMeO)C₆H₂-propane gave the corresponding products (±)-**5.2i,j**, respectively, with high yields and diastereoselectivities [entries **9, 10**, Table **5.3**]. On the other hand, although the reaction of *p*-CF₃-Bn sulfoxide (substrate (±)-**5.1c**) with 1-Br-3-Ph-propane at -60°C afforded the desired (±)-**5.2k**, the yield and diastereoselectivity were low and, when the reaction temperature was raised to rt, in order to increase the yield, and inversion of diastereoselectivity was observed [entries **11 and 12**, Table **5.3**]. The reaction of less nucleophilic *p*-NO₂-Bn-sulfoxide (±)-**5.1d** with 1-Br-3-Ph-propane did not give the desired alkylated product and a complex mixture of products was formed when the temperature was allowed to reach rt [entry **13**, Table **5.3**]. Reaction of sulfoxide (±)-**5.1f** with *p*-MeO-benzyl chloride and 1-Br-3-Ph-propane resulted in the formation of alkylated products (±)-**5.2l,m**, respectively, with high yields [entries **14, 15**, Table **5.3**]. The ethyl sulfoxide (±)-**5.1e** did not give satisfactory results, when it was treated with *p*-MeO-benzyl

chloride and 1-Br-pentane. In the latter case, an almost equimolar ratio of diastereoisomers (\pm)-**5.2o** was observed.

Importantly, no reaction occurred when the dimethylamide (\pm)-**5.1g** was treated with highly reactive benzyl bromide [entry 18, Table 5.3], thus suggesting that the *ortho*-lithiated amide function is involved in the reaction mechanism.

Finally, the treatment of enantiomerically pure (+)-**5.1i** with benzyl bromide failed in giving the desired alkylated product, probably because of steric factors [entry 19, Table 5.3], while when the less hindered enantiomerically pure sulfoxide (S)-(-)-**5.1a** was reacted with 1-Br-3-methylbutane, the corresponding product (-)-**5.2a** was obtained without loss of ee [entry 20, Table 5.3].

5.2.3 Use of *umpolung* sulfoxide reagents 5.2

The sulfoxides **5.2** were thought to provide NOPR and NOCPR-like outcomes, when we noticed the spontaneous decomposition of sulfoxide (\pm)-**5.2b** to (*E*)-stilbene and benzisothiazolone **5.6** after prolonged storage at rt.

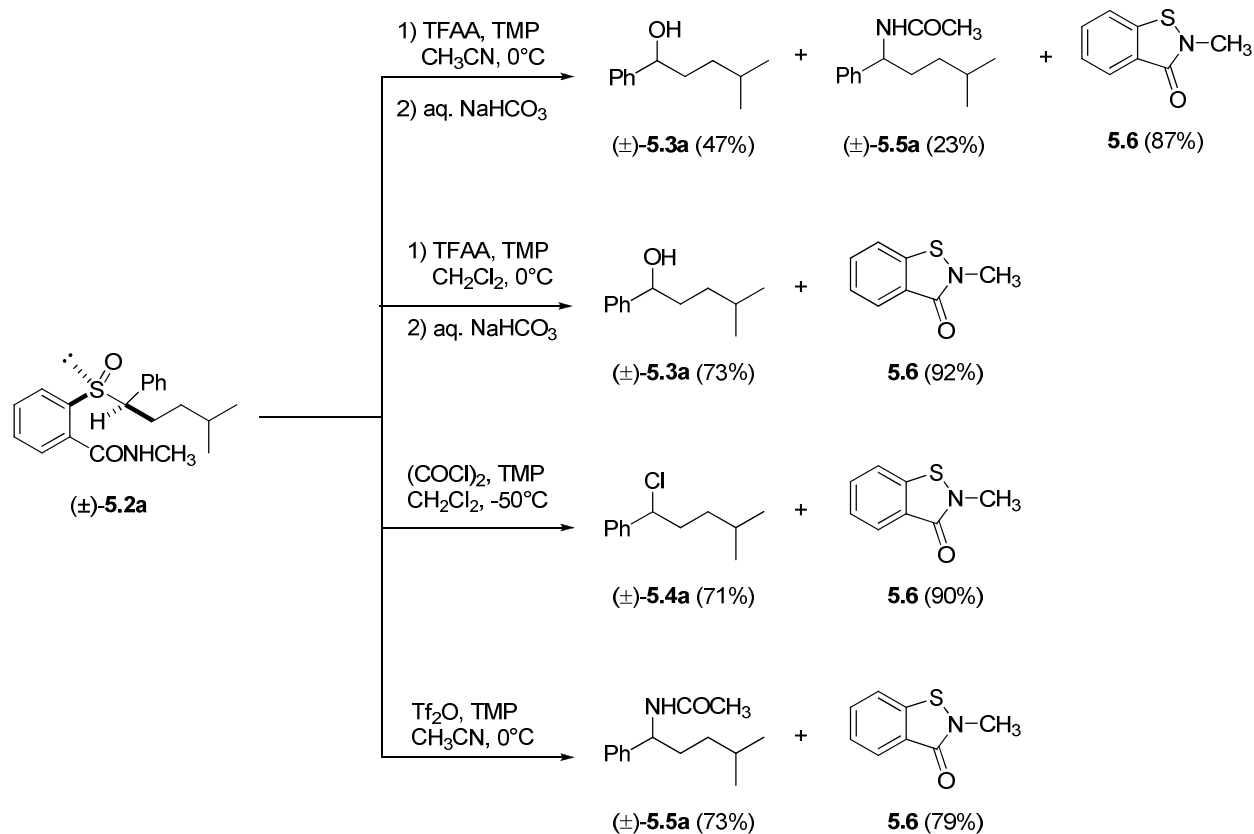
Accordingly, the sulfoxides **5.2** were proved to be suitable substrates for Pummerer reaction when they were submitted to NOCPR and NOPR conditions, giving rise to the chlorides **5.4** and alcohols **5.3**, respectively.

In fact, the treatment of sulfoxide (\pm)-**5.2a** under NOCPR conditions, namely oxalyl chloride, in the presence of *sym*-collidine in DCM at -50°C, afforded the corresponding chloride **5.4a** in very good yield, together with the heterocycle **5.6** [Scheme 5.6].

However, the treatment of sulfoxide (\pm)-**5.2a** under classical NOPR conditions, namely with TFAA, in the presence of TMP in CH₃CN at 0°C, followed by treatment with aqueous NaHCO₃, resulted in the formation of the expected alcohol **5.3a** and heterocycle **5.6** along with the acetamide **5.5a** [23%, Scheme 5.6].

Notably, when the reaction was performed in DCM instead of CH₃CN, the exclusive formation of alcohol **5.3a** and benzisothiazolone **5.6** was observed, thus suggesting the role of sulfoxides **5.2** not only as α -hydroxy carbanion and α -chloro carbanion synthetic equivalents but also as α -acetamido carbanion equivalents.

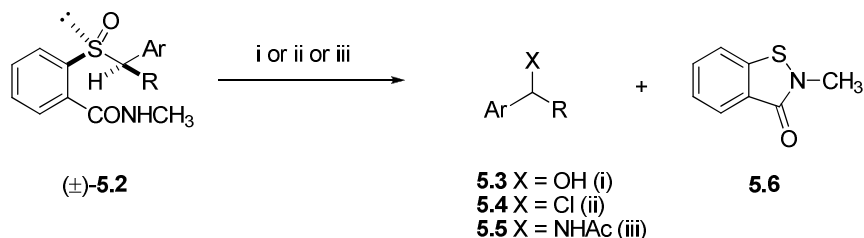
Presumably, the reaction proceeded through a carbocationic intermediate, which is trapped by the nucleophilic acetonitrile, thus leading to the formation of the acetamide, after hydrolysis during reaction quenching.



Scheme 5.6. NOPR on sulfoxide (\pm) -**5.2a**.

Hence, we assumed that the replacement of TFAA by another Pummerer reaction promoter as Tf_2O could give rise to the formation of the target acetamide along with the co-product **5.6**. Finally, the treatment of sulfoxide (\pm) -**5.2a** with Tf_2O , using TMP as a base in CH_3CN at 0°C , afforded the desired acetamide **5.5a** with a good yield and bezisothiazolone **5.6** [Scheme 5.6].

Since the racemic sulfoxide (\pm) -**5.2a** afforded the expected alcohol **5.3**, chloride **5.4** and acetamide **5.5** under the different Pummerer conditions, several alkylated sulfoxides, were submitted to the same conditions [Scheme 5.7 and Table 5.4].



i. TFAA, TMP, DCM, 0°C , then aq. NaHCO_3 ; ii. $(\text{COCl})_2$, TMP, DCM, -50°C ; iii. Tf_2O , TMP, CH_3CN , 0°C .

Scheme 5.7. Synthesis of alcohols **5.3**, chlorides **5.4** and acetamides **5.5**.

Table 5.4. Synthesis of alcohols **5.3**, chlorides **5.4** and acetamides **5.5**.

Substrate	Ar	R	Product	X	Yield ^a (%)
(±)- 5.2e	Ph	Ph(CH ₂) ₃	(±)- 5.3e	OH	86
(±)- 5.2f	Ph	CH ₂ =CH(CH ₂) ₃	(±)- 5.3f	OH	72
(±)- 5.2i	4-MeO-Ph	Ph(CH ₂) ₃	(±)- 5.3i	OH	67
(±)- 5.2k	4-CF ₃ -Ph	Ph(CH ₂) ₃	(±)- 5.3k	OH	77
(±)- 5.2e	Ph	Ph(CH ₂) ₃	(±)- 5.4e	Cl	90
(±)- 5.2f	Ph	CH ₂ =CH(CH ₂) ₃	(±)- 5.4f	Cl	60
(±)- 5.2i	4-MeO-Ph	Ph(CH ₂) ₃	(±)- 5.4i	Cl	63
(±)- 5.2k	4-CF ₃ -Ph	Ph(CH ₂) ₃	(±)- 5.4k	Cl	78
(±)- 5.2g	Ph	CH ₃ (CH ₂) ₅	(±)- 5.5g	NHAc	62
(±)- 5.2h	Ph	CH ₃ (CH ₂) ₂	(±)- 5.5h	NHAc	67
(±)- 5.2j	4-MeO-Ph	3,4,5-TriMeO-Ph-(CH ₂) ₃	(±)- 5.5j	NHAc	48 ^b
(±)- 5.2k	4-CF ₃ -Ph	Ph(CH ₂) ₃	(±)- 5.5k	NHAc	57 ^b

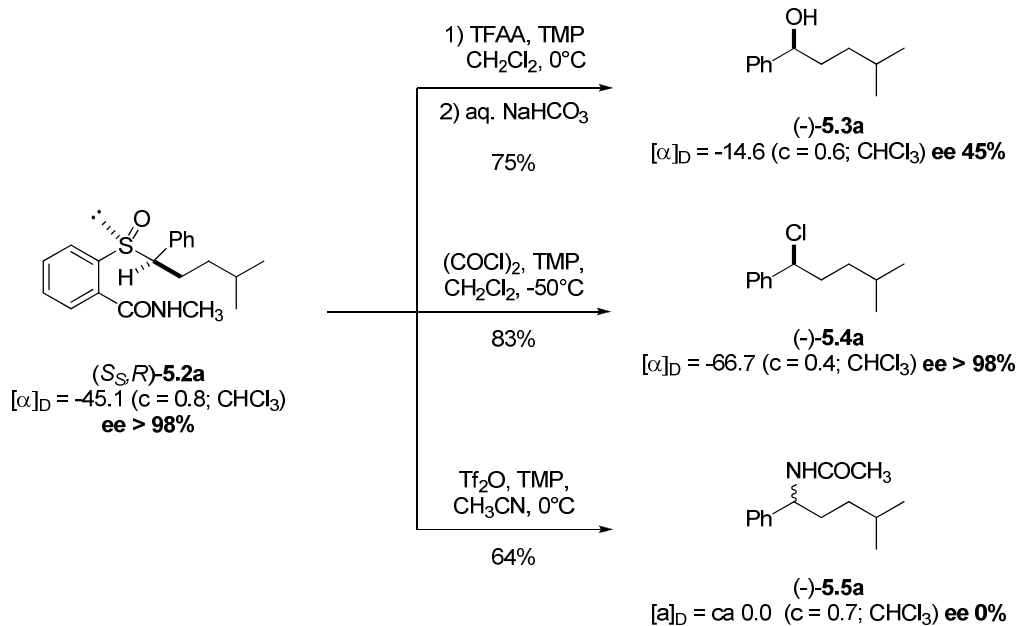
^a Overall isolated yield.

^b Formation of the corresponding tetralines as by-products was observed.

The NOPR on substrates (±)-**5.2e,f** afforded the corresponding alcohols **5.3e,f** in good yield. The NOPR outcomes were isolated also starting from alkylated sulfoxides (±)-**5.2i** and (±)-**5.2k**, thus demonstrating the reaction to work well with sulfoxides bearing either an electron-rich or an electron-poor ring as aryl substituent, respectively.

Similarly, the treatment of sulfoxides (±)-**5.2e,f,i,k** under NOCPR conditions gave rise to the desired chlorides from moderate to very good yield.

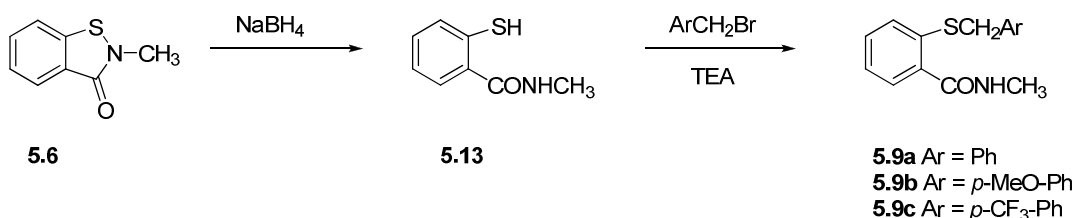
Finally, the acetamides (±)-**5.5g-k** were achieved by using Tf₂O as a promoter of Pummerer reaction, although the products **5.5j,k** were formed in low yield, because of the formation of tetraline derivatives as by-products⁵⁹. Afterwards, we aimed at synthesising enantiomerically pure alcohols, chlorides and acetamides, starting from the enantiomerically pure sulfoxide (-)-**5.2a** using the same conditions described above, in order to assess more information about the mechanism of reaction [Scheme 5.8].



Scheme 5.8. Pummerer reaction on enantiomerically pure (S,S,R) -**5.2a**

The NOPR on (S,S,R) -**5.2a** afforded the enantiomerically pure alcohol $(-)$ -**5.3a** in good yield with inversion of configuration at the benzylic stereocenter, however a partial loss of enantiomeric purity was observed (ee 45%, starting from sulfoxide (S,S,R) -**5.2a** with $ee > 98\%$). This result confirmed that the reaction did not occur exclusively *via* a $\text{S}_{\text{N}}2$ pathway. On the other hand, the treatment of (S,S,R) -**5.2a** under NOCPR gave rise to the expected chloride $(-)$ -**5.4a** without any loss of ee as evidenced by chiral HPLC. Finally the reaction with Tf_2O in CH_3CN afforded the racemic acetamide **5.5a**, thus confirming that this reaction probably proceeds through the formation of a carbocationic intermediate.

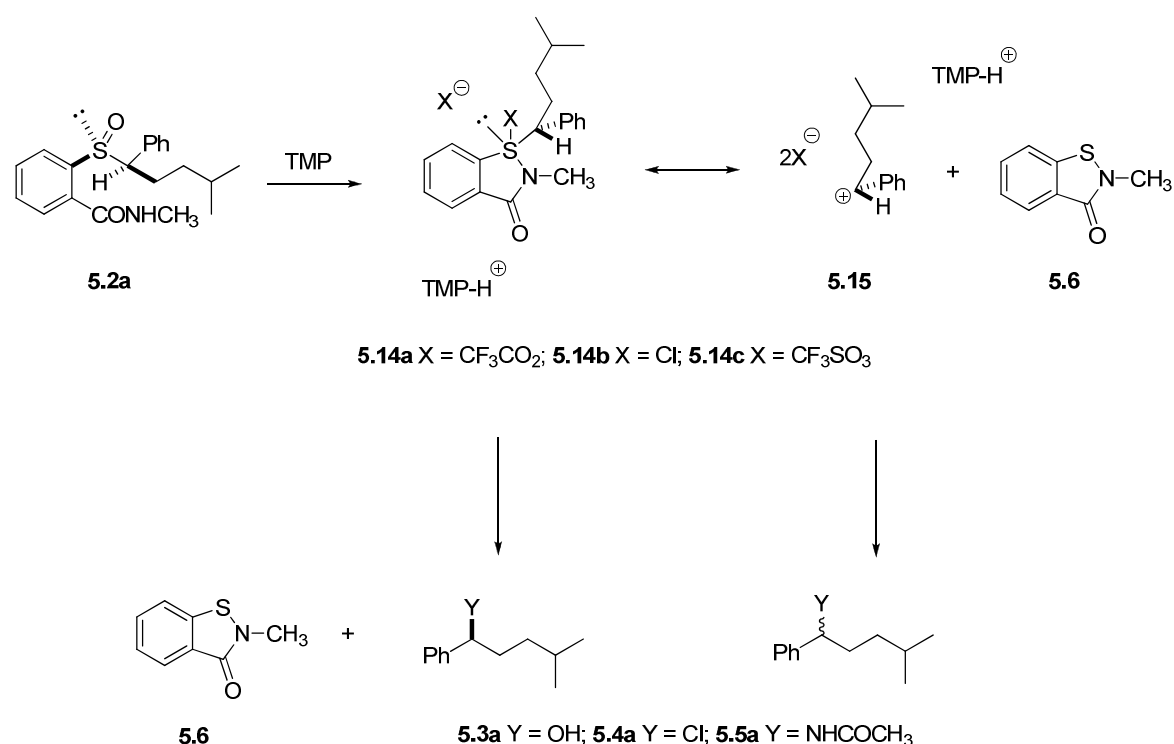
The benzisothiazolone **5.6** resulting from the Pummer reactions was sequentially submitted to regioselective reduction of S-N bond with NaBH_4 , followed by S-alkylation with arylalkyl bromide to give the starting sulfide **5.9** [Scheme 5.9].



Scheme 5.9. Recycle of the co-product **5.6**.

The stereochemical outcome of the investigated non-oxidative Pummerer reactions was thought to be dependent on Pummerer initiators (TFAA , $(\text{COCl})_2$ and Tf_2O).

The reaction starts with the acylation of sulfinyl oxygen by TFAA, $(\text{COCl})_2$ or Tf_2O , leading to the formation of a cyclic intermediate **5.14a-c** [Scheme 5.10], derived from the attack of *ortho*-carbamoyl nitrogen (deprotonated by TMP) to the sulfur cation.



Scheme 5.10. Proposed mechanism for the Pummerer reactions.

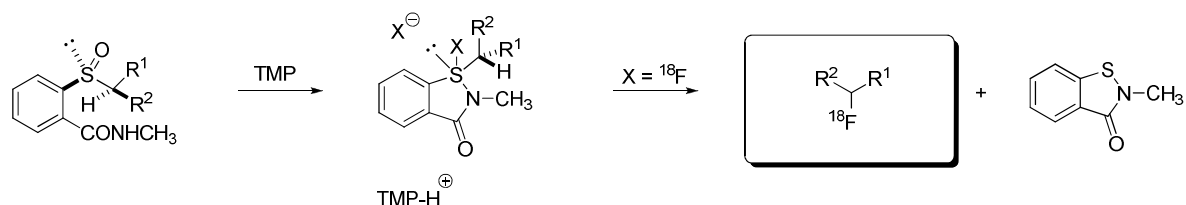
Conceivably, if the nucleophile X^- is sufficiently strong, such as Cl^- , the intermediate **5.14** probably undergoes an internal rearrangement, involving S-X and C-S bonds breaking, along with the formation of a new C-Cl bond, thus giving rise to the corresponding chloride **5.4a** and heterocycle **5.6**.

On the other hand, the Pummerer promoter Tf_2O produces the weak nucleophile Tf_2O^- , thereby the internal rearrangement cannot occur and the carbocationic species **5.15** which takes place can be trapped by the nucleophilic solvent CH_3CN , leading to the acetamide **5.5a**, after hydrolysis.

This assumption was confirmed when a better ee was obtained by using TCAA instead of TFAA ($\text{CCl}_3\text{CO}_2^-$ is a stronger nucleophile than CF_3CO_2^-) as initiator.

Presumably, the ability of *N*-methyl *ortho*-carbamoylaryl sulfoxides to work as umpolung reagents could be exploited to synthesise an important variety of enantiomerically pure molecules of biological interest. With regard to the synthesis of ^{18}F -labelled compounds as PET radiotracers, the mechanisms described above could be useful to carry out the ^{18}F -fluorination of selected

precursors, by using several ^{18}F -fluoride sources, and achieve new potential radiotracers for PET. [Scheme 5.11].



Scheme 5.11. Potential synthetic strategy for the introduction of fluorine-18 and production of new PET-tracers.

5.3 Conclusions

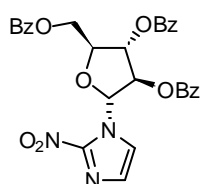
In conclusion, we have synthesised α -benzyl alcohols, chlorides and acetamides, starting from alkylated sulfoxides, which were obtained in satisfactory to very good yields and high diastereoselectivity.

N-methyl *ortho*-carbamoylaryl benzyl sulfoxides can be efficiently exploited as synthetic equivalents of α -hydroxy, α -chloro and α -acetamido benzyl carbanions. They can be easily converted to the corresponding α -benzyl alcohols, chlorides and acetamides by means of a two-step procedure, involving a high stereoselective C-C bond forming reaction followed by ‘non-oxidative’ Pummerer reactions, which allow the replacement of sulfinyl moiety by an hydroxyl, a chloride and an acetamido group.

The use of enantiomerically pure sulfoxides as substrates for the ‘non-oxidative’ Pummerer reactions provided different stereochemical results, thus suggesting that the formation of Pummerer-like outcomes takes place through different mechanisms, namely a $\text{S}_{\text{N}}2$ pathway and the formation of a carbocationic intermediate, both dependent on the nucleophilic character of the species X^- .

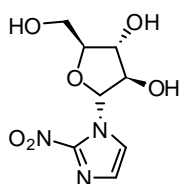
In fact when X^- is a strong nucleophile, such as Cl, enantiomerically pure chlorides can be achieved through a $\text{S}_{\text{N}}2$ mechanism, whereas if X^- is a poor nucleophile, such as TfO^- , a carbocationic species is formed and trapped by the solvent CH_3CN , producing the acetamides as racemates. Moreover, when X^- has an intermediate nucleophilic strength, such as CF_3CO_2^- , both mechanisms are involved and enantiomerically pure benzylic alcohols are formed.

Chapter 6. Experimental section



1-(α -D-2,3,5-Tri-O-benzoylarabinofuranosyl)-2-nitroimidazole (3.10):

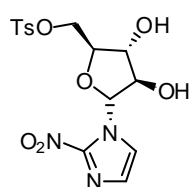
To a stirred suspension of 2-nitroimidazole (0.50 g, 4.42 mmol) in hexamethyldisilazane (15.25 ml), a catalytic amount of ammonium sulphate (0.06 g, 0.44 mmol) was added, under nitrogen atmosphere. After heating at reflux for 4 hours, 2-nitroimidazole had completely dissolved and the reaction was complete. Excess HMDS was then removed under N₂ gas stream, and the product was kept under high vacuum to remove the traces of HMDS. A solution of 2,3,5-Tri-O-benzoyl- α -D-arabinofuranosyl bromide (1.90 g, 3.62 mmol) in anhydrous acetonitrile (200 ml) was added to the flask containing 1-*N*-trimethylsilyl-2-nitroimidazole, under nitrogen atmosphere, then mercuric cyanide (2.01 g, 7.96 mmol) was added. The reaction mixture was heated at 50°C for 16 h, and monitored via TLC, which showed the complete consumption of the starting material. The solvent was evaporated under vacuum and the residue was dissolved in CH₂Cl₂ and washed sequentially with 30% w/v aqueous potassium iodide and then cold water. The organic layer was dried over Na₂SO₄, filtered and solvent was removed under reduced pressure. Purification over silica gel chromatography (Hexane/EtOAc 7:3) afforded 0.97 g (48% yield) of spongy white solid; R_f = 0.36 (Hexane/EtOAc 63:37); ¹H NMR (400 MHz, CDCl₃) δ : 8.02 (d, J = 7.3 Hz, 4H), 7.73 (d, J = 7.1 Hz, 2H), 7.60-7.29 (m, 9H), 7.19 (s, 1H), 6.90 (d, J = 1.4 Hz, 1H), 5.83 (s, 1H), 5.56 (s, 1H), 4.98 (m, 1H), 4.79 (dd, J = 11.8, 6.7 Hz, 1H), 4.61 (dd, J = 11.8, 5.1 Hz, 1H); ¹³C NMR (400 MHz CDCl₃) δ : 166.1, 164.9, 164.5, 134.1, 133.4, 130.1, 129.8, 129.8, 128.8, 128.7, 128.5, 122.2, 93.5, 86.1, 82.0, 63.6. ESI MS m/z : 580.2 [M + Na⁺], 596.1 [M + K⁺].



1-(α -D-Arabinofuranosyl)-2-nitroimidazole (α -AZA) (3.1):

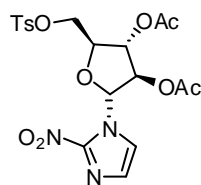
3.10 (0.97 g, 1.74 mmol) was dissolved in a 2M NH₃/MeOH solution (125 ml) and stirred under nitrogen at 0°C. After 10 h stirring, the reaction mixture was allowed to reach room temperature and stirred for 48 h. The solvent was removed under vacuum (rotavap.) and the residue purified via flash column chromatography on silica gel (CH₂Cl₂/CH₃OH 9:1) to give compound **3.1** (0.38 g, 87% yield) as a spongy white solid; R_f = 0.29 (CH₂Cl₂/CH₃OH 9:1); ¹H NMR (400 MHz, CD₃OD) δ : 7.65 (d, J = 1.0 Hz, 1H), 7.13 (d, J = 1.0 Hz, 1H), 6.43 (d, J = 1.1 Hz, 1H), 4.84 (s, 3H), 4.50 (td J = 5.0, 2.3, Hz,

1H), 4.25 (t, $J = 1.4$ Hz, 1H), 4.13 (t, $J = 2.0$ Hz, 1H), 3.79-3.75 (m, 2H); ^{13}C NMR (400 MHz CD_3OD) δ 126.7, 123.9, 95.9, 90.4, 82.5, 76.6, 61.8; ESI MS m/z : 268.0 [$\text{M} + \text{Na}^+$], 513.1 [$2\text{M} + \text{Na}^+$].



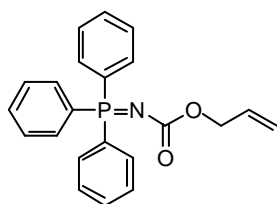
1-α-D-(5'-O-Toluenesulfonyl-arabinofuranosyl)-2-nitroimidazole (Ts-AZA) (3.11):

Tosyl chloride (0.46 g, 2.4 mmol) was added to a solution of **3.1** (0.39 g, 1.6 mmol) in dry pyridine (6 ml) at 5°C . The reaction mixture was stirred at this temperature for 48 h and then quenched by adding few pieces of ice. The solvent was removed *in vacuo* and the crude was purified by silica gel chromatography ($\text{CH}_2\text{Cl}_2/\text{CH}_3\text{OH}$ 95:5); to obtain the product **3.11** (0.54 g, 88% yield) as a spongy white solid; $R_f = 0.37$ ($\text{CH}_2\text{Cl}_2/\text{CH}_3\text{OH}$ 95:5); ^1H NMR (400 MHz, d_6 -DMSO) δ 7.76 (d, $J = 8.4$ Hz, 2H), 7.63 (s, 1H), 7.44 (d, $J = 8.0$ Hz, 2H), 7.11 (s, 1H), 6.19 (s, 1H), 6.00 (s, 1H), 5.41 (s, 1H), 4.53 – 4.47 (m, 1H), 4.17 (dd, $J = 12.0, 4.0$ Hz, 1H), 4.11 (dd, $J = 8.0, 4.0$ Hz, 1H), 3.85 (s, 1H), 2.45 (s, 2H), 2.37 (s, 3H); ^{13}C NMR (400 MHz CDCl_3) δ 145.3, 132.3, 130.0, 128.3, 128.0, 123.2, 96.2, 86.8, 83.6, 68.3, 29.7, 21.6; ESI MS m/z : 422.0 [$\text{M} + \text{Na}^+$], 438.0 [$\text{M} + \text{K}^+$].



1-α-D-(5'-O-Toluenesulfonyl-2',3'-di-O-acetyl-arabinofuranosyl)-2-nitroimidazole (DAcTs-AZA) (3.12):

Acetic anhydride (0.63 ml) was added to a solution of **3.11** (0.33 g, 0.83 mmol) in dry pyridine (2.0 ml) and the mixture was stirred overnight at room temperature. After the completion of reaction, acetic anhydride was quenched with water. The resulting mixture was concentrated under reduced pressure by azeotropic distillation with toluene. The crude residue was purified by flash chromatography on silica gel ($\text{CH}_2\text{Cl}_2/\text{CH}_3\text{OH}$ 99:1) to give the corresponding product **3.12** (0.34g, 84% yield) as a spongy white solid; $R_f = 0.31$ ($\text{CH}_2\text{Cl}_2/\text{CH}_3\text{OH}$ 99:1); ^1H NMR (400 MHz, CDCl_3) δ 7.83 (d, $J = 8.0$ Hz, 2H), 7.38 (d, $J = 8.0$ Hz, 2H), 7.29 (s, 1H), 7.20 (s, 1H), 6.54 (s, 1H), 5.39 (s, 1H), 5.12 (s, 1H), 4.63 (m, 1H), 4.30 (d, $J = 8.0$ Hz, 2H), 2.46 (s, 3H), 2.18 (s, 3H), 2.00 (s, 3H). ^{13}C NMR (400 MHz CDCl_3) δ 169.2, 168.8, 145.5, 132.3, 130.0, 128.6, 128.0, 121.9, 93.1, 85.1, 81.0, 67.6, 21.7, 20.5; ESI MS m/z : 506.1 [$\text{M} + \text{Na}^+$], 522.0 [$\text{M} + \text{K}^+$].

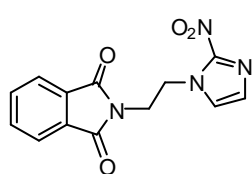


(Allyloxycarbonyl)amino triphenylphosphorane (4.6):

To a solution of trimethylsilylazide (1.0 g, 8.7 mmol) and allyl chloroformate (0.66 ml, 6.2 mmol) in dry benzene (10 ml) under nitrogen atmosphere, three drops of pyridine were added, and the solution was heated at reflux temperature for 30 min, then diluted with

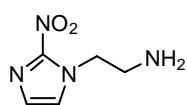
benzene (10 ml) and cooled to 0°C. This solution was slowly added to a solution of PPh₃ (1.63 g, 6.2 mmol) in benzene (15 ml) at 0°C. When nitrogen evolution ceased, the mixture was stirred for 30 min at rt., then the solvent was removed under reduced pressure.

The crude residue was purified by flash chromatography on silica gel (Hexane/EtOAc 5:5) to give the phosphorane **4.6** (2.13 g, 95% yield) as a white solid; $R_f = 0.24$ (Hexane/EtOAc 6:4); ¹H NMR (400 MHz, CDCl₃) δ 7.79–7.71 (m, 6H), 7.56 (td, $J = 7.2, 1.6$ Hz, 3H), 7.46 (td, $J = 7.5, 3.0$ Hz, 6H), 5.94 (ddd, $J = 22.9, 10.5, 5.7$ Hz, 1H), 5.22 (dd, $J = 17.2, 1.6$ Hz, 1H), 5.10 (dd, $J = 10.4, 1.4$ Hz, 1H), 4.51 (d, $J = 5.7$ Hz, 2H); ¹³C NMR (400 MHz CDCl₃) δ 161.7, 134.1, 133.1, 133.0, 132.4, 132.3, 128.7, 128.6, 128.5, 127.5, 116.6, 66.4; ESI MS m/z : 362.1 [M + H⁺], 745.2 [2M + Na⁺].



2-(2-Nitro-1H-imidazolyl)ethylphthalimide (4.16):

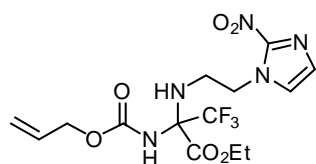
A stirred solution of 2-nitroimidazole (1.80 g, 15.9 mmol), 2-bromoethylphthalimide (4.24 g, 16.7 mmol), and K₂CO₃ (2.30 g, 16.7 mmol) in DMF (45 ml) was heated at 110°C for 2 h. The solvent was removed under reduced pressure and the residue was poured into water and extracted with CH₂Cl₂. The organic layer was dried over Na₂SO₄, filtered and evaporated *in vacuo*. Purification of the crude by flash chromatography on silica gel (Hexane/EtOAc 4:6) afforded compound **4.16** (3.63 g, 80% yield) as a pale yellow solid; $R_f = 0.28$ (Hexane/EtOAc 4:6); ¹H NMR (400 MHz, d₆-DMSO) δ 7.83 (s, 4H), 7.60 (d, $J = 0.8$ Hz, 1H), 7.06 (d, $J = 1.2$ Hz, 1H), 4.63 (t, $J = 4.0$ Hz, 2H), 4.05 (t, 8.0 Hz, 2H); ¹³C NMR (400 MHz d₆-DMSO) δ 167.4, 144.7, 134.5, 131.3, 128.4, 128.0, 123.2, 48.3, 37.1; ESI MS m/z : 287.1 [M + H⁺], 309.0 [M + Na⁺].



2-(2-Nitro-1H-imidazolyl)ethylamine (4.8):

A stirred solution of **4.16** (1.34 g, 4.67 mmol) and hydrazine monohydrate (0.46 ml, 9.34 mmol) in EtOH (20 ml) was heated under reflux for 2 h. The resulting suspension was cooled to 0°C and filtered, and the filtrate was evaporated under reduced pressure.

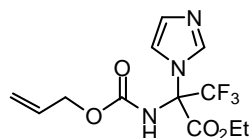
The residue was purified by flash chromatography (CH₂Cl₂/CH₃OH 9:1) affording 0.46 g (63% yield) of **4.8** as a yellow solid; $R_f = 0.23$ (CH₂Cl₂/CH₃OH 7:3); ¹H NMR (400 MHz, CD₃OD) δ 7.39 (d, $J = 1.2$ Hz, 1H), 7.03 (d, $J = 1.2$ Hz), 4.90 (s, 2H), 4.57 (t, $J = 4.0$ Hz, 2H), 3.17 (t, $J = 8.0$ Hz); ¹³C NMR (400 MHz CD₃OD) δ 160.3, 133.1, 130.2, 128.7, 128.6, 126.8, 52.5, 42.2; ESI MS m/z : 157.1 [M + H⁺], 179.0 [M + Na⁺].



Ethyl-2-(allyloxycarbonylamino)-3,3,3-trifluoro-2-(2-(2-nitro-1H-imidazol-1-yl)ethylamino)propanoate (4.13):

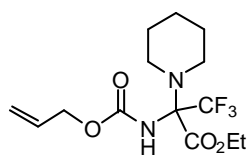
To a solution of **4.6** (1.03 g, 2.86 mmol) in dry THF (6.0 ml) under nitrogen atmosphere 3,3,3-ethyl trifluoropyruvate (0.54 g, 3.15 mmol) was added. After stirring for 30 min at rt., compound **4.8** (0.45 g, 2.86 mmol) was added. The reaction was complete after 30 min. (TLC monitoring). The solvent was evaporated under reduced pressure and the crude was purified by flash chromatography (Hexane/EtOAc 6:4) to give the product **4.13** (1.0 g, 85% yield) as a pale yellow oil; $R_f = 0.37$ (Hexane/EtOAc 1:1); $^1\text{H NMR}$ (400 MHz, CDCl_3) δ 7.21 (d, $J = 1.2$ Hz, 1H), 7.08 (d, $J = 0.8$ Hz), 6.15 (s, 1H), 5.87-5.77 (m, 1H), 5.27-5.17 (m, 2H), 4.51-4.44 (m, 4H), 4.30-4.15 (m, 2H), 3.26 (bs, 1H), 3.12-3.06 (m, 1H), 2.93-2.87 (m, 1H), 1.21 (t, $J = 8.0$ Hz); $^{13}\text{C NMR}$ (400 MHz CDCl_3) δ 165.0, 154.3, 131.9, 128.13, 127.5, 124.0, 118.7, 75.3, 66.4, 64.3, 50.3, 42.5, 29.8, 13.8;

$^{19}\text{F NMR}$ (600 MHz CDCl_3) δ -77.7; ESI MS m/z : 410.1 [$\text{M} + \text{H}^+$], 432.1 [$\text{M} + \text{Na}^+$].



ethyl 2-(allyloxycarbonylamino)-3,3,3-trifluoro-2-(1H-imidazol-1-yl)propanoate (4.9b):

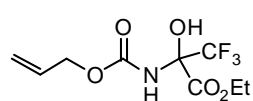
To a solution of **4.6** (1.0 equiv.) in dry THF under nitrogen atmosphere 3,3,3-ethyl trifluoropyruvate (1.1 equiv.) was added. After stirring for 30 min at rt., 1-*H*-imidazole (1.0 equiv.) was added. After completion of reaction the solvent was evaporated under reduced pressure and the crude was purified by flash chromatography (Hexane/EtOAc 3:7) to give the compound **4.9b** (0.50 g, 55% yield) as a white solid; $R_f = 0.50$ (Hexane/EtOAc 2:8); $^1\text{H NMR}$ (400 MHz, CDCl_3) δ 7.80 (s, 1H), 7.15 (d, $J = 8.0$ Hz, 1H), 6.97 (dd, $J = 4.0$ Hz, 1H), 5.77 (m, 1H), 5.17 (dd, $J = 16.0, 12.0$ Hz, 2H), 4.49 (d, $J = 4.0$ Hz, 2H), 4.28 (q, $J = 8.0$ Hz, 2H), 1.21 (t, $J = 8.0$ Hz, 3H); ESI MS m/z : 322.1 [$\text{M} + \text{H}^+$], 344.1 [$\text{M} + \text{Na}^+$].



ethyl 2-(allyloxycarbonylamino)-3,3,3-trifluoro-2-(piperidin-1-yl)propanoate (4.9c):

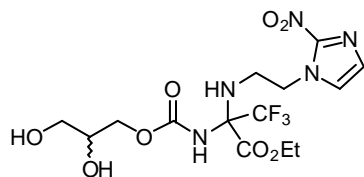
To a solution of **4.6** (1.0 equiv.) in dry THF under nitrogen atmosphere 3,3,3-ethyl trifluoropyruvate (1.1 equiv.) was added. After stirring for 30 min at rt., piperidine (1.0 equiv.) was added. After completion of reaction the solvent was evaporated under reduced pressure and the crude was purified by flash chromatography (Hexane/EtOAc 9:1) to afford the compound **4.9c** (0.02 g, 25% yield) as a white solid; $R_f = 0.37$ (Hexane/EtOAc 9:1); $^1\text{H NMR}$ (400 MHz, CDCl_3) δ 5.95 – 5.85 (m, 2H), 5.56 (bs, 1H), 5.23 (dq, $J = 4.0, 8.0$ Hz, 1H), 4.56 (dt, $J = 4.0, 8.0$ Hz, 2H), 4.33 (dq, 2H), 2.83 – 2.73 (m, 4H), 1.60 – 1.54 (m, 4H), 1.52 - 1.44 (m, 2H), 1.32 (t, $J = 4.0$ Hz, 3H); $^{13}\text{C NMR}$ (400 MHz

CDCl₃) δ 165.0, 153.7, 132.2, 118.2, 66.1, 62.9, 48.5, 26.6, 24.4, 14.0; ESI MS m/z : 339.1 [M + H⁺], 361.1 [M + Na⁺].



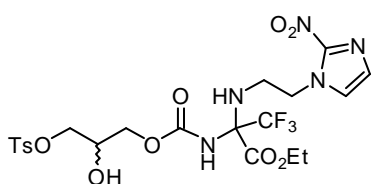
ethyl 2-(allyloxycarbonylamino)-3,3,3-trifluoro-2-hydroxypropanoate

(4.9a): (white solid, 36% yield); R_f = 0.71 (Hexane/EtOAc 7:3); ¹H NMR (400 MHz, CDCl₃) δ 5.92 – 5.75 (m, 2H), 5.26 (dd, J = 4.0, 20.0 Hz, 2H), 5.19 (dd, J = 4.0, 12.0 Hz, 1H), 4.53 (dt, J = 8.0, 4.0 Hz, 2H), 4.34 (q, J = 8.0 Hz, 2H), 1.28 (t, J = 4.0 Hz, 3H); ESI MS m/z : 272.1 [M + H⁺], 294.1 [M + Na⁺].



Ethyl 2-((2,3-dihydroxypropoxy)carbonylamino)-3,3,3-trifluoro-2-(2-(2-nitro-1H-imidazol-1-yl)ethylamino)propanoate **(4.19)**:

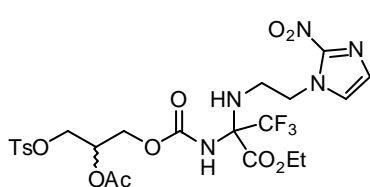
To a solution of **4.13** (1.00 g, 2.45 mmol) in acetone/water (1.0: 1.0 ml) *N*-methylmorpholine-*N*-oxide (0.32 g, 2.7 mmol) and a catalytic amount of osmium tetroxide 2.5% in *t*-BuOH (0.115 ml) were added. When the reaction was complete (TLC monitoring), a saturated solution of Na₂SO₃ was added. The resulting solution was extracted with EtOAc. The collected organic phase was dried over Na₂SO₄, filtered and evaporated under reduced pressure. The purification of the residue by flash chromatography (CH₂Cl₂/CH₃OH 95:5) afforded the desired compound **4.19** (1.0 g, 92% yield) as a brown oil with tendency to get solid; R_f = 0.46 (CH₂Cl₂/CH₃OH 9:1); ¹H NMR (400 MHz, CDCl₃) δ 7.21 (d, J = 0.8 Hz), 7.15 (d, J = 0.8 Hz), 6.19 (bs, 1H), 4.53-4.49 (m, 2H), 4.35-4.10 (m, 4H), 3.92-3.87 (m, 1H), 3.75-3.56 (m, 3H), 3.25 (t, J = 8.0 Hz), 3.18-3.10 (m, 1H), 2.99-2.91 (m, 1H), 1.27 (t, J = 4.0 Hz, 3H); ¹³C NMR (400 MHz CDCl₃) δ 165.0, 154.8, 144.6, 127.8, 122.6, 74.9, 70.0, 66.6, 64.0, 63.0, 55.2, 50.3, 46.2, 42.0, 13.7; ESI MS m/z : 444.1 [M + H⁺], 466.1 [M + Na⁺].



Ethyl 3,3,3-trifluoro-2-((2-hydroxy-3-(tosyloxy)propoxy)carbonylamino)-2-(2-(2-nitro-1H-imidazol-1-yl)ethylamino)propanoate **(4.20)**:

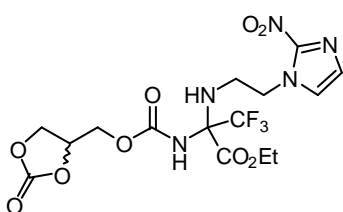
To a solution of **4.19** (1.10 g, 2.48 mmol) in dry pyridine (6 ml) at 5°C, tosyl chloride (0.71 g, 3.72 mmol) was added. The resulting solution was stirred overnight. The reaction was quenched by adding few pieces of ice and the mixture was evaporated under reduced pressure and by azeotropic distillation with toluene. The residue was purified by flash chromatography (CH₂Cl₂/CH₃OH 98:2) to give 1.11 g (75% yield) of **4.20** as a white solid; R_f = 0.29 (CH₂Cl₂/CH₃OH 97:3); ¹H NMR (400 MHz, CDCl₃) δ 7.78 (d, J = 8.0 Hz, 2H), 7.37 (d, J = 8.0 Hz, 2H), 7.27 (m, 1H), 7.11 (m, 1H), 6.50 (bs, 1H), 4.53-4.50 (m, 2H),

4.33-4.23 (m, 2H), 4.17-4.03 (m, 5H), 3.29 (t, $J = 8.0$ Hz, 1H), 3.17-3.09 (m, 1H), 3.00-2.92 (m, 1H), 2.45 (s, 1H), 1.26 (t, $J = 8.0$ Hz); ^{13}C NMR (400 MHz CDCl_3) δ 164.8, 154.2, 149.2, 145.3, 144.6, 129.9, 127.5, 124.0, 75.4, 70.1, 67.4, 64.2, 50.13, 42.2, 21.6, 13.7; ESI MS m/z : 598.2 $[\text{M} + \text{H}^+]$, 620.2 $[\text{M} + \text{Na}^+]$, 636.2 $[\text{M} + \text{K}^+]$.



Ethyl 2-((2-acetoxy-3-(tosyloxy)propoxy)carbonylamino)-3,3,3-trifluoro-2-(2-(2-nitro-1H-imidazol-1-yl)ethylamino)propanoate (4.18):

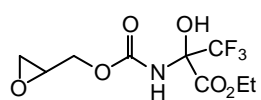
To a solution of **4.20** (1.11 g, 1.86 mmol) in dry pyridine (6.0 ml) acetic anhydride (1.52 g, 14.9 mmol) was added. The solution was stirred at rt. overnight and, after the completion of the reaction, water was added. The solvent was removed under reduced pressure and azeotropic distillation with toluene. The residue was washed with 1N HCl, 5% NaHCO_3 and brine and extracted with CH_2Cl_2 . The organic layer was dried over Na_2SO_4 , filtered and evaporated *in vacuo*. The crude residue was purified by flash chromatography ($\text{CH}_2\text{Cl}_2/\text{CH}_3\text{OH}$ 99:1) to give compound **4.18** (1.13 g, 95% yield) as a pale yellow oil; $R_f = 0.29$ ($\text{CH}_2\text{Cl}_2/\text{CH}_3\text{OH}$ 99:1); ^1H NMR (400 MHz, CD_3OD) δ 7.65 (d, $J = 8.0$ Hz, 2H), 7.37 (d, $J = 8.0$ Hz, 2H), 7.36 (m, 1H), 7.01 (m, 1H), 5.08-5.05 (m, 1H), 4.45 (t, $J = 8.0$ Hz, 2H), 4.17-4.11 (m, 4H), 4.04-3.80 (m, 1H), 3.22-3.23 (m, 1H), 2.98-2.95 (m, 2H), 2.37 (s, 3H), 1.88 (s, 3H), 1.14 (t, $J = 8.0$ Hz, 3H); ^{13}C NMR (400 MHz CDCl_3) δ 168.9, 163.7, 152.5, 152.5, 144.4, 143.7, 131.3, 129.0, 127.0, 126.9, 126.3, 74.5, 67.4, 66.2, 66.1, 63.3, 61.9, 49.1, 41.4, 20.6, 19.6, 12.7; ESI MS m/z : 640.1 $[\text{M} + \text{H}^+]$, 662.1 $[\text{M} + \text{Na}^+]$.



ethyl 3,3,3-trifluoro-2-(2-(2-nitro-1H-imidazol-1-yl)ethylamino)-2-(((2-oxo-1,3-dioxolan-4-yl)methoxy)carbonylamino)propanoate (4.21):

A solution of diol **4.19** (0.17 g, 0.38 mmol) in CH_2Cl_2 (3 ml) at -78 $^\circ\text{C}$ was treated with pyridine (0.15 ml, 1.91 mmol) and triphosgene (0.09 g, 0.32 mmol) in CH_2Cl_2 (2 ml). The resulting yellow solution was stirred at -78 $^\circ\text{C}$ for 10 min, then left to slowly warm to 0 $^\circ\text{C}$ over 1.5 h. After quenching with saturated aqueous NaHCO_3 (5 ml) under concomitant gas formation, the phases were separated and the aqueous layer was extracted with CH_2Cl_2 (3 x 5 ml). The combined organic phases were washed with saturated aqueous NaCl (5 ml), then dried over MgSO_4 , filtered and concentrated *in vacuo*. Purification by chromatography on silica gel ($\text{CH}_2\text{Cl}_2/\text{CH}_3\text{OH}$ 95:5) provided 0.123 g (69% yield) of carbonate **4.21** as a white solid; $R_f = 0.49$ ($\text{CH}_2\text{Cl}_2/\text{CH}_3\text{OH}$ 9:5); ^1H NMR (400 MHz, CDCl_3) δ 7.28 (s, 1H), 7.12 (s, 1H), 6.87 (d, $J = 16.0$ Hz, 1H), 4.97 (m, 1H), 4.66 - 4.51 (m, 3H), 4.41 - 4.21 (m, 4H), 3.30 - 3.10 (m, 2H), 3.10 - 2.94 (m, 1H), 1.29 (t, $J = 8.0$

Hz, 3H); ^{13}C NMR (400 MHz CDCl_3) δ 164.8, 154.7, 153.7, 144.8, 128.0, 127.6, 123.9, 121.0, 75.3, 74.2, 65.9, 64.3, 64.1, 50.2, 42.1, 29.7, 15.3, 13.8; ESI MS m/z : 470.1 [$\text{M} + \text{H}^+$], 492.1 [$\text{M} + \text{Na}^+$], 508.1 [$\text{M} + \text{K}^+$].

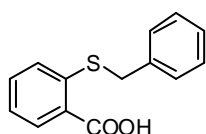


ethyl **3,3,3-trifluoro-2-hydroxy-2-((oxiran-2-ylmethoxy)carbonylamino)propanoate (4.24):**

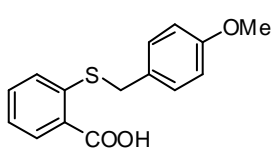
A solution of MCPBA (0.04 g, 0.25 mmol) in CH_2Cl_2 (1 ml) was added dropwise to a solution of **4.13** (0.09 g, 0.21 mmol) in CH_2Cl_2 (1 ml). The resulting mixture was stirred at room temperature overnight. After the completion of reaction (TLC monitoring) the mixture was quenched with saturated aqueous Na_2SO_3 (1 ml) and sequentially washed with NaHCO_3 and saturated aqueous NaCl . The organic phase was then collected, dried over MgSO_4 , filtered and concentrated *in vacuo*. Purification of the residue by flash chromatography (Hexane/EtOAc 6:4) afforded the compound **4.24** (0.07 g, 80% yield); $R_f = 0.27$ (Hexane/EtOAc 6:4); ^1H NMR (400 MHz, CDCl_3) δ 6.03 (bs, 1H), 5.30 (bs, 1H), 4.47 – 4.37 (m, 3H), 3.97 – 3.90 (m, 1H), 3.23 – 3.17 (m, 1H), 2.87 – 2.84 (m, 1H), 2.65 – 2.63 (m, 1H), 1.34 (td, 3H); ESI MS m/z : 448.0 [$\text{M} + \text{Na}^+$].

General procedure for the synthesis of compounds 5.8.

To a cooled solution of thiosalicylic acid (1 equiv.) and TEA (2.1 equiv.) in dioxane (0.1 M) benzyl bromide (1.1 equiv.) was added drop-wise at 0 °C. After 10 min the organic solvent was evaporated, the residue diluted in 1N HCl aqueous solution and extracted with AcOEt. The collected organic layers were dried on anhydrous Na_2SO_4 , filtered and the solvent evaporated *in vacuo*.

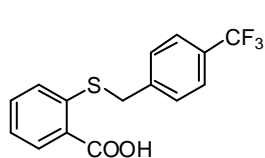


2-(benzylthio)benzoic acid (5.8a): $R_f = 0.47$ (Hexane/AcOEt 50:50); m.p. = 180-182 °C (MeOH); FTIR (film) 3440, 1639, 1255 cm^{-1} ; ^1H NMR (500 MHz, DMSO-d_6) δ 7.88 (d, $J = 7.8$ Hz, 1H), 7.49 (m, 2H), 7.42 (m, 2H), 7.33 (m, 2H), 7.26 (m, 1H), 7.20 (m, 1H), 4.20 (s, 2H); ^{13}C NMR (100.6 MHz, DMSO-d_6) δ 167.6, 141.5, 136.8, 132.6, 131.1, 129.4, 128.7, 127.8, 127.4, 125.9, 124.2, 35.9; MS (70 eV): e/z (%): 244 (12) [$\text{M}^+ + 1$], 91 (100).

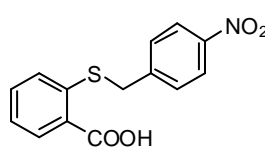


2-(4-methoxybenzylthio)benzoic acid (5.8b): $R_f = 0.57$ ($\text{CHCl}_3/\text{MeOH}$ 95:5); m.p. 213-215 °C (H_2O); FTIR (microscope) ν 3459, 1674 cm^{-1} ; ^1H NMR (400 MHz, DMSO-d_6) δ 7.84 (d, $J = 7.6$ Hz, 1H), 7.44 (m, 2H), 7.33 (d, $J = 8.6$ Hz, 2H), 7.17 (m, 1H), 6.88 (d, $J = 8.6$ Hz, 2H), 4.12 (s, 2H), 3.73 (s, 3H); ^{13}C

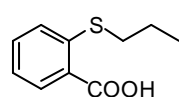
NMR (100.6 MHz, DMSO-d₆) δ 167.7, 158.3, 140.7, 131.5, 130.5, 130.2, 128.3, 125.6, 123.7, 113.8, 55.0, 35.2; EIMS (m/z) 274 [M^+ , (18)], 121 (100).



2-(4-(trifluoromethyl)benzylthio)benzoic acid (5.8c): R_f = 0.49 (CHCl₃/MeOH 95:5); FTIR (microscope) ν 2941, 1690 cm⁻¹; ¹H NMR (400 MHz, DMSO-d₆) δ 7.87 (d, J = 7.6 Hz, 1H), 7.67 (m, 4H), 7.46 (m, 2H), 7.21 (m, 1H), 4.31 (s, 2H); ¹⁹F NMR (235.4 MHz, DMSO-d₆) δ -61.0 (s, 3F); ¹³C NMR (100.6 MHz, DMSO-d₆) δ 167.6, 142.1, 140.5, 132.5, 131.1, 128.1, 127.6, 125.8, 125.4 (q, J = 3.7 Hz), 124.4 (q, J = 271.9 Hz), 124.3, 122.2, 35.0; EIMS (m/z) 312 [M^+ +1, (26)], 159 (100), 153 (59).



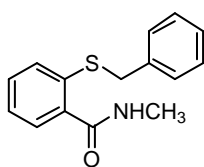
2-(4-nitrobenzylthio)benzoic acid (5.8d): R_f = 0.59 (CHCl₃/MeOH 95:5); m.p. 205-206 °C (MeOH); FTIR (microscope) ν 3460, 1682 cm⁻¹; ¹H NMR (400 MHz, DMSO-d₆) δ 8.18 (d, J = 8.6 Hz, 2H), 7.87 (d, J = 7.6 Hz, 1H), 7.71 (d, J = 8.6 Hz, 2H), 7.46 (m, 2H), 7.22 (m, 1H), 4.37 (s, 2H); ¹³C NMR (100.6 MHz, DMSO-d₆) δ 167.3, 146.5, 145.3, 139.7, 132.2, 130.8, 130.2, 128.3, 126.0, 124.3, 123.5, 34.9; EIMS (m/z) 289 [M^+ , (100)], 153 (81), 89 (77).



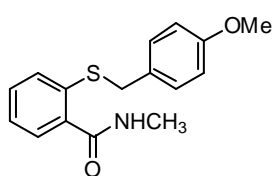
2-(propylthio)benzoic acid (5.8e): R_f = 0.55 (Hexane/AcOEt 50:50); FTIR (film) 1734, 1681, 1252 cm⁻¹; ¹H NMR (500 MHz, CD₃OD) δ 7.88 (d, J = 7.5 Hz, 1H), 7.40 (m, 2H), 7.15 (m, 1H), 2.89 (t, J = 7.2 Hz, 2H), 1.69 (sextet, J = 7.2 Hz, 2H), 1.06 (t, J = 7.2 Hz, 3H); ¹³C NMR (100.6 MHz, CD₃OD) δ 170.5, 142.3, 132.9, 132.0, 130.9, 127.3, 124.9, 35.0, 22.9, 13.9; MS (70 eV): e/z (%): 197 (34) [M^+ +1], 153 (100).

General procedure for the synthesis of compounds 5.9.

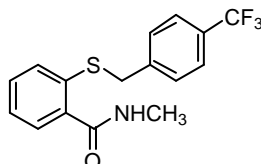
To a solution of crude **5.8** (17.9 mmol, 4.38 g) in DMF (0.1 M) were added respectively solid BOP (1 equiv.), the amine (1.1 equiv.) and DIPEA (2 equiv.). The solution was stirred at room temperature over-night. The organic solvent was evaporated and the residue purified by flash-chromatography.



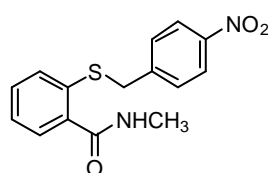
2-(benzylthio)-N-methylbenzamide (5.9a): R_f = 0.39 (Hexane/AcOEt 50:50); m.p. = 134-136 °C (AcOEt); FTIR (film) 3250, 1630, 1405 cm⁻¹; ¹H NMR (500 MHz, CDCl₃) δ 7.59 (dd, J = 7.3 and 1.8 Hz, 1H), 7.40 (m, 1H), 7.30 (dt, J = 7.3 and 1.8 Hz, 1H), 7.28-7.21 (m, 5H), 7.16 (m, 2H), 4.06 (s, 2H), 2.90 (d, J = 4.6 Hz, 3H); ¹³C NMR (100.6 MHz, CDCl₃) δ 168.7, 138.2, 137.2, 133.0, 132.5, 130.4, 128.8, 128.5, 127.3, 127.2, 40.3, 26.7; MS (70 eV): e/z (%): 257 (4) [M^+ +1], 166 (75), 91 (100).



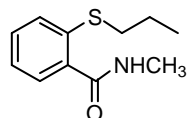
2-(4-methoxybenzylthio)-N-methylbenzamide (5.9b): $R_f = 0.57$ (Hexane/AcOEt 80:20); FTIR (microscope) ν 3430, 1638, 1510 cm^{-1} ; ^1H NMR (400 MHz, CD_3OD) δ 7.39 (d, $J = 7.7$ Hz, 1H), 7.33 (m, 2H), 7.21 (m, 1H), 7.17 (d, $J = 8.6$ Hz, 2H), 6.79 (d, $J = 8.6$ Hz, 2H), 4.06 (s, 2H), 3.73 (s, 3H), 2.84 (s, 3H); ^{13}C NMR (100.6 MHz, CD_3OD) δ 171.9, 160.2, 139.0, 136.0, 131.7, 131.2, 131.1, 130.4, 128.6, 127.1, 114.8, 55.7, 39.3, 26.7; EIMS (m/z) 287 [M^+ , (100)].



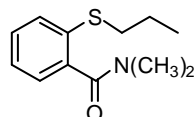
N-methyl-2-(4-(trifluoromethyl)benzylthio)benzamide (5.9c): $R_f = 0.49$ (Hexane/AcOEt 50:50); FTIR (microscope) ν 3435, 1643, 1435 cm^{-1} ; ^1H NMR (400 MHz, CD_3OD) δ 7.53 (d, $J = 8.2$ Hz, 2H), 7.46 (d, $J = 8.2$ Hz, 2H), 7.37 (m, 2H), 7.30 (m, 1H), 7.23 (m, 1H), 4.20 (s, 2H), 2.87 (s, 3H); ^{13}C NMR (100.6 MHz, CD_3OD) δ 171.9, 143.6, 139.7, 135.1, 132.1, 131.2, 130.6, 130.1, 128.8, 127.6, 126.2 (q, $J = 3.6$ Hz), 125.6 (q, $J = 271.4$ Hz), 39.2, 26.7; EIMS (m/z) 325 [M^+ , (100)].



N-methyl-2-(4-nitrobenzylthio)benzamide (5.9d): FTIR (microscope) ν 3427, 1636, 1518 cm^{-1} ; ^1H NMR (400 MHz, CD_3OD) δ 8.08 (d, $J = 8.6$ Hz, 2H), 7.48 (d, $J = 8.6$ Hz, 2H), 7.36 (m, 2H), 7.31 (m, 1H), 7.24 (m, 1H), 4.22 (s, 2H), 2.88 (s, 3H); ^{13}C NMR (100.6 MHz, CD_3OD) δ 171.8, 148.3, 147.0, 139.9, 134.5, 132.5, 131.3, 131.0, 128.8, 127.9, 124.4, 39.1, 26.7; EIMS (m/z) 302 [M^+ , (15)], 166 (100).



N-methyl-2-(propylthio)benzamide (5.9e): $R_f = 0.42$ (Hexane/AcOEt 50:50); FTIR (film) 3340, 1638, 1004 cm^{-1} ; ^1H NMR (400 MHz, CDCl_3) δ 7.49 (dd, $J = 7.8$ and 1.4 Hz, 1H), 7.33 (m, 1H), 7.28 (m, 1H), 7.12 (dt, $J = 7.8$ and 1.4 Hz, 1H), 7.04 (br s, 1H), 2.90 (d, $J = 4.9$ Hz, 3H), 2.82 (t, $J = 7.3$ Hz, 2H), 1.61 (sextet, $J = 7.3$ Hz, 2H), 0.98 (t, $J = 7.3$ Hz, 3H); ^{13}C NMR (100.6 MHz, CDCl_3) δ 168.6, 136.3, 134.7, 129.9, 129.4, 128.4, 125.4, 35.8, 26.2, 21.9, 13.4; MS (70 eV): e/z (%): 210 (30) [$\text{M}^+ + 1$], 152 (100).

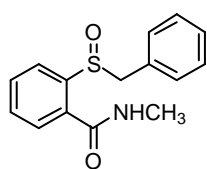


2-(benzylthio)-N,N-dimethylbenzamide (5.9g): $R_f = 0.49$ (Hexane/AcOEt 50:50); FTIR (film) 3420, 1652, 947 cm^{-1} ; ^1H NMR (400 MHz, CDCl_3) δ 7.30-7.16 (m, 9H), 4.10 (s, 2H), 3.09 (s, 3H), 2.70 (s, 3H); ^{13}C NMR (100.6 MHz, CDCl_3) δ 169.8, 139.5, 137.2, 132.1, 131.6, 128.8, 128.2, 127.0, 126.9, 126.4, 39.1, 38.0, 34.4; MS (70 eV): e/z (%): 272 (24) [$\text{M}^+ + 1$], 91 (100).

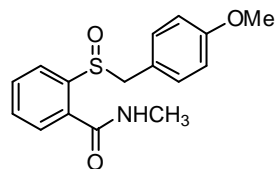
General procedure for the synthesis of compounds 5.1.

To a cooled solution of **5.9** (1 equiv.) in CHCl_3 (0.1 M) was added drop-wise a 50% in weight solution of MCPA (1 equiv.) in CHCl_3 (0.1 M) at 0 °C. After the addition was complete (ca. 30

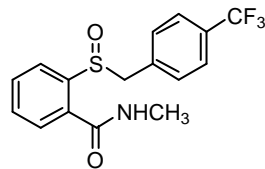
min) the solution was stirred for additional 20 min, quenched with a saturated aqueous solution of NaHCO₃ and the temperature was raised to rt. The mixture was extracted with CHCl₃, the collected organic layers dried on anhydrous Na₂SO₄, filtered and the solvent evaporated *in vacuo*. The residue was purified by flash-chromatography.



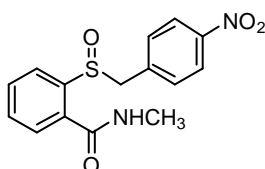
(S)-2-(benzylsulfinyl)-N-methylbenzamide ((S)-(-)-5.1a): $R_f = 0.38$ (CHCl₃/MeOH 95:05); m.p. 167-169 °C (AcOEt/MeOH); $[\alpha]_D^{20} = -258.3^\circ$ ($c = 1.1$, CHCl₃); FTIR (film) 3478, 1633, 1027 cm⁻¹; ¹H NMR (250 MHz, CDCl₃) δ 7.60 (m, 2H), 7.38 (m, 3H), 7.21 (m, 3H), 7.10 (m, 2H), 4.48 (d, $J = 12.4$ Hz, 1H), 4.03 (d, $J = 12.4$ Hz, 1H), 2.89 (d, $J = 4.6$ Hz, 3H); ¹³C NMR (100.6 MHz, CDCl₃) δ 166.9, 144.4, 132.1, 131.3, 130.7, 130.5, 130.4, 128.2, 128.0, 126.6, 125.7, 62.5, 26.9; MS (70 eV): m/z (%): 274 (41) [M⁺+1], 182 (83), 91 (100).



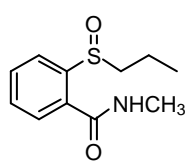
2-(4-methoxybenzylsulfinyl)-N-methylbenzamide (5.1b): $R_f = 0.20$ (Hexane/AcOEt 20:80); m.p. 154-156 °C (AcOEt/MeOH = 1:1); FTIR (microscope) ν 3296, 1646, 1513 cm⁻¹; ¹H NMR (400 MHz, CDCl₃) δ 7.59 (m, 2H), 7.43 (m, 1H), 7.37 (m, 1H), 7.10 (br s, 1H), 7.03 (d, $J = 7.7$ Hz, 2H), 6.74 (d, $J = 7.7$ Hz, 2H), 4.43 (d, $J = 12.4$ Hz, 1H), 3.99 (d, $J = 12.4$ Hz, 1H), 3.74 (s, 3H), 2.92 (d, $J = 3.5$ Hz, 3H); ¹³C NMR (100.6 MHz, CDCl₃) δ 167.0, 159.5, 144.8, 132.1, 131.8, 131.1, 130.2, 126.6, 125.5, 122.7, 113.6, 62.2, 55.2, 26.8; EIMS (m/z) 303 (100) [M⁺+1].



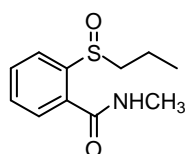
N-methyl-2-(4-(trifluoromethyl)benzylsulfinyl)benzamide (5.1c): $R_f = 0.30$ (AcOEt/Hexane 70:30); m.p. 204-205 °C (AcOEt/MeOH = 1:1); FTIR (microscope) ν 3282, 1646, 1322 cm⁻¹; ¹H NMR (400 MHz, CDCl₃) δ 7.58 (m, 2H), 7.48 (d, $J = 7.7$ Hz, 2H), 7.43 (m, 2H), 7.24 (d, $J = 7.7$ Hz, 2H), 6.76 (br s, 1H), 4.52 (d, $J = 12.4$ Hz, 1H), 4.16 (d, $J = 12.4$ Hz, 1H), 2.98 (d, $J = 4.6$ Hz, 3H); ¹⁹F NMR (235.4 MHz, CDCl₃) δ -63.6 (s, 3F); ¹³C NMR (100.6 MHz, CDCl₃) δ 166.9, 144.7, 134.9, 132.0, 131.4, 130.9, 130.6, 126.4, 125.6, 124.9 (q, $J = 3.6$ Hz), 124.2 (q, $J = 271.8$ Hz), 62.2, 26.9; EIMS (m/z) 342 [M⁺+1, (39)], 182 (100), 159 (96).



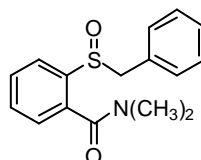
N-methyl-2-(4-nitrobenzylsulfinyl)benzamide (5.1d): $R_f = 0.52$ (AcOEt); m.p. 177-179 °C (AcOEt/MeOH 1:1); FTIR (microscope) ν 3296, 1646, 1519 cm⁻¹; ¹H NMR (400 MHz, CDCl₃) δ 8.07 (d, $J = 8.5$ Hz, 2H), 7.59 (m, 2H), 7.46 (m, 2H), 7.27 (d, $J = 8.5$ Hz, 2H), 6.66 (br s, 1H), 4.56 (d, $J = 12.4$ Hz, 1H), 4.28 (d, $J = 12.4$ Hz, 1H), 3.02 (d, $J = 4.6$ Hz, 3H); ¹³C NMR (100.6 MHz, CDCl₃) δ 166.8, 147.7, 144.5, 138.3, 131.9, 131.6, 131.4, 130.7, 126.3, 125.6, 123.1, 61.9, 26.9; EIMS (m/z) 319 [M⁺+1, (10)], 182 (100).



***N*-methyl-2-(propylsulfinyl)benzamide (5.1e):** $R_f = 0.24$ (AcOEt); FTIR (film) 3419, 1644, 998 cm^{-1} ; ^1H NMR (400 MHz, CDCl_3) δ 8.07 (d, $J = 7.8$ Hz, 1H), 7.87 (br s, 1H), 7.75 (d, $J = 7.8$ Hz, 1H), 7.62 (t, $J = 7.8$ Hz, 1H), 7.44 (t, $J = 7.8$ Hz, 1H), 3.26 (ddd, $J = 17.4, 12.8$ and 6.4 Hz, 1H), 2.93 (d, $J = 4.6$ Hz, 3H), 2.71 (ddd, $J = 17.4, 12.8$ and 5.0 Hz, 1H), 1.92 (m, 1H), 1.72 (m, 1H), 1.02 (t, $J = 7.8$ Hz, 3H); ^{13}C NMR (100.6 MHz, CDCl_3) δ 166.7, 145.7, 131.8, 131.4, 130.0, 127.0, 124.4, 59.5, 26.6, 16.5, 12.9; MS (70 eV): e/z (%): 226 (25) [$\text{M}^+ + 1$], 182 (46), 152 (100).



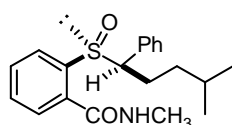
***N*-methyl-2-(propylsulfinyl)benzamide (5.1f):** see Kita, Y.; Tamura, O.; Shibata, N.; Miki, T. *Chem. Pharm. Bull.* **1990**, 38, 1473-1478.



2-(benzylsulfinyl)-*N,N*-dimethylbenzamide (5.1g): $R_f = 0.41$ (AcOEt); m.p. 90-91 $^\circ\text{C}$ (AcOEt); FTIR (film) 1626, 1397, 1032 cm^{-1} ; ^1H NMR (500 MHz, CDCl_3) δ 7.51 (d, $J = 7.8$ Hz, 1H), 7.45 (t, $J = 7.8$ Hz, 1H), 7.38 (t, $J = 7.8$ Hz, 1H), 7.31 (d, $J = 7.8$ Hz, 1H), 7.23 (m, 3H), 7.12 (m, 2H), 4.42 (d, $J = 12.8$ Hz, 1H), 4.08 (d, $J = 12.8$ Hz, 1H), 3.13 (s, 3H), 2.89 (s, 3H); ^{13}C NMR (100.6 MHz, CDCl_3) δ 168.0, 141.1, 133.2, 130.4, 130.3, 129.8, 129.4, 127.9, 127.8, 126.2, 125.4, 61.9, 38.9, 34.8; MS (70 eV): e/z (%): 287 (33) [M^+], 196 (64), 91 (100).

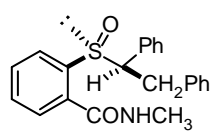
General procedure for the synthesis of compounds 5.2.

To a cooled solution of **5.1** (1.83 mmol, 500 mg) and dry HMPA (5 equiv.) in dry THF (0.05 M) was added drop-wise, at -70 $^\circ\text{C}$ and under Ar atmosphere, a 2.5 M solution of BuLi (1.2 equiv.). After 10 min, at -78 $^\circ\text{C}$ 3-methyl-1-bromo-butane (1.2 equiv.) was added. After the reaction was complete (TLC monitoring), saturated aqueous NH_4Cl was added, the temperature raised to rt and the solution extracted with AcOEt. The collected organic layers were dried on anhydrous Na_2SO_4 , filtered and the solvent evaporated *in vacuo*. The residue was purified by flash-chromatography.

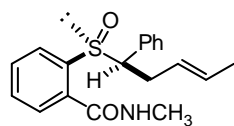


***N*-methyl-2-(4-methyl-1-phenylpentylsulfinyl)benzamide ((*Ss*, *R*) 5.2a):** $R_f = 0.50$ (AcOEt); $[\alpha]_{23}^D = -45.1$ (c 0.8, CHCl_3 , e.e. 98 %); m.p. = 108-109 $^\circ\text{C}$ (AcOEt); FTIR (film) 3383, 1653, 1000 cm^{-1} ; ^1H NMR (500 MHz, CDCl_3) δ 7.91 (d, $J = 7.5$ Hz, 1H), 7.62 (d, $J = 7.5$ Hz, 1H), 7.54 (t, $J = 7.5$ Hz, 1H), 7.44 (t, $J = 7.5$ Hz, 1H), 7.37-7.22 (m, 5H), 6.82 (br s, 1H), 4.25 (dd, $J = 11.3$ and 3.8 Hz, 1H), 2.90 (d, $J = 4.2$ Hz, 3H), 2.05 (m, 1H), 1.80 (m, 1H), 1.39 (m, 1H), 0.89 (m, 2H), 0.70 (d, $J = 6.3$ Hz, 6H); ^{13}C NMR (125.7 MHz, CDCl_3) δ 166.9, 143.1, 136.5, 133.5, 130.8, 130.6, 129.1, 128.6, 128.0,

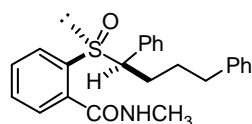
127.8, 126.8, 68.8, 35.5, 27.8, 26.8, 22.7, 21.8; MS (70 eV): e/z (%): 344 (2) [$M^+ + 1$], 183 (91), 117 (100), 91 (100).



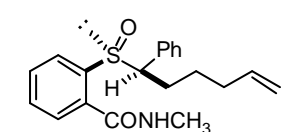
2-(1,2-diphenylethylsulfinyl)-N-methylbenzamide (5.2b), major diast.: $R_f = 0.51$ (AcOEt); $^1\text{H NMR}$ (400 MHz, CDCl_3) δ 8.23 (d, $J = 7.8$ Hz, 1H), 7.83-7.76 (m, 3H), 7.60-7.07 (m, 9H), 6.91 (m, 2H), 4.67 (dd, $J = 11.4$ and 3.9 Hz, 1H), 3.44 (dd, $J = 14.2$ and 11.4 Hz, 1H), 3.24 (dd, $J = 14.2$ and 3.9 Hz, 1H), 3.04 (d, $J = 3.9$ Hz, 3H); MS (70 eV): e/z (%), mixture of both diastereoisomers: 364 (12) [$M^+ + 1$], 91 (100). *Minor diast.*: $R_f = 0.51$ (AcOEt); $^1\text{H NMR}$ (400 MHz, CDCl_3) δ 8.12 (d, $J = 7.8$ Hz, 1H), 7.83-7.76 (m, 3H), 7.60-7.07 (m, 9H), 6.96 (m, 2H), 4.84 (dd, $J = 9.6$ and 6.2 Hz, 1H), 3.87 (dd, $J = 14.2$ and 6.2 Hz, 1H), 3.65 (dd, $J = 14.2$ and 9.6 Hz, 1H), 3.04 (d, $J = 3.9$ Hz, 3H).



(E)-N-methyl-2-(1-phenylpent-3-enylsulfinyl)benzamide (5.2c), major diast.: $R_f = 0.60$ (AcOEt); $^1\text{H NMR}$ (500 MHz, CDCl_3) δ 7.98 (d, $J = 7.7$ Hz, 1H), 7.64-6.75 (m, 9H), 5.28 (m, 1H), 5.01 (m, 1H), 4.36 (dd, $J = 11.5$ and 4.4 Hz, 1H), 2.92 (d, $J = 4.9$ Hz, 3H), 2.78 (m, 1H), 2.43 (m, 1H), 1.42 (d, $J = 6.6$ Hz, 3H); MS (70 eV): e/z (%), mixture of both diastereoisomers: 327 (15) [M^+], 91 (100). *Minor diast.*: $R_f = 0.60$ (AcOEt); $^1\text{H NMR}$ (500 MHz, CDCl_3) δ 8.05 (d, $J = 8.2$ Hz, 1H), 7.64-6.75 (m, 9H), 5.63 (m, 1H), 5.44 (m, 1H), 4.53 (dd, $J = 8.8$ and 7.1 Hz, 1H), 3.08 (m, 1H), 2.98 (d, $J = 4.4$ Hz, 3H), 2.91 (m, 1H), 1.60 (d, $J = 6.6$ Hz, 3H).

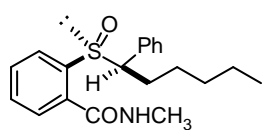


2-(1,4-diphenylbutylsulfinyl)-N-methylbenzamide (5.2e), major diast.: $R_f = 0.59$ (AcOEt); m.p. 130-131 °C (AcOEt); FTIR (film) 3451, 1661, 1019 cm^{-1} ; $^1\text{H NMR}$ (400 MHz, CDCl_3) δ 7.92 (d, $J = 7.9$ Hz, 1H), 7.61 (d, $J = 7.9$ Hz, 1H), 7.53 (t, $J = 7.9$ Hz, 1H), 7.42 (t, $J = 7.9$ Hz, 1H), 7.40-7.24 (m, 5H), 7.11 (m, 3H), 6.91 (m, 2H), 6.85 (br s, 1H), 4.35 (dd, $J = 11.7$ and 4.1 Hz, 1H), 2.89 (d, $J = 4.1$ Hz, 3H), 2.42 (m, 2H), 2.12 (m, 1H), 1.74 (m, 1H), 1.44 (m, 1H), 1.29 (m, 1H); $^{13}\text{C NMR}$ (125.7 MHz, CDCl_3) δ 166.9, 143.2, 141.7, 136.4, 133.3, 130.9, 130.5, 129.2, 128.7, 128.2, 128.1, 128.0, 127.6, 126.8, 125.6, 68.3, 35.3, 28.1, 26.8, 24.1; MS (70 eV): e/z (%): 392 (2) [$M^+ + 1$], 332 (87), 165 (78), 117 (100).



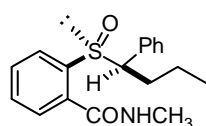
N-methyl-2-(1-phenylhex-5-enylsulfinyl)benzamide (5.2f), major diast.: $R_f = 0.52$ (AcOEt); FTIR (film) 3279, 1639, 996 cm^{-1} ; $^1\text{H NMR}$ (400 MHz, CDCl_3) δ 7.94 (d, $J = 8.0$ Hz, 1H), 7.63 (d, $J = 8.0$ Hz, 1H), 7.56 (t, $J = 8.0$ Hz, 1H), 7.45 (t, $J = 8.0$ Hz, 1H), 7.39-7.25 (m, 5H), 6.78 (br s, 1H), 5.57 (m, 1H), 4.81 (m, 2H), 4.31 (dd, $J = 11.5$ and 3.5 Hz, 1H), 2.93 (d, $J = 3.5$ Hz, 3H), 2.09 (m, 1H), 1.90 (m, 2H), 1.79 (m, 1H), 1.22 (m, 1H), 1.09 (m, 1H); $^{13}\text{C NMR}$ (100.6 MHz, CDCl_3) δ 167.0, 140.2,

137.0, 134.1, 131.7, 130.7, 129.3, 128.7, 126.7, 126.1, 125.5, 120.3, 114.8, 69.0, 33.6, 33.3, 32.4, 26.0; MS (70 eV): m/z (%): 342 (31) [$M^+ + 1$], 166 (90), 117 (100).



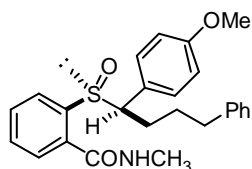
***N*-methyl-2-(1-phenylhexylsulfinyl)benzamide (5.2g)**, major diast.: R_f

= 0.56 (AcOEt); FTIR (film) 3290, 1643, 1554, 996 cm^{-1} ; m.p. 110-111 °C (AcOEt); ^1H NMR (400 MHz, CDCl_3) δ 7.91 (d, $J = 7.7$ Hz, 1H), 7.62 (d, $J = 7.7$ Hz, 1H), 7.50 (dt, $J = 7.7$ and 1.3 Hz, 1H), 7.47 (dt, $J = 7.7$ and 1.3 Hz, 1H), 7.35-7.24 (m, 5H), 6.64 (br s, 1H), 4.28 (dd, $J = 11.6$ and 4.1 Hz, 1H), 2.95 (d, $J = 4.9$ Hz, 3H), 2.08 (m, 1H), 1.82 (m, 1H), 1.35 (m, 6H), 0.74 (m, 3H); ^{13}C NMR (125.7 MHz, CDCl_3) δ 167.0, 143.0, 136.3, 133.8, 130.9, 130.7, 129.2, 128.6, 128.0, 127.3, 68.9, 31.4, 26.9, 26.3, 25.3, 22.2, 13.9; MS (70 eV): m/z (%): 344 (2) [$M^+ + 1$], 136 (84), 117 (75), 91 (100).



***N*-methyl-2-(1-phenylbutylsulfinyl)benzamide (5.2h)**, major diast.: R_f =

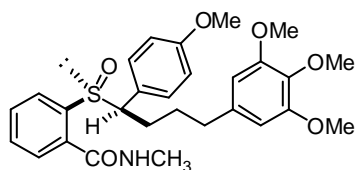
0.25 (AcOEt); FTIR (film) 3285, 1653, 1016 cm^{-1} ; m.p. 123-125 °C (AcOEt); ^1H NMR (400 MHz, CDCl_3) δ 7.92 (d, $J = 7.6$ Hz, 1H), 7.62 (d, $J = 7.6$ Hz, 1H), 7.56 (dt, $J = 7.6$ and 1.2 Hz, 1H), 7.48 (dt, $J = 7.6$ and 1.2 Hz, 1H), 7.33-7.26 (m, 5H), 6.55 (br s, 1H), 4.30 (dd, $J = 11.4$ and 3.8 Hz, 1H), 2.95 (d, $J = 5.0$ Hz, 3H), 2.09 (m, 1H), 1.79 (m, 1H), 1.18 (m, 1H), 1.02 (m, 1H), 0.76 (t, $J = 7.3$ Hz, 3H); ^{13}C NMR (125.7 MHz, CDCl_3) δ 167.0, 136.2, 134.0, 131.7, 131.0, 129.2, 128.6, 128.1, 127.4, 126.7, 125.5, 68.7, 27.6, 26.9, 19.9, 13.7; MS (70 eV): m/z (%): 316 (34) [$M^+ + 1$], 165 (88), 117 (77), 91 (100).



2-(1-(4-methoxyphenyl)-4-phenylbutylsulfinyl)-*N*-methylbenzamide

(5.2i), major diast.: R_f = 0.53 (AcOEt); FTIR (microscope) ν 3291,

1646, 1512 cm^{-1} ; ^1H NMR (400 MHz, CDCl_3) δ 7.90 (d, $J = 7.7$ Hz, 1H), 7.60 (d, $J = 7.5$ Hz, 1H), 7.52 (m, 1H), 7.41 (m, 1H), 7.28 (m, 2H), 7.12 (m, 3H), 6.93 (d, $J = 8.5$ Hz, 2H), 6.89 (br s, 1H), 6.85 (d, $J = 8.5$ Hz, 2H), 4.34 (dd, $J = 11.4$ and 3.6 Hz, 1H), 3.78 (s, 3H), 2.90 (d, $J = 4.9$ Hz, 3H), 2.43 (m, 2H), 2.07 (m, 1H), 1.71 (m, 1H), 1.46 (m, 1H), 1.27 (m, 1H); ^{13}C NMR (100.6 MHz, CDCl_3) δ 166.9, 159.5, 143.1, 141.7, 133.3, 130.9, 130.6, 130.3, 128.4, 128.2, 128.1, 127.6, 126.7, 125.6, 114.1, 67.5, 55.2, 35.3, 28.1, 26.8, 24.1; ESI (m/z) 441 ($M^+ + \text{Na}$).

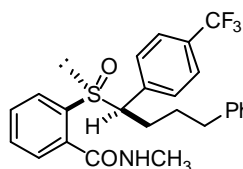


2-(1-(4-methoxyphenyl)-4-(3,4,5-

trimethoxyphenyl)butylsulfinyl)-*N*-methylbenzamide (5.2j),

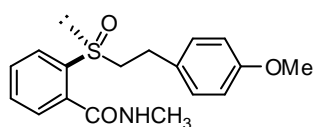
major diast.: R_f = 0.22 (AcOEt); FTIR (microscope) ν 3316, 1663 cm^{-1} ; ^1H NMR (400 MHz, CDCl_3) δ 7.90 (d, $J = 7.7$ Hz, 1H), 7.61 (m, 1H), 7.54 (m, 1H), 7.45 (m, 1H), 7.27 (m, 3H), 6.85 (d, $J = 8.3$ Hz, 2H), 6.69 (br d, $J = 3.6$ Hz, 1H), 6.17 (s, 2H), 4.32 (dd, $J = 11.6$ and 3.9 Hz, 1H), 3.79 (s, 3H), 3.78 (s, 3H), 3.75

(s, 6H), 2.94 (d, $J = 3.6$ Hz, 3H), 2.41 (m, 2H), 2.10 (m, 1H), 1.75 (m, 1H), 1.48 (m, 1H), 1.31 (m, 1H); ^{13}C NMR (100.6 MHz, CDCl_3) δ 167.0, 159.6, 153.0, 131.8, 130.8, 130.6, 130.5, 130.4, 129.0, 128.2, 128.0, 127.6, 127.0, 114.1, 105.4, 67.8, 60.8, 56.0, 55.3, 35.7, 28.0, 26.9, 24.3; ESI (m/z) 550 ($\text{M}^+ + \text{K}$), 534 ($\text{M}^+ + \text{Na}$).



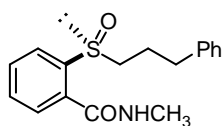
***N*-methyl-2-(4-phenyl-1-(4-(trifluoromethyl)phenyl)butylsulfinyl)benzamide (5.2k)**, major diast.:

$R_f = 0.50$ (AcOEt/hexane 70:30); FTIR (microscope) ν 3322, 1649 cm^{-1} ; ^1H NMR (400 MHz, CDCl_3) δ 8.00 (d, $J = 8.0$ Hz, 1H), 7.67-7.05 (m, 5H), 6.90 (d, $J = 7.2$ Hz, 2H), 6.81 (br s, 1H), 4.48 (dd, $J = 11.6$ and 3.6 Hz, 1H), 2.94 (d, $J = 3.6$ Hz, 3H), 2.43 (m, 2H), 2.14 (m, 1H), 1.68 (m, 1H), 1.41 (m, 1H), 1.26 (m, 1H); ^{13}C NMR (100.6 MHz, CDCl_3) δ 166.6, 143.1, 141.3, 141.1, 132.5, 131.3, 130.7, 129.6, 128.4, 128.3, 128.2, 127.2, 126.6, 125.8, 125.6 (q, $J = 3.6$ Hz), 67.6, 35.2, 27.9, 26.9, 23.4, CF_3 signal is obscured due to its low intensity; EIMS (m/z) 460 [$\text{M}^+ + 1$, (2)], 276 (43), 165 (73), 104 (72), 91 (100).



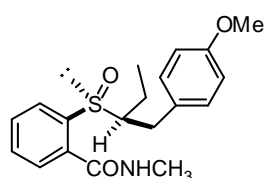
2-(4-Methoxyphenethylsulfinyl)-*N*-methylbenzamide (5.2l).

Yellowish oil, $R_f = 0.43$ (AcOEt/hexane 70:30); ^1H NMR (400 MHz, CDCl_3) δ 8.18 (m, 1H), 7.65 (m, 2H), 7.50 (m, 1H), 7.12 (d, $J = 8.2$ Hz, 2H), 6.90 (br s, 1H), 6.78 (d, $J = 8.2$ Hz, 2H), 3.75 (s, 3H), 3.20-2.95 (m, 4H), 2.98 (d, $J = 4.8$ Hz, 3H); ^{13}C NMR (100.6 MHz, CDCl_3) δ 167.8, 157.8, 143.0, 134.1, 133.2, 131.7, 131.2, 129.8, 128.4, 123.7, 114.2, 56.1, 55.8, 33.0, 26.7;



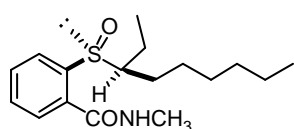
***N*-methyl-2-(4-phenylbutylsulfinyl)benzamide (5.2m)**: ^1H NMR (500 MHz, CDCl_3) δ 8.10 (d, $J = 8.1$ Hz, 1H), 7.60 (m, 2H), 7.45 (m, 1H), 7.23 (m, 2H), 7.13 (m, 3H), 6.97 (br s, 1H), 3.31 (m, 1H), 2.93 (d, $J = 4.6$ Hz, 3H), 2.77 (m,

1H), 2.61 (m, 2H), 1.96 (m, 1H), 1.75 (m, 3H); MS (70 eV): m/z (%): 316 (4) [$\text{M}^+ + 1$], 152 (75), 91 (100).



2-(1-(4-Methoxyphenyl)butan-2-ylsulfinyl)-*N*-methylbenzamide (5.2n).

Yellowish oil, inseparable mixture of diastereoisomers, $R_f = 0.63$ (AcOEt/hexane 70:30); ^1H NMR (400 MHz, CDCl_3) δ 8.22 (m, 2H), 7.64 (m, 4H), 7.51 (m, 2H), 7.10 (m, 4H), 6.91 (br s, 2H), 6.80 (m, 4H), 3.77 (s, 3H), 3.72 (s, 3H), 3.22-2.98 (m, 6H), 2.96 (m, 6H), 1.63 (m, 4H), 0.98 (t, $J = 7.5$ Hz, 3H), 0.92 (t, $J = 7.5$ Hz, 3H); MS (70 eV): m/z (%): 346 (19) [$\text{M}^+ + 1$], 84 (100).



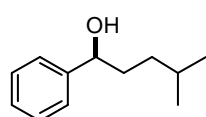
***N*-methyl-2-(nonan-3-ylsulfinyl)benzamide (5.2o)**, one diast.: $R_f =$

0.41 (AcOEt); FTIR (film) 3298, 1651, 1550, 1000 cm^{-1} ; ^1H NMR

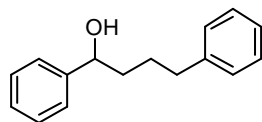
(400 MHz, CDCl₃) δ 8.03 (d, *J* = 7.5 Hz, 1H), 7.63 (m, 2H), 7.47 (m, 1H), 6.99 (br s, 1H), 3.00 (m, 1H), 2.96 (d, *J* = 6.6 Hz, 3H), 1.78 (m, 2H), 1.47 (m, 2H), 1.31 (m, 11H), 0.71 (t, *J* = 7.5 Hz, 3H); ¹³C NMR (125.7 MHz, CDCl₃) δ 166.8, 142.8, 131.1, 130.3, 128.6, 127.6, 126.9, 64.4, 31.7, 29.6, 29.4, 26.8, 26.6, 22.6, 17.9, 14.0, 11.4; MS (70 eV): *m/z* (%): 310 (17) [M⁺], 183 (25), 84 (100). *Other diast.*: *R*_f = 0.33 (AcOEt); FTIR (film) 3298, 1651, 1550, 1000 cm⁻¹; ¹H NMR (400 MHz, CDCl₃) δ 8.03 (d, *J* = 7.5 Hz, 1H), 7.63 (m, 2H), 7.48 (m, 1H), 6.81 (br s, 1H), 3.01 (m, 1H), 2.97 (d, *J* = 4.9 Hz, 3H), 1.85 (m, 2H), 1.44 (m, 2H), 1.17 (t, *J* = 7.5 Hz, 3H), 1.14 (m, 4H), 1.06 (m, 4H), 0.79 (t, *J* = 7.2 Hz, 3H); ¹³C NMR (125.7 MHz, CDCl₃) δ 166.9, 143.4, 132.7, 131.0, 130.2, 127.3, 126.6, 64.2, 31.4, 29.0, 26.9, 23.9, 23.4, 22.4, 14.0, 11.3; MS (70 eV): *m/z* (%): 310 (17) [M⁺], 183 (25), 84 (100).

General procedure for the synthesis of compounds 5.3.

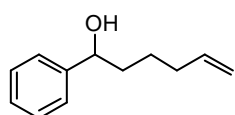
To a cooled solution of **5.2** (1 equiv.) and TMP (3 equiv.) in dry DCM (0.1 M) was added neat TFAA (5 equiv.) at 0 °C and under Ar atmosphere. The temperature was left to reach rt and the reaction was stirred until complete disappearance of the starting material was monitored (TLC). The organic solvent was evaporated, the residue diluted with MeOH and water and an excess of solid K₂CO₃ was added until basic pH was reached. The mixture was extracted with AcOEt, the collected organic layers dried on anhydrous Na₂SO₄, filtered and the solvent evaporated in vacuo. The residue was purified by flash-chromatography.



4-methyl-1-phenylpentan-1-ol ((-)-5.3a): *R*_f = 0.66 (AcOEt/Hexane 70:30); [α]_D²³ = - 14.6 (*c* 0.6, CHCl₃, e.e. 45 %); ¹H NMR (400 MHz, CDCl₃) δ 7.34-7.25 (m, 5H), 4.62 (t, *J* = 6.8 Hz, 1H), 1.83-1.68 (m, 2H), 1.60-1.50 (m, 1H), 1.37-1.26 (m, 2H), 1.18-1.09 (m, 1H), 0.87 (d, *J* = 3.0 Hz, 3H), 0.86 (d, *J* = 3.0 Hz, 3H); ¹³C NMR (100.6 MHz, CDCl₃) δ 144.9, 128.4, 127.5, 125.9, 75.0, 37.0, 34.9, 28.0, 22.6, 22.5; EIMS (*m/z*) 178 [M⁺+1, (100)].

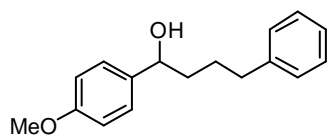


1,4-diphenylbutan-1-ol (5.3e): *R*_f = 0.60 (AcOEt/Hexane 70:30); ¹H NMR (400 MHz, CDCl₃) δ 7.25-7.03 (m, 10H), 4.45 (t, *J* = 5.0 Hz, 1H), 2.75 (s, 1H), 2.51 (t, *J* = 7.0 Hz, 2H), 1.75-1.44 (m, 4H); ¹³C NMR (100.6 MHz, CDCl₃) δ 144.5, 141.9, 128.1, 128.03, 127.97, 127.1, 125.6, 125.4, 74.0, 38.4, 35.6, 27.4; EIMS (*m/z*) 225 [M⁺+1, (100)].

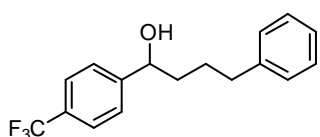


1-phenylhex-5-en-1-ol (5.3f): *R*_f = 0.70 (AcOEt/Hexane 60:40); ¹H NMR (400 MHz, CDCl₃) δ 7.33-7.21 (m, 5H), 5.75 (m, 1H), 5.00-4.90 (m, 2H),

4.58 (m, 1H), 2.55 (br s, 1H), 1.32-2.07 (m, 6H); ^{13}C NMR (100.6 MHz, CDCl_3) δ 144.9, 128.5, 128.4, 127.6, 114.6, 74.7, 65.3, 38.4, 33.5; EIMS (m/z) 176 [$\text{M}^+ + 1$, (100)].



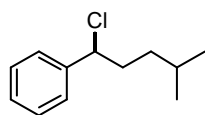
1-(4-methoxyphenyl)-4-phenylbutan-1-ol (5.3i): R_f = 0.64 (AcOEt/hexane 60:40); ^1H NMR (400 MHz, CDCl_3) δ 7.26-7.13 (m, 7H), 6.87 (d, J = 8.6 Hz, 2H), 4.63 (t, J = 5.3 Hz, 1H), 3.80 (s, 3H), 2.62 (t, J = 7.1 Hz, 2H), 1.90-1.57 (m, 5H); ^{13}C NMR (100.6 MHz, CDCl_3) δ 158.5, 142.0, 136.8, 128.1, 127.9, 126.8, 125.4, 113.4, 73.4, 54.8, 38.2, 35.4, 27.3; EIMS (m/z) 257 [$\text{M}^+ + 1$, (100)].



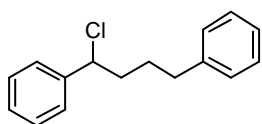
4-phenyl-1-(4-(trifluoromethyl)phenyl)butan-1-ol (5.3k): R_f = 0.68 (AcOEt/Hexane 60:40); ^1H NMR (400 MHz, CDCl_3) δ 7.55 (d, J = 8.0 Hz, 2H), 7.36 (d, J = 8.0 Hz, 2H), 7.50-7.11 (m, 5H), 4.66 (br s, 1H), 2.60 (t, J = 6.8 Hz, 2H), 2.31 (br s, 1H), 1.81-1.52 (m, 4H); ^{13}C NMR (100.6 MHz, CDCl_3) δ 148.5, 141.9, 129.5, (q, J = 32.3 Hz), 128.3, 126.0, 125.8, 125.2 (q, J = 3.6 Hz), 125.1, 124.2 (q, J = 272.2 Hz), 73.6, 38.5, 35.5, 27.2; EIMS (m/z) 294 [$\text{M}^+ + 1$, (100)].

General procedure for the synthesis of compounds 5.4.

To a cooled solution of **5.2** (1 equiv.) and TMP (3 equiv.) in dry DCM (0.1 M) was added neat oxalyl chloride (1.2 equiv.) at $-50\text{ }^\circ\text{C}$ and under Ar atmosphere. After complete disappearance of the starting material (TLC), the reaction was quenched with 1N HCl, the temperature raised to rt and the mixture extracted with DCM. The collected organic layers were dried on anhydrous Na_2SO_4 , filtered and the solvent evaporated *in vacuo*. The residue was purified by flash-chromatography.

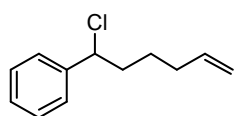


(1-chloro-4-methylpentyl)benzene ((-)-5.4a): $[\alpha]_{23}^D = -66.7$ (c 0.4, CHCl_3 , e.e. > 98%); FTIR (film) 1651, 1456, 1023 cm^{-1} ; ^1H NMR (400 MHz, CDCl_3) δ 7.44-7.27 (m, 5H), 4.83 (dd, J = 8.0 and 6.2 Hz, 1H), 2.10 (m, 2H), 1.59 (m, 1H), 1.40 (m, 1H), 1.20 (m, 1H), 0.90 (d, J = 7.1 Hz, 6H); ^{13}C NMR (100.6 MHz, CDCl_3) δ 142.1, 128.6, 128.2, 126.9, 64.2, 38.0, 36.2, 27.7, 22.5, 22.4; MS (70 eV): e/z (%): 198 (7) [$\text{M}^+ + 2$], 196 (21) [M^+], 125 (100), 91 (55).



(1-chloro-4-phenylpentyl)benzene (5.4e): R_f = 0.67 (AcOEt/Hexane 90:10); ^1H NMR (400 MHz, CDCl_3) δ 7.35-7.11 (m, 10H), 4.84 (dd, J = 8.0 and 6.5 Hz, 1H), 2.63 (t, J = 7.7 Hz, 2H), 2.14 (m, 1H), 2.06 (m, 1H),

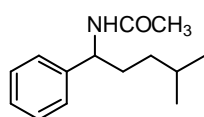
1.83 (m, 1H), 1.66 (m, 1H); ^{13}C NMR (100.6 MHz, CDCl_3) δ 141.7, 128.6, 128.4, 128.2, 126.9, 125.9, 63.6, 39.4, 35.2, 28.7.



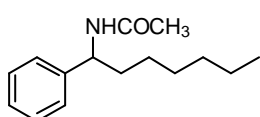
(1-chloro-4-methylpentyl)benzene (5.4f): $R_f = 0.70$ (AcOEt/Hexane 90:10); ^1H NMR (400 MHz, CDCl_3) δ 7.20-7.05 (m, 5H), 5.75 (m, 1H), 4.93 (m, 2H), 4.81 (br s, 1H), 2.03 (m, 4H), 1.59-1.41 (m 2H); ^{13}C NMR (100.6 MHz, CDCl_3) δ 141.9, 138.1, 128.6, 128.3, 126.9, 115.1, 63.7, 39.4, 33.1, 29.7, 26.3.

General procedure for the synthesis of compounds 5.5.

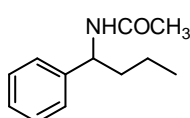
To a cooled solution of **5.2** (1 equiv.) and TMP (3 equiv.) in dry CH_3CN (0.1 M) was added neat Tf_2O (5 equiv.) at $-50\text{ }^\circ\text{C}$ and under Ar atmosphere. After complete disappearance of the starting material (TLC), the reaction was quenched with 1N HCl, the temperature raised to rt and the mixture extracted with AcOEt. The collected organic layers were dried on anhydrous Na_2SO_4 , filtered and the solvent evaporated *in vacuo*. The residue was purified by flash-chromatography.



N-(4-methyl-1-phenylpentyl)acetamide (5.5a): $R_f = 0.34$ (AcOEt/Hexane 60:40); ^1H NMR (400 MHz, CDCl_3) δ 7.45 (m, 5H), 5.63 (br s, 1H), 4.91 (br s, 1H), 2.03 (s, 3H), 1.78 (m, 2H), 1.54 (m, 1H), 1.98 (m, 1H), 1.06 (m, 1H), 0.80 (m, 6H); ^{13}C NMR (100.6 MHz, CDCl_3) δ 142.5, 128.7, 127.3, 126.6, 53.8, 35.3, 34.0, 27.9, 23.5, 22.5, 22.4; MS (70 eV): e/z (%): 220 (21) [M^+], 106 (100).



N-(1-phenylheptyl)acetamide (5.5g): $R_f = 0.42$ (AcOEt/Hexane 50:50); ^1H NMR (400 MHz, CDCl_3) δ 7.34-7.12 (m, 5H), 5.81 (br d, $J = 7.8$ Hz, 1H), 4.87 (dd, $J = 8.0$ Hz both, 1H), 1.88 (s, 3H), 1.70 (m, 2H), 1.19 (m, 8H), 0.78 (t, $J = 8.0$ Hz, 3H); ^{13}C NMR (100.6 MHz, CDCl_3) δ 169.1, 142.6, 128.6, 127.2, 126.6, 53.5, 36.2, 31.6, 29.0, 26.1, 23.3, 22.5, 13.9; MS (70 eV): e/z (%): 256 (100) [$\text{M}^+ + \text{Na}$].



N-(1-N-(1-phenylbutyl)acetamide (5.5h): $R_f = 0.29$ (AcOEt/Hexane 50:50); ^1H NMR (400 MHz, CDCl_3) δ 7.39-7.18 (m, 5H), 5.80 (br s, 1H), 4.97 (dd, $J = 8.0$ Hz, both, 1H), 1.98 (s, 3H), 1.83-1.68 (m, 2H), 1.34 (m, 2H), 0.92 (t, $J = 8.0$ Hz, 3H); ^{13}C NMR (100.6 MHz, CDCl_3) δ 169.7, 142.4, 128.8, 127.5, 126.7, 38.4, 29.8, 23.5, 19.6, 13.9; MS (70 eV): e/z (%): 214 (100) [$\text{M}^+ + \text{Na}$].

Chapter 7. References

-
- ¹ Paans, A.M.J., van Waarde, A., Elsinga, P.H., Willemsen, A.T.M., Vaalburg, W. Positron emission tomography: the conceptual idea using a multidisciplinary approach. *Methods* **2002**, 27, 195-207.
- ² Partridge, M., Spinelli, A., Ryder, W., Hindorf, C. The effect of β^+ energy on performance of a small animal PET camera. *Nucl. Instr. and Meth. A* **2006**, 568, 933-936.
- ³ Pauling, L. *Nature of the chemical bond*. Cornell University press: New York, **1940**, p 189.
- ⁴ Leo, A., Hansch, C., Elkins, D. *Chem Rev.* **1971**, 71, 525.
- ⁵ Haubner, R. PET radiopharmaceuticals in radiation treatment planning-Synthesis and biological characteristics. *Radiother. and Onc.* **2010**, 96, 280-287.
- ⁶ Wadsak, W., Mitterhauser, M. Basics and principles of radiopharmaceuticals for PET/CT. *Eur. J. Rad.* **2010**, 73, 461-469.
- ⁷ De Rosales, R.T.M., Årstad, E., Blower, P.J. Nuclear imaging of molecular processes in cancer. *Targ. Oncol.* **2009**, 4, 183-197.
- ⁸ Ametamey, S.M., Honer, M., Schubiger, P.A. Molecular imaging with PET. *Chem. Rev.* **2008**, 108, 1501-1516.
- ⁹ Le Bars, D. Fluorine-18 and medical imaging: radiopharmaceuticals for positron emission tomography. *J. F. Chem.* **2006**, 127, 1488-1493.
- ¹⁰ Laszlo, J., Humphreys, S.R., Goldin, A. Effects of glucose analogues (2-deoxy-D-glucose, 2-deoxy-D-galactose) on experimental tumors. *J. Natl. Cancer. Inst.*, **1960**, 24, 267-281.
- ¹¹ Pacák, J., Cerny, M., History of the first synthesis of 2-Deoxy-2-Fluoro-D-Glucose the Unlabeled Forerunner of 2-Deoxy-2- [¹⁸F]Fluoro-D-Glucose. *Mol. Imaging Biol.* **2002**, 4, 353-354.
- ¹² Jackowski, S. Coordination of membrane phospholipid synthesis with the cell cycle. *J. Biol. Chem.* **1994**, 269, 3858-3867.
- ¹³ Clary, G.L., Tsai, C.F., Guynn, R.W., et al. Substrate specificity of choline kinase. *Arch. Biochem. Biophys.* **1987**, 254, 214-221.
- ¹⁴ De Certaines, J.D., Larsen, V.A., Podo, F., Carpinelli, G., Briot, O., Henriksen, O. In vivo 31P MRS of experimental tumours. *NMR Biomed.* **1993**, 6, 345-365.

- ¹⁵ Hara, T., Kosaka, N., Shinoura, N., et al. PET imaging of brain tumor with [methyl-¹¹C] choline. *J. Nucl. Med.* **1997**, 38, 842-847.
- ¹⁶ Lisheng, C., Shuiyu, L., Victor, W., P. Chemistry with [¹⁸F]fluoride ion. *Eur. J. Org. Chem.* **2008**, 2853-2873.
- ¹⁷ Kieseewetter, D.O., Kilbourn, M.R., Landvatter, S.W., et al. Preparation of four fluorine-18 labeled estrogens and their selective uptakes in target issues of immature rats. *J. Nucl. Med.* **1984**, 25, 1212-1221.
- ¹⁸ Ido, T., Wan, C.N., Casella, J.S., et al. Labeled 2-deoxy-D-glucose analogs: ¹⁸F-labeled 2-deoxy-2-fluoro-D-mannose and ¹⁴C-2-deoxy-2-fluoro-D-glucose. *J. Label. Compd. Radiopharmacol.* **1978**, 14, 175-183.
- ¹⁹ Hara, T., Yuasa, M., Yoshida, H. Automated synthesis of fluorine-18 labeled choline analogue: 2-fluoroethyl-dimethyl-2-oxyethylammonium [abstract]. *J. Nucl. Med.* **1997**, 38, 44P.
- ²⁰ Grierson, J.R., Link, J.M., Mathis, C.A., Rasey, J.S., Krohn, K.A. A radiosynthesis of fluorine-18-fluoromisonidazole. *J. Nucl. Med.* **1989**, 30, 343-350.
- ²¹ Lim, J.L., Berridge, M.S. An efficient radiosynthesis of [¹⁸F]fluoromisonidazole. *Appl. Radiat. Isot.* **1993**, 44, 1085-1091.
- ²² Grierson, J.R., Link, J.M., Mathis, C.A., Rasey, J.S., Krohn, K.A. A radiosynthesis of fluorine-18-fluoromisonidazole. *J. Nucl. Med.* **1989**, 30, 343-350.
- ²³ Dong W., K., Doo-S. A., Young-Ho, O., Sungyul, L., Hee, S. K., Seung, J. O., Sang, J. L., Jae, S. K., Jin, S. R., Dae, H. M., Dae., Y. C. A new class of S_N2 reactions catalyzed by protic solvents: facile fluorination for isotopic labeling of diagnostic molecules. *J. Am. Chem. Soc.* **2006**, 128, 16394-16397.
- ²⁴ Dong, W. K., Hwan., J. J., Seok, T. L., Myung, H. S., John, A.K., Dae, Y. C. Facile nucleophilic fluorination reactions using *tert*-alcohols as a reaction medium: significantly enhanced reactivity of alkali metal fluorides and improved selectivity *J. Org. Chem.* **2008**, 73, 957-962.
- ²⁵ Dolci, L., Dollé, F., Jubeau, S., Vaufrey, F., Crouzel, C., *J. Labelled Compd. Radiopharm.* **1999**, 42, 975-985.
- ²⁶ Zhang, Y., Hall, W., Horti, A. G. *J. Labelled Compd. Radiopharm.* **2004**, 47, 385-392.
- ²⁷ Zhang, Y., Horti, A. G. *J. Labelled Compd. Radiopharm.* **2004**, 47, 947-952.
- ²⁸ Abraham, A., Angelberger, P., Kletter, K., Müller, M., Joukhadar, C., Erker, T., Langer, O. *J. Labelled Compd. Radiopharm* **2006**, 49, 345-356.
- ²⁹ Carrol, M. A., Nairne, J., Woodcraft, J. L., *J. Labelled Compd. Radiopharm* **2007**, 50, 452-454.
- ³⁰ Martin-Santamaria, S., Carrol, M. A., Carrol, C. M., Carter, C. D., Pike, V. W., Rzepa, H. S., Widdowson, D. A. *Chem. Commun.* **2000**, 649-650.
- ³¹ Ross, T., Ermert, J., Coenen, H. H., *J. Labelled Compd. Radiopharm* **2005**, 48 (Suppl), S153.

-
- ³² Pike, W. V., Aigbirhio, F. I., *J. Labelled Compd. Radiopharm* **1995**, *37*, 120-122.
- ³³ Höckel, M., Vaupel, P. *J. Natl. Cancer Inst.* **2001**, *93*, 266-276.
- ³⁴ Vaupel, P., Harrison, L. *The Oncologist* **2004**, *9* (suppl 5), 4-9.
- ³⁵ Imam, S.K. Review of positron emission tomography tracers for imaging of tumor hypoxia. *Cancer Biotherapy and Radiopharmaceuticals* **2010**, *25*, 365-373.
- ³⁶ Mees, G., Dierckx, R., Vangestel, C., Van de Wiele, C. Molecular imaging of hypoxia with radiolabeled agents. *Eur. J. Nucl. Med. Mol. Imaging* **2009**, *36*, 1674-1686.
- ³⁷ Mees G., Dierckx R., Vangestel C., et al. Molecular imaging of hypoxia with radiolabelled agents. *Eur. J. Nucl. Med. Mol. Imaging* **2009**, *36*, 1674.
- ³⁸ Chapman, J.D. Hypoxic sensitizers: implications for radiation therapy. *N. Engl. J. Med.* **1979**, *301*, 1429-1432.
- ³⁹ (a) Chapman, J.D., Franko, A.J., Sharplin, J. A marker for hypoxic cells in tumours with potential clinical applicability. *Br. J Cancer* **1981**, *43*, 546-550.
- ⁴⁰ Jerabek, P.A., Dischino, D.D., Kilbourn, M.R., Welch, M.J. *J. Labelled Compd. Radiopharm* **1984**, *21*, 1234.
- ⁴¹ Evans, S.M., Kachur, A.V., Shiue, C.Y., et al. Noninvasive detection of tumor hypoxia using the 2-nitroimidazole [¹⁸F]EF1. *J. Nucl. Med.* **2000**, *41*, 327-336.
- ⁴² (a) Mahy, P., Geets, X., Lonneux, M., et al. Determination of tumour hypoxia with [¹⁸F]EF3 in patients with head and neck tumours: A phase I study to assess the tracer pharmacokinetics, biodistribution and metabolism. *Eur. J. Nucl. Med. Mol. Imaging* **2008**, *35*, 1282-1289.
- (b) Mahy, P., De Bast, M., Leveque, P.H., et al. Preclinical validation of the hypoxia tracer 2-(2-nitroimidazol-1-yl)-N-(3,3,3-[¹⁸F]trifluoropropyl) acetamide, [¹⁸F]EF3. *Eur. J. Nucl. Med. Mol. Imaging* **2004**, *31*, 1263.
- ⁴³ (a) Komar, G., Seppanen, M., Eskola, O., Lindholm, P., et al. ¹⁸F-EF5: A new PET tracer for imaging hypoxia in head and neck cancer. *J. Nucl. Med.*, **2008**, *49*, 1944-1951. (b) Evans, S.M., Hahn, S., Pook, D.R., et al. Detection of hypoxia in human squamous cell carcinoma by EF5 binding. *Cancer Res.* **2000**, *60*, 2018.
- ⁴⁴ Koch, C.J., Evans, S.M., Lord, E.M. Oxygen dependence of cellular uptake of EF5 [2-(2-nitro-1H-imidazol-1-yl)-N-(2,2,3,3,3-pentafluoropropyl)acetamide]: analysis of drug adducts by fluorescent antibodies vs bound radioactivity. *Br. J. Cancer* **1995**, *72*, 869-874.
- ⁴⁵ Kumar, P., Stypinski, D., Xia, H., McEwan, A.J.B., Machulla, H.J., Wiebe, L.I. Fluoroazomycin arabinoside (FAZA): synthesis, 2H and 3H-labelling and preliminary evaluation of a novel 2-nitroimidazole marker of tissue hypoxia. *J. Label. Comp. Radiopharmaceuticals* **1999**, *42*, 3-16.

- ⁴⁶ Dehdashti, F., Grigsby, P.W., Lewis, J.S., et al. Assessing tumor hypoxia in cervical cancer by PET with ⁶⁰Cu-labeled diacetyl-bis(*N*⁴-methylthiosemicarbazone). *J. Nucl. Med.* **2008**, *49*, 201-205.
- ⁴⁷ Lewis, J.S., Laforest, R., Dehdashti, F., et al. An imaging comparison of ⁶⁴Cu-ATSM and ⁶⁰Cu-ATSM in cancer of the uterine cervix. *J. Nucl. Med.* **2008**, *49*, 1177-1182.
- ⁴⁸ Chapman, J.D. Hypoxic sensitizers: implications for radiation therapy. *N. Engl. J. Med.* **1979**, *301*, 1429-1432.
- ⁴⁹ Kumar, P., Stypinski, D., Xia, H., McEwan, A. J. B., Machulla, H-J., Wiebe, L. I. FLUOROAZOMYCIN ARABINOSIDE (FAZA): Synthesis, ²H and ³H-labeling and preliminary biological evaluation of a novel 2-nitroimidazole marker of tissue hypoxia. *J. Labelled Cpd. Radiopharm.* **1999**, *42*, 3-16.
- ⁵⁰ Kumar, P., Emami, S., McEwan, A. J. B., Wiebe, L. I. Development of an economical, single step synthesis of FAZA, a clinical hypoxia marker, and potential synthons to prepare its positional analogs. *Letters in Drug Design & Discovery* **2009**, *6*, 82-85.
- ⁵¹ Bravo, P., Capelli, S., Valdo, M., V., Viani, F., Zanda, M. Synthesis of optically pure (R)- and (S)- α -trifluoromethyl-alanine *Tetrahedron Asymmetry*, **1994**, *5*, 2009-2018.
- ⁵² VanRheenen, V., Cha, D., Hartley, W. M., *Organic Syntheses*, Wiley & Sons: New York, **1988**, Collect. Vol VI, p. 342.
- ⁵³ Dong, W.K., Hwan-Jeong, J., Seok, T.L., Myung-Hee, S., Katzenellenbogen, A. J., Dae, W. C. Facile nucleophilic fluorination reactions using *tert*-alcohols as a reaction medium: significantly enhanced reactivity of alkali metal fluorides and improved selectivity *J. Org. Chem.* **2008**, *73*, 957-962.
- ⁵⁴ Dong, W.K., Doo-Sik, A., Young-Ho, O., Sungyul, L., Hee, S. K., Seung, J. O., Sang, J. L., Jae, S. K., Jin, S. R., Dae, H. M., Dae, J. C. A new class of S_N2 reactions catalyzed by protic solvents: facile fluorination for isotopic labeling of diagnostic molecules *J. Am. Chem. Soc.* **2006**, *128*, 16394-16397.
- ⁵⁵ Corey, E. J., Seebach, D. *Angewandte. Chem. Int. Ed. Engl.* **1965**, *4*, 1075-1077.
- ⁵⁶ Seebach, D. *Angew. Chem. Int. Ed. Engl.* **1979**, *18*, 239-258.
- ⁵⁷ Volonterio, A., Bravo, P., Pesenti, C., Zanda, M. *Tetrahedron Lett.* **2001**, *42*, 3985-3988.
- ⁵⁸ Volonterio, A., Bravo, P., Panzeri, W., Pesenti, C., Zanda, M. *Eur. J. Org. Chem.* **2002**, 3336-3340.
- ⁵⁹ Volonterio, A., Zanda, M. *Tetrahedron Lett.* **2005**, *46*, 8723-8726.